Ana Sofia Matias da Silva

Mestre em Ciências Biomédicas

Multifunctional nano-in-micro formulations for lung cancer theragnosis

Dissertação para obtenção do Grau de Doutor em Bioengenharia

Orientador: Doutora Ana Isabel Nobre Martins Aguiar de Oliveira Ricardo, Professora Catedrática da FCT-UNL

Orientador: Doutor Ilídio Joaquim Sobreira Correia, Professor Auxiliar da UBI

Júri:

Presidente: Doutor Manuel Luís de Magalhães Nunes da Ponte, Professor Catedrático da FCT- UNL

Arguente: Doutora Maria Luísa Teixeira de Azevedo Rodrigues Corvo, Investigadora Auxiliar da Faculdade de Farmácia da Universidade de Lisboa

Arguente: Doutora Eunice Margarida Santos Costa, Cientista – Investigação e Desenvolvimento – Hovione FarmaCiência

Vogais: Doutor Carlos Lodeiro Espiño, Professor Auxiliar da FCT-UNL

FACULDADE DE CIÊNCIAS E TECNOLOGIA
UNIVERSIDADE NOVA DE LISBOA

Novembro 2015

Multifunctional nano-in-micro formulations for lung cancer theragnosis

ACKNOWLEDGMENTS

The last four years were, undoubtedly, the most challenging years of my life. More than gathering “tons” of scientific knowledge this PhD truly challenged my personal resistance and also, faith. Yes, faith. For many, faith and science to not hold hands, but to me, they are tightly bound to each other. You must have strong believes, faith and resilience to face day-by-day failures until a tremendous success is obtained. I truthfully doubted myself so many times. Luckily, I was always surrounded by amazing and special people that never let me sank in my own sea of doubting. Fortunately, they always remembered me to have faith and most importantly, to believe in my own abilities. To all the people that walked this tortuous path by my side I give to you the most sincere Thank You! I also do believe that a PhD and all the success that arises from it, is not only a very big individual battle, but also a collective effort from supervisors, colleagues, family and friends. These acknowledgments are entirely for you.

To begin with, I would like to acknowledge to my supervisors Professor Ana Aguiar Ricardo and Professor Ilídio Correia for giving me the opportunity to work and develop this outstanding project. I am very grateful for all the effort and dedication you both deposited on me and the work that together we were able to develop. Professor Ana Aguiar-Ricardo, there are not enough words to acknowledge all that you have done for me in these last years. You were more than a supervisor. You were a friend and a counselor and also, an important piece of energy that struck me whenever my light was somehow off. You never gave up on me you and always believed in me, both as researcher and a person. Professor Ilídio Correia, I’m very thankful for all of your effort to make me a good and proactive researcher. My initial steps in research and the way I build myself as a researcher are strongly owed to our first years together. I still remember your enthusiastic gesture when I was given this fellowship. I still remember where I came from.

I would also like to acknowledge to the Polymer Synthesis and Processing Group and to the Biomaterials and Tissue Engineering Group. To all of you that shared all my happy and sad days I have some special words for you. Starting with the Polymer Synthesis and Processing Group: Raquel Viveiros, more than a colleague you were an amazing friend that I will always treasure in my heart. Thank you so much for all the trust and motivation you always deposited on me. Thank you for your everyday good morning texts while I was an entire ocean apart. Your friendship is a blessing ☺; Renato Cabral, my friend in health and sickness ☺. Thank you for all your teachings, but most importantly thank you for true friendship; Telma Barroso thank you for your friendship, for constantly remembering me that ‘the sky is the limit’ and for begin

the positive person that you are and whose good vibes infect all the people surrounding you; Marta Chaves, thank you for being an excellent apprentice and for making me feel a good teacher. Remember that you are also a great research…trust in yourself and everything will be much easier; Rita Pires, keep with the excellent work that always fascinates all of us. You got it all. Do not stop until you reach the top. Thank you for all your supercritical advices and NMR teachings; Ana Sousa, you too are a fascinating research that also contributed to my scientific evolution. I am really glad we met and worked together. Thank you for your teachings and also life advices; Patrícia Morgado, our path together is longer than the course of this PhD. I will always keep a special memory of us. Thank you for the learnings we did together; Vanessa Correia, thank you our enthusiastic brainstorming moments and long outpourings about our PhDs; Márcia Tavares, thank you making part of this chapter of my life. It was a pleasure to have worked with you and to meet your easygoing way of life; Vanessa Almeida, a special thank you for your effort in helping me to achieve an important matter to pursue my last research in this PhD; Zé Jorge, thank you for all the good and funny moments you have spent together; Anita Lourenço thank you for the good moments we shared; Rita Restani thank you for the good moments we shared in the first year of my PhD. Two special thanks to two very important researchers that I was lucky to encounter. Thank you so much Vasco Bonifácio for all your teachings and patient with me and our collaborative works. The time and effort you have devoted to my PhD is truly marked in my heart; and thank you so much Teresa Casimiro. Your unconditional help, devotion and friendship will always be treasured. Without you 'baby SASD' would never have been born. It was a blessing having you around.

For the Biomaterials and Tissue Engineering group I would like to start by acknowledging to Maximiano Ribeiro, a mentor, a friend, a listener and very special person that I will never forget. Thank you for all the conversations, advices and teachings; Sónia Miguel, thank you so much for your sincere friendship and caring; Paulo Machado and Edgar Silva, thank you so much for making the first year of this PhD such an amazing challenge. It was a pleasure to teach you both in the best way I could. Elisabete Costa, João Marques and Bernardo Antunes thank you for all the good moments we shared.

To Professor Manuel Nunes da Ponte and Eunice Costa, thank you so much for your guidelines.

To Ana Pina, thank you so much for the friendship we developed during these last years. You are an extraordinary person with an outstanding spirit. To Javier Lodeiro, thank you so much for all the good working times we have shared. You are an amazing research that I strongly admire. To Nuno Costa, Luz Fernandes and Carla Rodrigues thank you for all the help in the

development of relevant analysis to my PhD. To Isabel Nogueira from IST thank you for SEM and TEM images acquisitions. To Maria José a special thank you for all assistance and availability to help.

I also have to give some special acknowledgments to all the people that make possible by MIT visiting and amazing staying. A sincere thank you to Professor Paula Hammond. Thank you so much for accepting me in your lab and for providing everything I needed to pursue my research in a successful way. I have no words to describe how grateful I am for this amazing opportunity. I would also like to acknowledge to Flavia Cardarelli for all the help upon arriving at the MIT. Thank you for contributing to an amazing experience. I would also like to express my gratitude to Liz for all the help and assistance given. Now the lab members' acknowledgements: Noemie Dorval and Samantha Collins, thank you so much for your friendship during those cold months. I will always have a special place for both of you in my heart. To Kevin Shopsowitz, Santiago Correa, Stephen Morton and Erik Dreaden thank you all for your teachings and help and our brainstorming moments. Thank you for letting me be a part of your extraordinary team. Also, thank you for the friendship we developed during those months. Mike McDonald it was such a pleasure to meet you. Thank you all the conversations and the laughs, and specially thank you for the friendship we have created. Li-Gu, Ki-Young, Mohi, Chibueze, Lawrence, Jouha, Marianna, Aishen and Kristianna, thank you so much for being part of this chapter of my life. Thank you for all the sharing. To Jeff Wyckoff a very special thank you for all the help in acquiring extraordinary images for my work. Other two important people from Koch Institute are Peter Jasen and David Gray. I'm very grateful to have met you both. To my MIT visiting colleagues with whom I shared my anxiety and happiness I would also like to acknowledge. In particular, a special thank you to Carlos Nuno, João França, Ricardo Greenfield and João Lopes. To Elaine Joseph that received me in her lovely house and treated me like her own daughter, my most sincere thank you. I will never forget you ☺. I would also like to acknowledge to Katie Trosen my great friend that I was lucky to find even before moving to Boston and that was always rooting for my success.

Because friends are the family that we can chose, I would like to express my sincere gratitude to: Marta Faria & Gonçalo Saldida, Céline Simões & Daniel Lopes, Cristina Nunes, Luísa Graça & Aníbal Pereira, Beta, Carina Castanheiro & Renato Nunes, Alexandra Castanheiro & Emanuel Silva, Marco Roriz & Guida Saloca, 'Tia' Nana & Susana, Branca Antunes & Armando Antunes, Frederico Martins, Luísa Figueiredo, Andreia Silva, Catarina Pires & David Mota, Liliana Carvalho, Mara Gonçalves, Márito, Bárbara & Luís, Márcia Gameiro, Márcia Boura, Ana Formiga, Tânia Leite, Joana Mourão & Hugo Gomes. Thanks to your unconditional sup-

port and friendship I was also to surpass another challenge. I would also like to acknowledge to the babies Babi, Eva, Rafael, Miguel and Carolina. You have been the light of eyes and the time stops when I'm with you. To my guardian angels Maria Manuela (Bebé) and Maria Celeste (Leta), I would like to thanks for the guidance in every single step of my life.

To my best friend for life and my soulmate Dário Antunes the words thank you are not enough. You have been my 'scaffold', my happiness and serenity. Your patient and unconditional love has been the turbine that keeps me spinning. Thank you for making me the luckiest women on earth.

Lastly, but not the least, my beautiful family. My final and biggest acknowledgment goes to them. To my grandparents, for helping to raise me as a child and to have risen the most amazing people on earth: my parents. To my sister, for being herself and understand how difficult it is to be me. Thank you for love ☺. To my parents, the ones that raised me in the best way they knew and did everything in their power so that I could have the life I have today. Thank you for all your love, caring and support even in the darkest times. Thank you for believing in me, when I didn't. Thank you for never giving up and for being who you are: the best parents on earth.

To conclude this vast acknowledgments section, I would also like to express my gratitude to the financial support from Fundação para a Ciência e a Tecnologia (FC&T), through the projects UID/QUI/50006/2013 (LAQV), PTDC/EQU-EQU/116097/2009, SFRH/BD/515842011, FEDER and FSE, and MIT-Portugal Program Bioengineering Systems.

ABSTRACT

Lung cancer is the most common and leading cause of cancer death worldwide. Despite the clinical and technological advances, the majority of the patients are lately diagnosed with either locally advanced or metastatic disease. Moreover, the current treatments are ineffective as the therapeutic molecules barely reach deep lung tumors.

To address this problem, nanotechnology and pulmonary delivery have been the focus for the generation of novel and potentially effective delivery systems, able to target the deep lungs. Hence, multifunctional nanodevices combining high doses of anti-cancer drugs and small interfering RNA (siRNA) can be efficiently delivered to a defined area of the respiratory tract where the tumor is confined, enhancing treatment efficacy while minimizing adverse side effects. In an attempt to engineer respirable microparticles, sustainable methodologies using supercritical carbon dioxide ($scCO_2$), like supercritical assisted spray drying (SASD), combined with nano and micro technologies were optimized. Therefore, two nanosystems were successfully engineered: i) gold nanoparticles (AuNPs) functionalized with biocompatible and fluorescent coatings (produced under $scCO_2$ conditions), and targeting sequences, able to target and enter into lung cancer cells; ii) and Layer-by Layer (LbL) assemblies comprising a nanolayer of siRNA to knockdown specific genes linked to lung cancer genetic pathway. Our results highlight the extraordinary outcomes that arise from the combination of $scCO_2$ technology in different steps of the process, with multifunctional nanocarriers in the development of ultrafine dry powders. Suitable aerodynamic performances for deep lung delivery, together with optimal release profiles (from 50 to 90% over a period of 4 or 5 days, at lung cancer pH), make these types of nano-in-micro formulations ideal for pulmonary delivery. Furthermore, the preliminary *in vivo* results of micronized LbL nanovehicles proved that the developed formulations are adequate for future lung cancer gene therapy through the pulmonary route.

Altogether, the work herein detailed represents a broad skill set for engineering and manufacturing dry powder formulations comprising nanodevices for the diagnosis and treatment of lung cancer.

Keywords: lung cancer, nanotechnology, pulmonary delivery, supercritical carbon dioxide, supercritical assisted spray drying.

.

RESUMO

O cancro do pulmão é o tipo de cancro mais comum e mortal em todo o mundo. Apesar dos avanços clínicos e tecnológicos, a maioria dos pacientes é diagnosticada tardiamente com doença local ou metastizada. Além disso, os tratamentos actuais são ineficientes, uma vez que os agentes terapêuticos não chegam à zona mais profunda do pulmão.

De forma a combater este problema, a combinação da nanotecnologia e engenharia de partículas tem permitido o desenvolvimento de sistemas de inalação eficientes capazes de atingir zonas alvo do pulmão. Assim sendo, nanosistemas multifuncionais que combinem elevadas doses de drogas anti-cancerígenas e ARN interferente silenciador (ARNsi), podem ser administrados de forma eficiente à região do tracto respiratório onde o tumor está confinado, melhorando a eficácia do tratamento e minimizando efeitos secundários adversos. Numa tentativa de desenvolver metodologias sustentáveis para produzir micropartículas respiráveis, combinou-se a atomização assistida por dióxido de carbono supercrítico (SASD), com tecnologias nano e micro. Assim, foram produzidos com sucesso dois tipos de nanosistemas: i) nanopartículas de ouro (AuNPs) funcionalizadas com revestimentos biocompatíveis e fluorescentes (produzidos em $scCO_2$), e com sequências de direccionamento, capazes de atingir e entrar de forma específica nas células do cancro do pulmão; ii) e sistemas de deposição em camada de polielectrólitos (LbL) contendo uma nanocamada de ARNsi para silenciar genes específicos associados com a via genética do cancro do pulmão. Os nossos resultados evidenciam os avanços extraordinários que surgem através da combinação de tecnologia $scCO_2$ em diferentes etapas de processamento, com os nanosistemas multifuncionais, na produção de pós secos ultrafinos. As adequadas características aerodinâmicas dos microsistemas capazes de atingir a zona mais profunda do pulmão, juntamente com os óptimos perfis de libertação dos nanosistemas (de 50 a 90%, por um período de 4 ou 5 dias), tornam estes tipos de formulações nano-em-micro ideais para administração pulmonar. Além disso, os resultados preliminares dos estudos *in vivo* realizados para os pós contendo os nanosistemas de LbL, provam que as formulações desenvolvidas são adequadas para futura terapia génica do cancro do pulmão através da administração pulmonar.

No seu todo, o trabalho constitui um amplo conjunto de ferramentas para a produção o desenvolvimento e produção de formulações para inalação contendo nanosistemas com aplicações no diagnóstico e tratamento de cancro do pulmão.

Palavras-chave: cancro do pulmão, nanotecnologia, libertação pulmonar, dióxido de carbono supercrítico, atomização assistida por dióxido de carbono supercrítico.

DEDICATION

I would like to dedicate this thesis to my parents, the best on earth.

TABLE OF CONTENTS

INDEX OF FIGURES

INDEX OF TABLES

ABBREVIATIONS

^{1}H NMR	Proton nuclear magnetic resonance
ACI	Andersen cascade impactor
AF 488 siRNA	Alexa Fluor 488 siRNA
ALT	Alanine aminotransferase
API	Active pharmaceutical ingredient
AST	Aspartate aminotransferase
Au-MPM	MPM functionalized AuNP
Au-MPM-OA	OA and MPM functionalized AuNP
AuNPs	Gold nanoparticles
Au-OA	AuNP coated with oligoaziridine
Au-OEI-CS	AuNP coated with OEI-CS
Au-OEI-CS-YIGSR	AuNP coated with OEI-CS and grafted with YIGSR
Au-OEtOx-SH	AuNP coated with OEtOx-SH
Au-OEtOx-SH-YIGSR	AuNP coated with OEtOx-SH and grafted with YIGSR
BET	Brunauer emmett teller
$BF_3.OEt_2$	Boron trifluoride etherate
BUN	Blood urine nitrogen
CHT	Chitosan
CLSM	Confocal laser scanning microscopy
COPD	Chronic obstructive pulmonary diseases
CREAT	Creatinine
CROP	Cationic ring-opening polymerization
CTAB	Cetyltrimethylammonioum bromide
d*ae*	Aerodynamic diameter
DLS	Dynamic light scattering
DMEM	Dulbecco's modified eagle's medium
DMF	Dimethylformadide
DMPE	Dimyristoylphosphatidylethanolamine
DP	Dry powders
DPI	Dry powder inhalers
DPPC	Dipalmitoylphosphatidylcholine
DUSA	Dosage unit sampling apparatus
Dv	Volume mean diameter
E%	Entrapment efficiency
ED	Emitted dose
EDX	Energy dispersive X ray spectroscopy
EtOH	Ethanol
FBS	Fetal bovine serum
FDA	Food and drug administration
FPF	Fine particle fraction
FTIR-ATR	Fourier transform infrared-attenuated total reflection

GFP	Green fluorescence protein
GNP	Gold nano probe
GSD	Geometric standard deviation
H&E	Hematoxylin and eosin
HA	Hyaluronic acid
$HAuCl_4.3H_2O$	Tetrachloroauric (III) acid
HD	Hydrodynamic diameter
Hdase	Hyaluronidase
HPLC	High-performance liquid chromatography
ICP	Inductively coupled plasma
ICP-AES	Inductively coupled plasma-atomic emission spectrometer
IR	Infrared
k	Rate constant
K-	Negative control
K+	Positive control
LbL	Layer-by-Layer
LPPS	Large porous particles
Maldi-TOF	Matrix assisted laser desorption ionization – Time of flight
MeOTH	Methanol
MeOPEGMa	PMMA-methoxy(polyethylene glycol)methacrylate
MMAD	Mass median aerodynamic diameter
mPES	Modified polyethersulfone
MPM	Homobifunctional maleimide poly(ethylene glycol)
MSN	Mesoporous silica nanoparticles
MSN_IR-780	IR-780 dye loaded MSN
MTS	3-(4,5-dimethylthiazol-2-yl)-5-(3-carboxymethoxyphenyl) -2-(4-sulfophenyl)-2H-tetrazolium
n	Diffusion exponent
NC siRNA	Silencer Negative Control siRNA (NC siRNA)
NIAD	National Institute of Allergy and Infectious Diseases
NIR	Near-infrared
NSCLC	Non-small cell lung cancer
OA	Oligoaziridine biosensor
OCT	Optimal cutting temperature
OEI-CS	Oligo(ethyleneimine-N-chromylium salt)
OEtOx	Oligo(2-ethyl-2 oxazoline)
OEtOx-OH	Oligo(2-ethyl-2 oxazoline) end capped with water
OEtOx-SH	Oligo(2-ethyl-2 oxazoline) end capped with cysteamine
OOxs	Oligo(2-alkyl-2-oxazolines)
PBS	Phosphate-buffered saline
PDI	Polydispersity Index
Pe	Peclet number
PEG	Poly(ethylene glycol)
PEI	Poly(ethyleneimine)

PGSS	Particles from gas saturated solutions
Pkase	Proteinase K
PLA	Poly-L-arginine
PLGA	Poly (lactic-co-glycol acid)
pMDI	Pressured metered dose inhalers
PMMA	Poly(methyl methacylate)
PMS	(Phenazine methosulfate)
PNAPs	Porous nanoparticle-aggregate particle
PTT	Photothermal therapy
RESS	Rapid expansion of supercritical solutions
ROI	Region of interest
SAS	Supercritical antisolvent
SASD	Supercritical assisted spray drying
$scCO_2$	Supercritical carbon dioxide
SCFs	Supercritical fluids
SCLC	Small cell lung cancer
SEM	Scanning electron microscopy
SFEE	Supercritical fluid extraction of emulsions
siRNA	Small interference ribonucleotide acid
STEM	Scanning TEM
TEM	Transmission electron microscopy
TEOS	Tetraehtyl orthosilicate
TFF	Tangential flow filtration
TGA	Thermal gravimetric analysis
TPCM	Two photon correlation microscopy
UV-Vis	Ultraviolet-visible
Wr%	Percent weight remaining
x	Particle dynamic shape factor
XRD	X-ray power diffraction
YIGSR	Laminin fragment (Cys-Asp-Pro-Gly-Tyr-Ile-Gly-Ser-Arg)
$\rho 0$	Unit density
ρp	Particle mass density

THESIS EVOLUTION

Lung cancer (including both non-small cell lung cancer (NSCLC) and small cell lung cancer (SCLC)) is the most common and leading cause of cancer death in both men and women worldwide. Despite the clinical and technological advances, the majority of the patients are lately diagnosed with either locally advanced or metastatic disease. In fact, only about 14 % of the patients with lung cancer survive for five years, while the rest dies within two years. [1,2]

The main reason for the poor survival rates among the patients with lung cancer is the limited efficiency of traditional treatments.[2] In fact, the efficacy of a treatment mostly depends on the techniques by which the drug is delivered and the optimum concentration to exert an accurate therapeutic effect.[3] The ideal anticancer therapy would involve the local administration of high drug concentration directly to the target tissue for the maximum treatment effect and thus low unwanted side effects.[2,4] Bearing this knowledge in mind, new strategies based on interdisciplinary approaches like polymer science, pharmaceutical technology, bioconjugate chemistry and molecular biology have been fully implemented to generate advanced drug delivery systems. For more than 20 years the potential benefits of nanotechnology have been providing extraordinary improvements in both drug delivery and targeting. In fact, nanotechnology-based therapeutics exhibited several benefits over the unmodified drugs, including improved half-lives, retention, and targeting efficiency, substantially decreasing patient side effects.[3,5] Theranostics (a combination of therapy and diagnosis) is considered the pathway to personalized medicine, which will lead to an entirely new era of healthcare delivery. Nano-based theranostics can offer many benefits for lung disease patients including real time diagnosis of lung inflammatory state and treatment, optimal therapy for individual patients and reduction in adverse drug effects. Therefore, innovative design of nanoparticles will allow for the tailoring of multifunctional airway targeting nanocarriers that allow for the integration of multiple functions, such as cell targeting, ultra-sensitivity imaging and therapy, all into one system. Surface functionalized gold nanoparticles, multifunctional quantum dot conjugated, liposomes and multi-layered assemblies have been extensively exploited to face the urgent need to further develop novel multifunctional nanosystem theragnosis of lung complications.[6–9]

In this context, this work starts by portraying the developed multifunctional theragnostic nanoparticles. There are many types of nanoparticulated systems being explored for lung delivery. In fact, nanoparticle systems can be engineered to exhibit several desirable features for diagnosis and therapy (theragnosis) of specific conditions. Gold nanoparticles (AuNPs), for instance, have been widely investigated as carriers and biosensors for lung cancer treatment.[10] AuNPs display interesting optical, electronic and molecular recognition properties not shown by

bulk gold. They are easily synthetized, reproducible and functionalized to perform specific functions. Actually, several works already described that functionalized AuNPs selectively target lung cancer cells enabling diagnosis and treatment of the disease.[11,12] Nanoparticles functionalization also provides a stealth surface to prevent opsonisation, therefore increasing their residence time and enhancing therapeutics delivery at the accurate site of action. Usually, such protection is performed by hydrophilic polymers like poly(ethylene glycol) (PEG). For imaging purposes, AuNPs are usually tagged with fluorescent probes.[13] However, the well-known plasmon resonance effect depicted by AuNPs usually self-quench these fluorescence coatings. In this concern, the work detailed in CHAPTER 2 aim to the development of robust gold biotags where a convergent strategy using PEG and a fluorescent oligoaziridine compound, produced in supercritical carbon dioxide ($scCO_2$) conditions, successfully resulted in a bilayered fluorescent, and non-quenched, gold nanoprobes (GNP).

As the time evolves, recent reports have been stating that increasing amounts of PEG may lead to undesired hepatic accumulation leading to an inflammatory response triggered by the liver. To overcome such problem, new oligomers (oligo-oxazolines), produced in $scCO_2$, a totally green process, have been widely investigated as PEG substitutes. Such oligo-oxazolines are highly stable, water-soluble, amphiphatic, non-toxic, very flexible and hydrated in water, and have already been used in several biological applications as an alternative to PEG. Moreover, due to the known tumor anatomical abnormalities like the existence of overexpressed receptors on the surface of cancer cells, it is possible to improve nanoparticles selectivity to promote the specific recognition by cancer cells. Hence, structures like antibodies, antibody fragments, small molecules, nucleic acids and peptides, vitamins and carbohydrates have all demonstrated ability to induce nanoparticle-targeting to cancer cells. Such modifications confer not only an additional benefit of sustaining systemic effects, but also the potential to reduce dosing frequency.[14,15] Bearing all this concepts in mind, CHAPTER 3 describes the substitution of both PEG and additional flourescent tagging, by totally "green" oligo-oxazolines produced under $scCO_2$ conditions, resulting in stable, biocompatible and non-quenched POxylated gold nanoparticles. Moreover, these nanoconstructs were further conjugated with a specific peptide sequence, known to bind to overexpressed receptors in the cancer cell line in study, enhancing cellular uptake by these nanosystems. A future conjugation of these nanovehicles with therapeutic drugs is envisaged for effective theragnostic applications.

Local administration of nanotherapeutics to the lungs is the best alternative to improve lung cancer outcomes.[1,2] Hence, the merging of nanotechnology and pulmonary delivery of aerosolizable drugs brings out new and exciting breakthroughs for the diagnosis and therapy of

several types of lung and systemic diseases. Such type of lung delivery is expected to circumvent the lack of effective methods for targeted delivery of therapeutics specifically to lung tissues and cells. However, nanoparticles are in a size range which is not suitable for deep lung delivery as they are easily exhaled or mucociliary cleared out before reaching the underlying epithelia.[9,16] Therefore, the major challenge for pulmonary delivery of nanoparticles is to find a proper carrier system. Prolonging nanoparticles or drugs presence in lung epithelium can be manipulated by using mucoadhesive materials such as the biodegradable polysaccharide chitosan.[17,18] Increased effectiveness of an inhalation treatment may be achieved by the quick dissolution of powder particles in the airway mucus and rapid diffusion to the destination tissue.[19–21] Hence, a novel particulate form incorporating nanoparticles into micro-scale structures has been engineered to overcome the issues of storing and delivering drugs and other biomolecules to the lungs. Micro and nanotechnologies are enabling the design of new materials and methods with enormous impact on medical technology, greatly improving the performance of many existing drugs and enabling the use of entirely new therapies. Full description of nano-in-micro particles engineering for pulmonary delivery can be accessed in CHAPTER 1, where a review of the most sustainable strategies to construct such formulations is given in detail. Targeted therapy of drugs to lungs provides maximum deposition of suitable therapeutic agents at the lung surface, minimizing potential drug side effects and reducing health care costs with increased efficacy.[9]

By bringing all these concepts together, nano-in-micro formulations comprising a chitosan matrix and POxylated gold nanoparticles were efficaciously engineered by using $scCO_2$ methodologies like Supercritical Assisted Spray Drying (SASD) and the work is detailed in CHAPTER 4. Our proof-of-concept systems show ideal characteristics for effective pulmonary delivery and optimal *in vitro* release profiles for lung cancer situation.

Notwithstanding, to achieve the clinical translation promise of this SASD technology, it is critical to adapt not only the carriers but also the materials used to build the nanoconstructs to a broad range of biodegradable and highly biocompatible polymers. Also, the nanosystems should be replaced by the most common and currently FDA approved nanocarriers, which are already accepted for several forms of cancer and can be readily adapted to a number of therapeutic approaches. In such attempt, our POxylated gold nanoparticles were substituted by layer-by-layer (LbL) nanosystems comprising of a mesoporous silica nanoparticles (MSN) core. This type of materials also offer several advantages related to good physical-chemical stability, high loading capacity and controlled and sustained released. Moreover, MSN have been found to be non-toxic, biocompatible and biodegradable [22] (which is an advantage over AuNPs that are

mainly eliminated from the body through urine). The simplicity of LbL has also led to recent and extremely accelerated growth of new drug delivery systems. The ability to incorporate a broad range of therapeutic molecules with meaningful loadings has greatly impaired to this revolution. Cancer therapy has been evolving in a way of minimizing the use of chemotherapeutic drugs.[23] Therefore, combined strategies of anti-cancer drugs with small interference RNA (siRNA) or isolated genetic therapy have been strongly investigated in the recent years and there already numerous successful studies proving the ability of siRNA to specifically silence mutated oncogenes.[24–27] Moreover, due to their unique advantages, combined strategy of LbL with siRNA has already been investigated by some authors with regard to the ability to target gene silencing both *in vitro* and *in vivo* cancer cell lines.[25]

Therefore, CHAPTER 5 describes the extraordinary outcomes that result through the merging of LbL technology with siRNA lung cancer therapy. Moreover, in order to produce particles that can be locally delivery to the lungs through the pulmonary route, LbL siRNA nanoconstructs were micronized into chitosan powders using SASD technology and effective gene silencing of the mutate oncogene was successfully achieve *in vitro*. Finally, the produced powders were administered to healthy mice in order to assess the biodistribution of this novel type of particles. The successful outcomes that resulted from this latest work are truly exciting and provide a potential strategy to deliver siRNA to the lungs and open new insights to effective gene therapy in lung adenocarcinoma situations.

Ultimately, CHAPTER 6 briefly revises all the investigation work developed during this thesis, while evaluating the accomplishment of the major goals of this PhD: i) to development of new biocompatible, biodegradable and targeted nanosystems to be use in theragnosis lung cancer situations; ii) to produce nano-in-micro dry powders formulations with suitable aerodynamic properties and adequate release and degradation profiles, while preserving nanoparticles integrity; and iii) to evaluate *in vivo* powders biodistribution in mice lungs. Future expectations and forthcoming works that can arise from this thesis are also given in this chapter.

THESIS ORGANIZATION AND OUTLINE

Based on the evolution attained during the development of this PhD, this thesis is based on five manuscripts (listed below) that are presented as individual chapters (1 to 5). The first two have already been published (the following two were submitted for publication at the time this thesis was concluded, and the remaining one was being prepared for submission) in peer reviewed international journals, being presented in this thesis mainly as a reproduction of the

published content. The chapters were organized considering the main goals for this PhD work, and are in agreement with the association between the scientific subjects addressed in each one. Each chapter is preceded by a title page containing the reference of the publication, conference attendances (if applicable), and the specific author contributions. Briefly, each chapter includes the following contents:

CHAPTER 1 – A.Sofia Silva, Márcia T.Tavares, Ana Aguiar-Ricardo. 2014. Sustainable strategies for nano-in-micro particle engineering for pulmonary delivery, Journal of Nanoparticle Research, 16:2602-2619.

CHAPTER 2 - A. Sofia Silva, Vasco D. B. Bonifácio, Vivek P. Raje, Paula S. Branco, Paulo F.B. Machado, Ilídio J. Correia and Ana Aguiar-Ricardo. 2015. Design of oligoaziridine-PEG coatings for efficient nanogold cellular biotagging Royal Society of Chemistry Advances, 5: 10733-10738.

CHAPTER 3 - A. Sofia Silva, Marta C. Silva, S P Miguel, Vasco D.B. Bonifácio, Ilídio J. Correia, Ana Aguiar-Ricardo. Nanogold POXylation: Towards always-on fluorescent lung cancer targeting. Submitted manuscript

CHAPTER 4 - A. Sofia Silva, A. M. Sousa, Renato Cabral, Marta C. Silva, S P Miguel, Vasco D.B. Bonifácio, T. Casimiro, Ilídio J. Correia, Ana Aguiar-Ricardo. Aerosolizable gold nano-in-micro dry powder formulations: New prospects for lung cancer theragnosis. Submitted manuscript.

CHAPTER 5 - A.Sofia Silva, Kevin E.Shopsowitz, Santiago Correa, Stephen W. Morton, Erik C. Dreaden, Teresa Casimiro, Ana Aguiar-Ricardo, Paula T. Hammond. Micronized Layer-by-Layer nanovehicles for siRNA pulmonary delivery: A novel approach for lung cancer therapy. Manuscript in preparation

CHAPTER 6 – Final overview, concluding remarks and future prospects.
This chapter provides an overall summary of the subjects addressed in the five chapters, highlighting the main results and conclusions achieved along the PhD thesis. Future prospects are also presented.

All chapters were formatted using a unique style of references being cited by sequential numbers and listed in the References section. Finally, appendixes relative to each chapter are also compiled in a single section at the end of this thesis named Appendix.

CHAPTER 1. Sustainable strategies for nano-in-micro particle engineering for pulmonary delivery

This chapter corresponds to the contents (with minor changes) of the following publication:

2014, Journal of Nanoparticle Research, 16:2602-2619

A.Sofia Silva, Márcia T.Tavares, Ana Aguiar-Ricardo

Sustainable strategies for nano-in-micro particle engineering for pulmonary delivery

Keywords: inhalation; pulmonary delivery; dry powders; nano-in-micro particles; spray drying; supercritical-assisted atomization

Personal contribution

A. Sofia Silva contributed to the design of the study, and wrote the majority of the manuscript.

1.1. ABSTRACT

With the increasing popularity and refinement of inhalation therapy, there has been a huge demand for the design and development of fine-tuned inhalable drug particles capable of assuring an efficient delivery to the lungs with optimal therapeutic outcomes. To cope with this demand, novel particle technologies have arisen over the last decade agreeing with the progress of pulmonary therapeutics that were commonly given by injection. Nanotechnology holds a considerable potential in the development of new release mechanisms of active ingredients to the deep lungs. For an accurate deep lung deposition and effective delivery of nanoparticles, respirable nano-in-micro formulations have been extensively investigated. Microparticles with nanoscale features can now be developed and their functionalities have contributed to stabilize and improve the efficacy of the particulated dosage form. This chapter reviews the different types of the aerosolizable nano-in-micro particles, as well as their sustainable production and characterization processes as dry powders. This review also intends to provide a critical insight of the current goals and technologies of particle engineering for the development of pulmonary drug delivery systems with a special emphasis on nano-micro dry powder formulations prepared by spray drying and supercritical fluid assisted techniques. The merits and limitations of these technologies are debated with reference to their application to specific drug and/or excipient materials. Finally, a list of most recent/ongoing clinical trials regarding pulmonary delivery of this type of formulation is described.

1.2. INTRODUCTION

In the last decade, investigation on the interactions between nanoparticles and lung tissue has been strengthened, specifically in terms of potential health risk of particle inhalation. Notwithstanding, the huge advances in the nanotech field also brought new insights for novel delivery strategies, diagnosis and therapeutic approaches through the inhalative route.[28] With rapid advances in nanotechnology, the use of drug nanoparticles has become a subject of a very active research, and it has triggered the interest in the lungs as a major route of drug delivery for both systemic and local treatment.[16] Nanoparticles have been foreseen as an efficient way to develop controlled release delivery systems for the lungs. There are many types of nanoparticulated systems being explored for lung delivery. In fact, nanoparticle systems can be engineered to exhibit several desirable features for diagnosis and therapy (theragnosis) of specific conditions. Despite their ability to protect therapeutics at both extracellular and intracellular levels and then release them in a sustained and controlled manner, they are still able to penetrate into deep tissue and then suffer cellular uptake, due to their nanometric scale. Nanoparticles functionalization also

provides a stealth surface to prevent opsonisation, therefore increasing their residence time and enhancing therapeutics delivery at the accurate site of action. Nano-based theranostics offer a pathway for personalized medicine allowing real time diagnosis of lung inflammatory state and carrying the optimal therapy for individual patients with reduction of the undesirable drug side effects. Innovative design of nanoparticles allows for the assimilation of several functions, such as cell targeting, ultra-sensitivity imaging and therapy, all into one system. Surface functionalized gold nanoparticles (AuNPs), multifunctional quantum dot conjugated, liposomes and multilayered assemblies have been extensively exploited to face the urgent need to further develop novel multifunctional nanosystem theragnosis of lung complications.[6–9] The combination of nanotechnology and the pulmonary route for administration of aerosolizable drugs brings out new and exciting breakthroughs for the diagnosis and therapy of several types of lung and systemic diseases. Such type of delivery to the lung (air-to-lung) and via the lung (air-to-blood) can circumvent the lack of effective methods via other routes of administration. However, nanoparticles are in a size range which is not suitable for deep lung delivery and be easily exhaled or mucociliary cleared out before reaching the underlying epithelia.[9,16] Moreover, nanoparticles' nature poses noteworthy challenges in powders development. Their increased surface area results in high Gibbs free energy, which may lead to particles agglomeration and consequent formulation instability. Therefore, the major challenge for pulmonary delivery of nanoparticles is to find a proper carrier system. Increased effectiveness of an inhalation treatment may be achieved by the quick dissolution of powder particles in the airway mucus and rapid diffusion to the destination tissue. Hence, a novel particulate form incorporating nanoparticles into microscale structures has been engineered to overcome the issues of storing and delivering the drugs and other biomolecules to the lungs. Aerosols for inhalation therapies may be produced by pneumatic or ultrasonic nebulizers, pressured metered dose inhalers (pMDI) and dry powder inhalers (DPI).[18] From all the formulations available for inhalation, dry powders are usually preferred as they exhibit the most suitable behavior for pulmonary delivery such as stability and bioavailability of active ingredients, when compared to their aqueous counterparts.[29,30] Moreover, storage and distribution in a cool-chain are not necessary as the usage of a DPI provides longer storage stability to the powders therein.[21] In DPI formulations, drug nanoparticles have been blended with carrier materials, producing nano-in-micro formulations like Trojan and Strawberry particles or particles with nanofeatures. In DPI, the lower density of such nanoparticles agglomerates results in smaller mass median aerodynamic diameter (MMAD) and consequently, increases lung deposition and powder flowability. Moreover, nanoparticles in inhaled therapeutics have also been demonstrating an increased residence time in the lung muco adhesive surfaces and reduced mucociliary clearance.[31]

Although microparticles can be manufactured by many different processing methods, this review focuses mainly on spray drying and supercritical fluids technology in the production of totally 'green' dry powders formulations. Wet chemistry, phase separation processes and other drying methods such as spray freeze drying, have also been widely used for particle engineering purposes and have already been reviewed elsewhere.[32,33]

1.2.1. The lung as a delivery target for nanomaterials: nano-delivery via aerosol

Lungs, skin and intestinal tract are in direct contact with the environment. Therefore, these organs are likely to be a first port of entry for nanomaterials into the body. In fact, epidemiological studies regarding the exposure of the body to atmospheric particles showed a positive correlation between the increase of such contact and the short-term increase in morbidity and mortality.[34,35] Since inhalation is by far, the most significant exposure route for air-borne nanoparticles, the number of studies regarding on nanoparticles deposition along the respiratory tract has been increasing. Bearing this knowledge in mind, the systemic administration of proteins or other macromolecules is being surpassed by the delivery of such molecules through the pulmonary inhalation route.[16,31,36–41] Actually, needle-free drug delivery systems have been receiving increased attention as a noninvasive alternative owing to the unique physiological features of the lungs.[42] Ones are characterized by large absorptive surface area (> 100 m^2), thin blood-barrier membrane (0.1 - 0.2 μm), elevated vascularization and low enzymatic activity which, together, facilitate macromolecule transport into systemic circulation, leading to very rapid action and high bioavailability. Furthermore, drug and other molecules delivery through lungs are not subjected to hepatic first pass-effect.[16,29,31,36,43] Moreover, the favorable physiological environment of the deep lungs, such as physiological pH and reduced mucociliary action, overcomes many problems of other non-invasive vaccine targets, like rapid clearance, poor absorption, exposure to digestive enzymes and the antigenic tolerance.[43] So far, several protein based drugs, such as insulin, human growth hormone, calcitonin and deslorelin, have been reported to reach the systemic circulation following aerosol administration. Hence, pulmonary delivery holds a great potential for the treatment of several respiratory diseases like asthma, tuberculosis, influenza, cystic fibrosis, Chronic Obstructive Pulmonary Diseases (COPD) and lung cancer. Actually, recent studies regarding cancer immunotherapy using genetically engineering T-cells to target cancer cells have shown remarkable results. With more people living beyond age 65, cancer's incidence is projected to rise even more in the coming years. Therefore, the population who might benefit from immunotherapy is potentially quite large. By combining this knowledge with pulmonary delivery, extraordinary outcomes may arise. First pass metabo-

lism may be avoided and cancer, especially non-small lung cancer (one of the leading cause of death worldwide) may be effectively treated.[44]

Localized drug delivery shows a great promise not only in the treatment of such diseases but also reduces the systemic toxicity.[40] Although advantageous, efficient pulmonary delivery and effective delivery of biologic drugs inside cells of the deep lung are also very challenging missions.[16] In fact, particle deposition and retention in the different pulmonary stages are determined by three main factors: respiratory tract anatomy, breathing pattern and droplet/particle size.[28] Though some conflicts regarding the range for optimal aerodynamic diameter (d_{ae}) to efficiently reach the deep lungs may exist, the most recent works state that the aerodynamic diameter of aerosol particles should be between 0.5 and 5 μm. Smaller particles may fail to deposit and are exhaled, whereas bigger ones may accumulate in the mouth and throat.[16,37,45] Moreover, smaller particles are more likely phagocytized and have the tendency to aggregate due to van der Waals and electrostatic forces[19] making large porous particles with low density suitable for lung delivery.[46] When the MMAD is more than 5 μm, inertial impaction exists in the oropharynx and large conducting airways, while the smaller airways are reached when the aerodynamic diameter is smaller than 5 μm.[32,47] Table 1.1 describes the mechanism of dry powder deposition along the respiratory tract.

Table 1.1-Mechanism of aerosol deposition.[32,47]

Site		**Particle size**	**Mechanism**
Large conducting airways		>5 μm	Inertial impaction
Respirable airways	Smaller airways	3-5 μm	Deposition
	Alveolar airspaces	1-2 μm	Deposition
		<0.5 μm	Exhalation

However, drugs and other biomolecules that are targeted to intracellular machinery, generally require nanocarriers to improve mucus diffusion and cellular uptake by the epithelial cells. These paradoxical requisites turn complex the development of an efficient carrier system: the particles should comprise sizes between 0.5 and 5 μm during the inhalation, then swell and increase their size upon depositing onto the lung, evade the macrophage clearance in the deep lung and enable the release of smaller particles that penetrate lung mucus and epithelial lining and deliver drugs, proteins or other biomolecules intracellularly, minimizing nonspecific side

effect to the healthy tissue, as displayed in Figure 1.1.[37,48] For suitable cellular internalization nanoparticles should not exhibit sizes larger than 150 nm.[49] Notwithstanding, particles comprising sizes ranging between 20 to 50 nm have shown to have higher cellular internalization.[50,51] Moreover, it has already been proved that if smaller nanoparticles (hydrodynamic diameter (HD) less than ≈ 34 nm and a noncationic surface charge) are used, specifically in pulmonary delivery, nanoparticles can rapidly translocate from the lung epithelium to mediastinal lymph nodes. This should provide high levels of drug to pulmonary lymph nodes, which could be used to deliver antibiotics and anti-inflammatory drugs to treat other lung infections, tumor metastases and inflammatory conditions.[45]

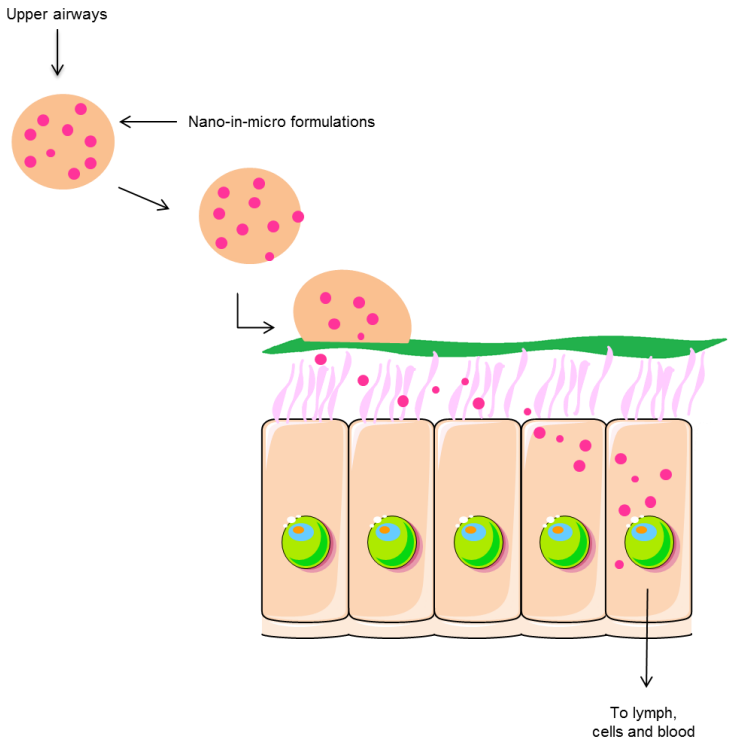

Figure 1.1-Mechanism of nanoparticle delivery through aerosol of nano-in-micro formulations - once in the lung epithelia, microcarriers must readily dissociate into the primary nanoparticles in an aqueous medium without significant destruction of the delivery advantages associated with the nanoparticulate systems. Then, nanocarriers may travel to their site of action, due to specific targeting exhibited in nanoparticles surface, and exert their theragnosis effect.

1.2.2. Devices for pulmonary inhalation – Dry powder inhalers

Lung delivery of nano-in-micro formulations may rely on either dry solid particles as in DPIs, suspensions of nanoparticles as in nebulizers and pMDIs, or the formation of

nanodroplets from solution.[31,52] Table 1.2 shows a comparison between the different types of existing inhalers.

Pulmonary drug delivery of controlled release formulations may provide an effective approach to orally deliver antibiotics for clearing persistent lung infections.

Table 1.2-Different types of inhalers: advantages and disadvantages.[53–55]

Type of inhaler	Advantages	Disadvantages
Nebulizers	Alveolar deposition can be easily achieved	Limited portability Difficult to use
pMDI	Easy portable Tamper Proof Multidose	Difficult to use Use of propellants
DPI	Propellant-free Easy to use Formulation stability	Complex development and manufacture Dose uniformity problems

Although the general reviews do allude to the use of different inhaler devices, we here narrow the focus to the recent studies regarding DPIs. For the sake of simplicity, the term nanoparticles will be used to cover either solid nanoparticles, or other biomolecules at the nanoscale. Thus, the term 'nano' refers to all particulates, droplets or solid particles for which at least one dimension is 1-1000 nm. DPIs are at the forefront in the pulmonary delivery technology. They overcome problems such as desynchronized dose discharge during the inhalation process as they are breath actuated.[30,56] DPIs are also suitable for delivering a broad range of drugs than pMDIs (which used to be the leading application form of inhalation but were surpassed by DPIs as they require difficult hand–lung coordination by the patient and use environmentally damaging CFC propellants). Moreover, DPIs can deliver a range of doses from less than 10 μg to more than 20 mg via a single inhalation.[56] Besides listing the marketed nebulizers and pMDIs, Table 1.3 also displays several types of DPIs that can be classified as "single-dose" devices, where a single dose is provided in a capsule; "multiple unit dose" devices, which contains a small amount of doses in capsules or blisters; or "multidose" devices; where the powder is stored in a reservoir and the doses are metered.[56,57] The working principle of a DPI is to deliver a pre-

scribed dose of powder aerosol into air inhaled by the patient during a single breath in a process designated ‘fluidization’, preventing the powder from air ambient exposure. The vast majorities of fine drug particles are micronized drug blended with large carrier particles which enhance flow, reduce aggregation, and assist in dispersion.[40] Pharmaceutical products to be used in the DPI may result in high local levels of drug in epithelial fluid of the airways and lower respiratory tract.[36] However, the application of drug nanoparticles for pulmonary delivery in DPIs is not straightforward, as it was already explained, since the direct inhalation of drug nanoparticles is not viable due to their easy aggregation. To overcome this problem, spray drying and, more recently, supercritical fluid-assisted atomization techniques have been used to manufacture large composite porous particles or hollow particles composed of nanoparticles aggregates, to be then delivered to the lungs using DPIs.[16]

Table 1.3-Examples of marketed inhalers. [58,59]

Type of inhaler							
Nebulizers		*pMDI*			*DPI*		
		Press-and-breath products		**Breath-actuated products**	**Single Dose**	**Multiple Unit Dose**	**Multidose**
		Bronchodilators	Steroids				
Atrovent	Flixotide	Maxair®	Beclazone™	AeroBec™ 100 Autohaler	Spinhaler®	Diskhaler®	Turbuhaler®
Duovent	Lomudal	Proventil®	Beclovent®	Beclazone™ 100	Rotahaler®	Diskus®	Easyhaler®
Duo-Medihaler		Sultanol	Becotide ™ 100	Maxair ™ Autohaler™	Aerolizer™	Aerohaler®	Novolizer®
Ventolin		Ventolin®	Flixotide™	QVAR ™ Autohaler™	Inhalator®	Flowcaps®	Clickhaler®
Pulmicort			Pulmicort		Eclipse	MicroDose DPI	Pulvinal®
Bisolvon					Turbospin	Delsys DPI	Ultrahaler®
Beclojet					AIRTM Inhaler	Technohaler®	Taifun®

1.2.3. Particle engineering

1.2.3.1. Spray drying technique

Spray drying technique has been extensively applied in the production of dry powder formulations due to its simplicity, scale-up, ease of operation and the ability to produce composite materials. In 2010 spray drying was considered as one of the most interesting technologies used in the pharmaceutical field.[60] Appealing to this technology, powders/particles properties such as size, morphology, density and level of residual solvent, can be manipulated. This remarkable feature has led to its application in the formulation of a wide variety of powders or advanced solid forms. A wide range of products may be obtained, mainly: very fine powders for inhalation to large particles for direct compression, solid dispersions for enhanced bioavailability and microcapsules for drug shelter and/or controlled release.[60] However, spray dryers scale up have to be strategically designed so that the quality of the resultant materials is maintained and no considerable and expensive losses are exhibited.[60,61] Spray drying technology is a one step process that comprises the atomization of the feed solution into a spray. The solvent in the atomized droplet is thermally removed in the spray drying chamber leading to the particles drying, which are then separated from the air through a cyclone or a filter bag. Typically, polymeric or lipid-based materials are used as carriers to prepare drug loaded nanoparticles in the form of suspension, followed by spray drying under specific conditions in order to form large porous nanoparticle aggregates with spherical geometry and rough surfaces. However, such technique has some disadvantages including the possible degradation of heat sensitive fine particles and inefficient yields.[31,32,40,56,62–66] Spray drying technique has been employed for decades in the manufacture of drug microparticles for inhalation therapy. Recently, Jun and colleagues produced micron-sized spherical agglomerates of pure sodium cromoglicate to improve aerosolization performance in dry powder inhalers. Such achievement was accomplished using combined technologies as liquid anti-solvent precipitation followed by instant agglomeration of nanoparticles into porous spherical microparticles by spray drying technique. The authors were able to increase in 50 % in vitro aerosol deposition in comparison with the control samples.[16,67]

1.2.3.2. Supercritical fluid assisted processes

Supercritical fluid assisted processes have lately emerged as green and innovative alternatives for a wide variety of processes such as: solubility enhancement of poorly soluble drugs, plasticization of polymers, surface modification, nanosizing and nanocrystal adjustment, and

chromatographic extraction. An increasing interest regarding this research area has been triggered by the numerous advantages that this technology offers over the conventional methods.[68] Supercritical fluids (SCFs) are defined as compressed gases or liquids above their critical pressures and temperatures. SCFs possess central advantages as solvents or antisolvents for pharmaceutical manufacturing. Due to its low critical temperature (31.1 °C), moderate pressure (7.38 MPa), inert and environmentally friendly nature, non-flammability and low cost, carbon dioxide is the most used fluid under supercritical conditions ($scCO_2$) for pharmaceutical approaches. One of the most extraordinary properties of $scCO_2$ in processing nanoparticles is its tunable solvent power that facilitates the extraction and separation of organic solvents allowing the production of pure and dry particles or as a pure aqueous suspension, while enabling a clean and recyclable precipitation process at very low temperatures. Due to these extensive properties, applications using SCFs, particularly CO_2, have been extensively investigated for respiratory delivery applications.[31,36] There were two main conventional methods for obtaining microparticles using $scCO_2$: the Rapid Expansion of Supercritical Solutions (RESS), where the solid material is dissolved in CO_2 under supercritical conditions, and then the solution is rapidly expanded by lowering the pressure, promoting a rapid cooling rate and inducing supersaturation leading to microparticle formation;[68–72] and supercritical antisolvent (SAS), where particles are produced when a solution is brought into contact with $scCO_2$ in a semi-continuous method. This process has the advantage of controlling the physical form of powders by varying the working conditions of temperature, pressure or solution flow rate. However, solvents used in this method must be completely miscible in $scCO_2$, which may pose a problem when aqueous solvents are used since water is not miscible with $scCO_2$.[32,56,68,72,73] Particles from Gas Saturated Solutions (PGSS) is a $scCO_2$ - assisted process based in two main steps, the first being the saturation of a solute-containing solution with CO_2 in a static mixer, and the second one the mixture's expansion through a nozzle into a spray tower. The CO_2 expansion from the resulting droplets leads to an atomization, which also happens due to the fast temperature and pressure reduction (Joule-Thomson effect).[74,75] Particle formation via polymerization-induced phase separation (PIPS) is a process that produces particles by means of a synthesis in a supercritical fluid medium, such as polymerization.[76] Moreover, Supercritical Fluid Extraction of Emulsions (SFEE) uses $scCO_2$ to extract the organic phase out of emulsions. Each emulsion droplet allow precipitation, encapsulation or blending resulting in uniform particles.[32] More recently, the supercritical-assisted spray drying (SASD), a process based on the solubilisation of controlled quantities of CO_2 into the liquid solution has proved to have many advantages over conventional methods. It offers the possibility of operating in a continuous mode in mild operating conditions and the ability to use both organic and inorganic solvents while providing a good control over particle size and distri-

bution.[77–80] Table 1.4 displays the advantages and disadvantages of spray drying technique and supercritical CO_2 - assisted processes.

Table 1.4-Spray drying vs $scCO_2$.[31,81]

Technique	Advantages	Disadvantages
Spray-drying	Furthest optimized On-step process to produce dry powder Control of particles' properties Potential for producing antigenic nanoparticles in-line with the aerosols	Production of a broad size distribution Possible degradation of heat sensitive drugs Inefficient yields
Supercritical CO_2 - assisted processes	Use of mild conditions Efficient solvent extraction Clean and environmentally friendly Benefic physical properties of the supercritical fluids Narrow particle distribution High yields Produces successful drug nanoparticles	Expensive equipment High critical pressure High pressure and associated hazards

1.2.4. Design of nano-in-micro dry powder formulations

As already mentioned, nanoparticles are unique carrier platforms of proteins and other macromolecules for pulmonary delivery due to their capacity to penetrate into intracellular compartments and the possibility of avoiding macrophages' phagocytosis from increasing the carrier's residence time in the lung therefore allowing a sustained drug release.[29,82]

For DPI formulation, nanoparticles have been designed to reduce the interparticle attraction forces and to improve the DPI blending with carrier materials, forming Trojan, strawberry and nanoparticles aggregates (particles with nano-features).[52] To be therapeutically effective, microparticles must readily dissociate into the primary nanoparticles in an aqueous medium without significant destruction on the delivery advantages associated with the nanoparticulate systems.[19] Inhalable powders have to fulfill certain requirements; the increase of the respirable fraction with a decreasing average particle diameter is a fundamental matter of fact.[20] The general assumption is that particles smaller than 5 µm are not deposited in the upper airways but are able to penetrate into the lung. Systemically effective drugs which have to attain the alveoli, should even have a mass median aerodynamic diameter of less than 2 µm.[21] To overcome these issues, the nanoparticles can be microencapsulated in order to improve their aerodynamic properties and stability and so, produce suitable lung delivery particles. Table 1.5 and Figure 1.2 display the most promising nano-in-microparticles already developed.

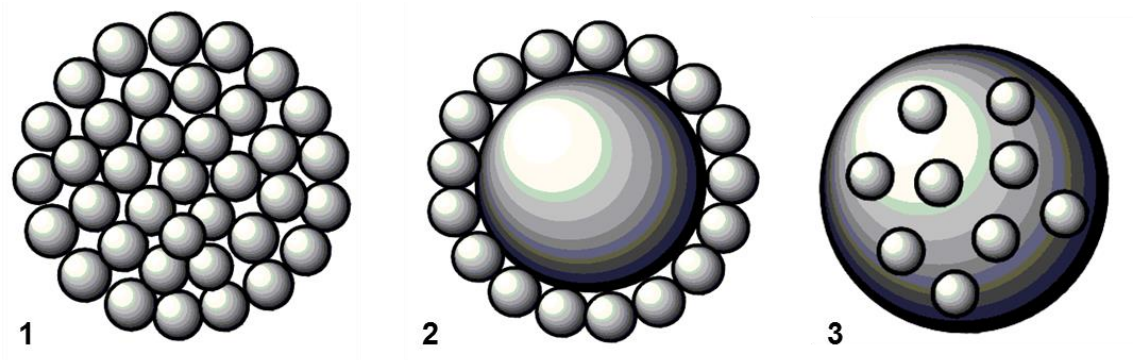

Figure 1.2-Nanoparticle-based dry powders for inhalation: 1 – Trojan particles; 2 – Strawberry particles; 3 – Particles with nanofeatures.

Table 1.5-Nano-in-micro formulations

Process	Type	Drug	Excipients	Particle size (µm)
Spray-drying	Trojan Particles	n.a.	DPPC-DMPE-lactose	4-8[83]
		Rifampicin	PLGA/L-leucine	4.2[84]
		Octreotide acetate	n.a.	5.7[85]
	Particles with nanofeatures	Human IgG	PLGA/lactose	4.2[86]
		Clarythromycin	PLGA/L-Leucine	5.3-8.9[87]
		Thymopentin	Mannitol/L-Leucine	4.1[19]
	Strawberry Particles	β-galactosidase	Lactose	226[88]
Supercritical CO_2	Particles with nanofeatures	Magnetite nanoparticles	PMMA/PLGA	0.97-1.55[89]
		Terbutaline sulphate	Lactose	3.2 – 3.4[90]
		Deslorelin-HPβCD	PLGA	2.2/ 13.8[91]
		pDNA	Chitosan	12.2-13.2[92]
		Lysozyme; Doxorubicin	PLGA	2.17-18.2[46]

n.a. – not available

1.2.4.1 Trojan particles

Trojan particles are micron-sized Large Porous Particles (LPPS) that get deposit in the lungs thanks to their aerosolization and physical properties and then dissociate to the primary nanoparticles, avoiding phagocytosis and taking advantage of its drug delivery properties. Tsapis and coworkers produced large porous nanoparticles composed of dipalmitoylphosphatidylcholine (DPPC), dimyristoylphosphatidylethanolamine (DMPE) and lactose using spray drying, which allows the control of the drying time of the droplet avoiding nanoparticle diffusion. By measuring the geometric and aerodynamic diameter they noticed that the LPPs properties and the Fine Particle Fraction (FPF) improved when the nanoparticles were encapsulated.[83]

Sung and coworkers formulated a dry powder for the treatment of tuberculosis by encapsulating rifampicin in PLGA nanoparticles and then spray dried into porous nanoparticle-aggregate particle (PNAPs) with L-leucine. Experiments showed that the particles have both systemic deliver and long levels of drug for up to eight hours.[84]

More recently, the spray freeze drying method was used to produce PNAPs containing a model peptide, octreotide acetate. When peptides are used in the process, temperature becomes a concern, which made this group to deviate from the conventional spray drying process to keep the model peptide active. The *in vivo* experiments showed higher levels of plasma aspartate amino-transferase when in comparison with delivery through subcutaneous injection. To improve the encapsulation efficacy and the drug loading, hydrophobic ion pair complexes was used.[85] Some examples of scanning electron microscopy (SEM) images of Trojan microparticles are depicted in Figure 1.3.

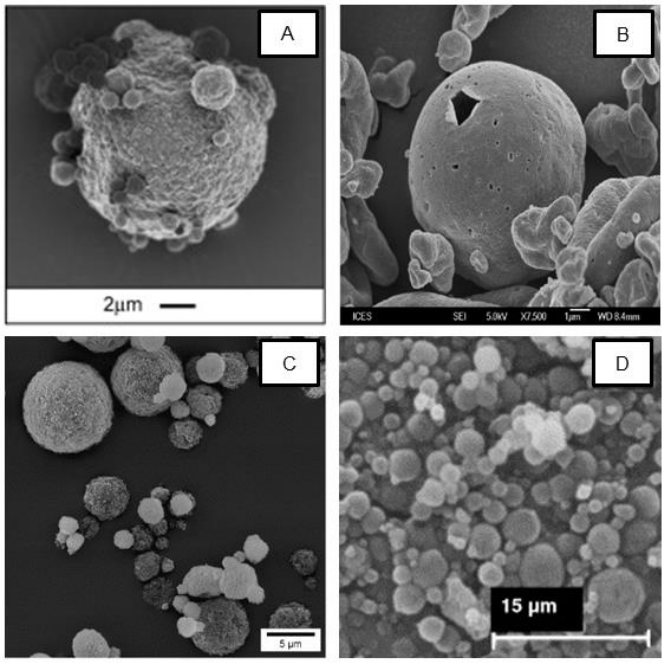

Figure 1.3-SEM pictures of a representative panel of Trojan microparticles reported in literature: A) Reproduced with the permission of Elsevier:[93] spray dried microparticles prepared with DPPC, hyaluronic acid (HA) and PLGA nanoparticles; B) Reproduced with the permission of Elsevier:[94] spray dried microparticles prepared with DPPC and PMMA-methoxy(polyethylene glycol)methacrylate (MeOPEG-Ma) nanoparticles; C) Reproduced with the permission of Elsevier:[29] spray dried microparticles prepared with mannitol and chitosan/TPP nanoparticles; D) Reproduced with the permission of Elsevier:[95] microparticles prepared with colloidal silicon dioxide as drying auxiliary and oily-core PCL nanocapsules.

1.2.4.2 Particles with nanofeatures

Even though Trojan particles have shown some success, there are some drawbacks when it comes to the preservation of the particles integrity and their aerodynamic properties due to drying process of the NPs suspension. Another type of particles produced are the nano-embedded microparticles that consist of micro-encapsulated drug-loaded NPs, which excipient is degraded when they reach the deep lung, releasing the nanoparticles.[82]

Lately, polymeric nanoparticles production has been growing once its effectiveness in sustained release and high drug capacity has been shown. One of the most used polymers is PLGA (polylactil-glycol acid) because of its biodegrability and biocompability, and also for its long clinical evidence.[96] Besides, it is used in a host of Food and Drug Administration (FDA)-approved therapeutic devices and has a long safety record.[97] Another common polymer is chitosan, a polysaccharide biopolymer which has a high interest due to its low toxicity, biocompability, biodegradability and mucoadhesive properties.[29,98] As for the inert excipients, sugars are the most used ones, such as lactose and mannitol, because of the stability they provide for the

spray dried particles.[99] Mannitol is said to be advantageous comparing to lactose because it has less hygroscopicity, no reducing effect and it is also nontoxic.[19,98] On the other hand, lactose is the only FDA-approved sugar carrier for dry powder aerosol formulations.[100] Some nano-in-microparticles were developed by co-spray-drying the nanoparticles with bulking agents and dispersibility enhancers, such as L-leucine, a nontoxic and nonirritant amino acid, known to improve flowability and dispersibility.[101,102] For instance, Kaye and colleagues produced nano-in-micro particles aimed for antibody delivery in the lungs by SIMANIM (Simultaneously Manufactured Nano-in-Micro).[86] A double-emulsion containing human IgG, lactose, PLGA and DPPC was spray-dried, leading to lactose microparticles loaded with PLGA nanoparticles, where the antibody was released for 35 days in a pH 2.5 media and was stable and active. With the addition of L-leucine the fine particle fraction improved from 37 % to 52 %, which was also concluded by Moghaddam and co-workers that spray-dried Clarythromycin-encapsulated PLGA nanoparticles with L-leucine to treat lung infections such as pseudomonas aeruginosa.[87] The resulting micro-carriers had diameters between 5.3 to 8.9 μm and the presence of L-leucine showed improvements in yield and in FPF since it reduced the particles cohesiveness. Li and coworkers produced thymopentin-loaded solid lipid nanoparticles encapsulated in mannitol/leucine microparticles. From *in vitro* and *in vivo* studies it was shown that the mannitol provided protection to the peptide, which had a strong therapeutic effect, since the layer formed around the nanoparticles avoids lipids coalescence. Also the moisture sorption and surface tension diminished thanks to the presence of L-leucine.[19]

Al-Qadi and colleagues developed microencapsulated chitosan nanoparticles for pulmonary protein delivery, by co-spray-drying them with mannitol. The resulting microspheres have a mean diameter of 2.5 and 2.8 μm and quantitive analyses of hypoglycemic effect and lung distribution studies showed that this delivery system gets to the deep lung and releases insulin in its bioactive form.[29] Even though spray-drying is the conventional technique to produce dry powders, the use of supercritical CO_2 has been growing over the years. An example is the supercritical antisolvent technique, used by Chattopadhyay and collaborators to coprecipitate poly(methyl methacylate) (PMMA), PLGA and Eudragit RS with a suspension of magnetite nanoparticles. This magnetic property of the particles allows a specific targeting due to the attractive forces with the magnetic field applied to the target site. It was observed a slight difference in morphology when the magnetite nanoparticles were added because the particles showed a roughened surface.[89]

1.2.4.3 Strawberry particles

This particle designation first appeared during the 2005 Aerosol Society meeting and it is associated with micro-carriers coated with active nanoparticles connected via physical absorption.[52] This formulation is advantageous because the use of micronized drug blended with larger carrier helps flow and prevents aggregation.[53] Once the coated nanoparticles work as spacers between the microparticles, the adhesion between them is diminished, making the handling easier. The coating process can be done by electrostatic forces, where the different size particles have opposite charges, avoiding aggregation between themselves and only with each other.[103] There are also capillary and van der Waals forces and mechanical interlocking responsible for particle-particle and particle-surface interactions. Usually, lactose particles are the chosen carrier because, besides all the advantages already mentioned, their large size, when the airflow is introduced, allow the generation of primary drug particles that can then be carried until the deep lungs while the carrier impacts in the oropharynx and is cleared.[20,53] It is also possible to nano-coat proteins in micro-carriers using an ultrasound technique. Genina and associates used β-galactosidase and lactose to produce appropriated pharmaceutical formulations for lactose intolerant patients and measured the proteins quantity in the surface by its enzymatic reaction product, D-galactose, with results between 0.2 and 5.7 mg/g of lactose.[88]

1.2.5. Characterization of inhaled particles

Upon testing a formulation for future lung delivery there are several parameters that should be confirmed, such as its safety, efficacy and quality.[104] To address these features, there are specific characterizations that need to be carefully addressed. In this review, the most important evaluations are described. One of the most important features is the particle size diameter, which must be known to evaluate the aerodynamic diameter (d_{ae}). The d_{ae} of a particle is defined as 'the diameter of a sphere with an unit density that has the same terminal settling velocity in still air as the particle in consideration' and is represented by the following equation:

$$d_{ae} = d_{geo}\sqrt{\frac{\rho_p}{\rho_o x}} \qquad \text{Equation 1.1}$$

where ρ_p is the particle mass density, ρ_o is the unit density and x, the particle dynamic shape factor. Such factor is also defined as the ratio of the drag force of the particle to that of a sphere of equivalent volume. From this equation it is possible to verify that the $d_{ae.}$ can be reduced by decreasing particle size or density, or by increasing the dynamic shape factor.[58] Both size and distribution can be determined with the use of automated microscopy and image analy-

sis and methods that use geometric features and physicochemical properties.[53,101] In the other hand, by means of an *in vitro* aerosolization study using a multistage cascade impactor, it is possible to obtain the MMAD, which is determined as the particle diameter corresponding to 50 % of the cumulative distribution and to find the fraction of emitted dose (ED%) that reach the deep lung. The fine particle fraction is the mass of particles under a certain cut-off diameter, usually around 5 μm, with reference to the emitted dose, i.e the particles proportion to exit the inhaler and which can also be determined using a Dosage Unit Sampling Apparatus (DUSA).[6,32]

The selection of the optimal solid form is a crucial aspect upon the development of pharmaceutical compounds, due to their ability to exist in more than one form or crystal structure (polymorphism). These polymorphs show different physical properties which affect their biopharmaceutical properties.[104] Solid state analyses are often used to guarantee both safety and efficacy of drugs or pharmaceutical compounds and to validate the control of the pharmaceutical manufacture process.[105] X-ray power diffraction (XRD) is one of the most used techniques to attest the solid state of a formulation and it is used to define the intermolecular spacing of the unit cell, which defines a crystalline system. For lung delivery applications, it is important to have an amorphous carrier, not only for storage proposes, but because it also increases dissolution rate and it has high water adsorption capacity. In the other hand, the Active Pharmaceutical Ingredient (API) is usually preferred in a crystalline form, since it maintains the bioavailablility of the drug, maximizing its efficiency and minimizing the required dosage.[20,32,53,106]

The dry powders' properties and performance in the lungs can be determined by *in vitro* studies that can match the regulatory body criteria, even though *in vivo* events such as lung deposition and pulmonary pharmacokinetics are difficult to experimentally test. The *in vitro* experiments for inhalation particles use lung epithelial cell models which have the advantages of being simpler, more controllable and cheaper than the *in vivo* approach. The main goal is to determine the transepithelial transport kinetics of test molecules in order to compare it with *in vivo* lung absorption.[107] However, cell cultures used in *in vitro* studies do not provide an accurate correlation with *in vivo* absorption and also present limitations in absorption kinetic studies, making *ex vivo* studies preferable since, despite the limitations, they can reproduce the kinetics region of the lung-region absorption. Moreover, *ex vivo* models allow for a complete study of most of cell types involved in the lung tissue.[108] Isolated perfused lung model, where the lung is outside the body, is commonly used as an *ex vivo* model. Even though the environment is artificial, the lung tissue keeps its architecture and functionality. The organ is maintained at a specific temperature and pressure and it is pumped with perfusate while the drug is delivered by the tracheal port. In order to obtain the rate of absorption the perfusate is sampled.[107,108] Notwith-

standing, *in vivo* methods enables the direct acquisition of pharmacokinetic data from lung tissue of live animals, usually small rodents, even though in this type of study, larger animals such as dogs, sheep or monkeys are more appropriate.[107] Gamma scintigraphy is an *in vivo* non-invasive imaging technique that uses radiopharmaceuticals that localize in different organs and are visualized in a gamma camera to determine drug delivery precisely, by giving a measurement of the local bioavailability through the lung. The results obtained are an accurate percentage of the delivered dose and also a specific rate and extent of the drug's action.[31,57]

1.3. CLINICAL TRIALS

Unlike other delivery systems, the current excipients approved by the Food and Drug Administration (FDA) are very limited and not accepted worldwide. Such issue renders some difficulties in finding suitable polymeric or lipid based materials authorized for inhalation for this technique.[16]

In 2007, Rogueda and Traini published a review paper about the delivery of nanoparticles through pulmonary routes. At that time, publications were scarce, only one patent regarding DPI's and covering sizes below 500 nm was available, and there were no available products on the market for the delivery of nanoparticles using DPI.[52] The FDA approved the use of insulin DPIs (Exubera, Pfizer) in 2006, to treat patients with type 1 and type 2 diabetes, which was a major breakthrough for research in DPIs.[109,110] However, one year later this product was removed from the market due to some uncertainties over patient compliance and long-term safety.[110,111] As the time goes by, Nolan and co-workers reported in 2011 an excipient free formulation approach of making sodium cromoglicate, an antiasthmatic and anti-allergenic drug whose use in a DPI was firstly reported in 1998 into spherical nanoporous microparticles via spray drying technique.[112,113] The results obtained by this group showed improved aerodynamic properties comparing to the drug by itself demonstrating that porosity and sphericity of drug particles are preponderant features to enhance aerosol deposition.[16,113] Further optimization, regarding the aerodynamic properties, was achieved by Hu and collaborators by coupling continuous liquid solvent precipitation with immediate spray drying. Spherical agglomerates of pure drug nanoparticles were achieved with sizes more suitable for pulmonary delivery (4.46 ± 0.14 μm), thus increasing the FPF in approximately 50 %.[16]

More recently, Nanotherapeutics Inc., challenged the National Institute of Allergy and Infectious Diseases (NIAD) to produce an inhaled version of the injectable antiviral drug Cidofovir for the treatment of smallpox and for non-invasive post-exposure prophylaxis. The devel-

opment of inhaled Cidofovir could decrease the amount of people that are still vulnerable to smallpox due to their inability to be vaccinated. Several studies have already proved that this new respirable formulation of Cidofovir is very efficient against multiple pox models, when compared to injectable administration. In turn, increases the amount of powder retained in the pulmonary level and, quite possibly avoids nephrotoxicity (so far caused by the injectable form). Amazingly, the use of gold nanoshells to deliver such drug, as already started in human models.[40] Table 1.6 summarizes the more recent ongoing clinical trials on dry powder formulations for a wide range of pulmonary diseases. The listed dry powder formulations under clinical trials comprise crystalline and/or amorphous APIs blended in excipients of, for example, phospholipid, monosaccharides, disaccharides, polysaccharides, additols, and surfactants such as oleic acid and 1,2 distearoyl-sn-glycero-3-phosphocholine (DSCP). These formulations could be classified as particles with nanofeatures.

Table 1.6-Clinical trials using dry powder formulations for a wide variety of pulmonary diseases.

Clinical Trials	Condition/ Drug	Formulation/production	MMAD(µm)/FPF	Sponsor	Status
A Twelve Month Long Term Safety Study to Evaluate the Safety of Albuterol in a Dry Powder Inhaler with both Repeated and as Needed Dosing	Asthma/Albuterol	Levalbuterol L-tartare; surfactant (e.g. oleic acid)/Milling	1.5-2.1/31.6- 4.6 %	Teva Branded Pharmaceutical Products, R&D Inc.	Completed
Pharmacokinetic Evaluation and Tolerability of Dry Powder Tobramycin by a Novel Device in Patients With Non Cystic Fibrosis Bronchiectasis	Bronchiectasis/Tobramycin	Tobramycin; sulfate; 1,2 distearoyl-sn-glycero-3-phosphocholine (DSPC);Calcium chloride ($CaCl_2$)/ spray drying	n.a.	University Medical Centre Groningen	Completed
A clinical trial to access the safety of a measles vaccine (dry powder) administered by two different devices (PMV-001)	Measles virus/Live attenuated Edmonstron-Zabgreb measles virus	Myo-inositol; Leucine/supercritical fluid drying (Clinical Trials.gov213)	n.a/~40%	Serum Institute of India Limited	Completed
To determine the relationship between baseline reversibility and the efficacy of indacaterol (REVERBREZ)	Chronic Obstructive Pulmonary Disease (COPD)/ Indacaterol	Indacaterol; glycopyrrolate;DSPC; trehalose; $CaCl_2$/ spray drying	2.3-2.8 /57-69%	Novartis Pharmaceuticals	Completed

Ciprofloxacin Dry Powder for Inhalation in Non-cystic Fibrosis Bronchiectasis (Non-CF BE) (RESPIRE 1)	Bronchiectas/Ciprofloxacin	n.a.	n.a.	Bayer	Recruiting
Sensitivity of Pharmacokinetics to Differences in Aerodynamic Particle Size Distribution	Asthma/ Fluticasone Propionate	Fluticasone Propionate crystals/ anti-solvent process	5.1-6.7/ n.a.	University of Florida	Recruiting

n.a. – not available

1.4. CONCLUSION

The present review has highlighted the current status as well as the major benefits and limitations of the already existing and the under development formulations for 'dry powder inhalers'. Particle engineering is a fresh and *in vogue* area that combines chemical engineering, biopharmaceuticals, biology, formulation science, colloid and interface science, solid state physics, aerosol and powder science and nanotechnology. Nanoparticulated systems have been showing a huge potential in the delivery of biological active substances. Recent progresses in aerosol formulations have led to the development of more efficient delivery systems able to produce small particle aerosols (nano-in-micro formulations) allowing higher powders deposition in the alveoli and deep lung region. The combination of nanotechnology and pulmonary delivery of aerosolizable drugs brings out new and exciting breakthroughs for the diagnosis and therapy of several types of lung and systemic diseases.

Particle engineering requires a deeper understanding of particle formation processes. A wide range of research experts from different but complementary areas, are already working in the design of safe and effective formulations to make these therapies safer and more effective. A detailed research in the possible combination of nano-in-micro dry powder formulations making use of spray drying and/or supercritical assisted-atomization is behind the scope of this review.

It is well-known that the new class of engineered spray dried particles and more specifically SASD formulations will definitely cause a shift in the thinking and structure of pharmaceutical organizations developing them. Although this type of research appears to be promising in lung disease therapeutics, some difficulties still need to be overcome before the potential for wide public use may be appreciated. The fate and effect of the particles, specifically the nanoparticles release from the micro platforms, needs to be fully understood before clinical trials may be performed. Safety and efficacy must be assured and optimization processes must be guaranteed so that large scale manufacturing processes can be achieved, reducing costs and waste materials. Despite the plentiful advantages and applications of supercritical fluid technology, there is still room for improvement in the pharmaceutical industry. The influence of operating parameters on particle size and its morphology needs to be completely discerned. Potential efforts must be performed to defeat these challenges, as supercritical fluid technology has added a totally new dimension to the pharmaceutical research and formulation development. Moreover, successful design of engineered particles requires a thorough understanding and predictive modelling, so that the early development process can be completed in an acceptable time with a high likelihood of success.

These are definitely the ultimate goals for the successful production and approval of dry powders produced through the use of sustainable strategies.

CHAPTER 2. Design of oligoaziridine-PEG coatings for efficient nanogold cellular biotagging

This chapter corresponds to the contents (with minor changes) of the following publication:
2015, Royal Society of Chemistry Advances, 5: 10733-10738
A. Sofia Silva, Vasco D. B. Bonifácio, Vivek P. Raje, Paula S. Branco, Paulo F.B. Machado, Ilídio J. Correia and Ana Aguiar-Ricardo

Keywords: Gold nanoparticles, maleimide poly(ethylene glycol), oligoaziridine

Personal contribution

A.Sofia Silva contributed to the design of the study, co-performed the synthesis of oligoaziridine, performed the rest of the experimental work, co-interpreted the data and wrote the manuscript.

2.1. ABSTRACT

Gold nanoparticles (AuNPs) are the most investigated nanomaterials for theragnosis applications. In a research field where live cell assays, as well as the tracking of nanomaterials into cell's environment, are of extremely importance, water-soluble AuNPs have been intensively studied to overcome the toxic effects exerted by coatings. Unfortunately, AuNPs fluorescent tagging often fails due to self-quenching and a careful design must be carried out to keep optoelectronic properties and biocompatibility. In this work, the synthesis of fluorescent gold nanoprobes, able to enter within cell's environment (biotags) and target the cell nucleus, was designed and the particles tracked by confocal laser scanning microscopy. The coating of AuNPs with maleimide poly(ethylene glycol) and fluorescent oligoaziridine biocompatible oligomers, resulted in robust, optical active biotags that open novel insights into cancer theragnosis.

2.2. INTRODUCTION

Cellular internalization and nuclear targeting are two subsequent and challenging tasks that have been increasingly investigated over the past decades. The cell nucleus is the place where the genetic information and transcription machinery of the cell can be encountered and, therefore, its targeting has been demonstrated to be crucial for several diagnostic and therapeutic purposes.[114] In such targeting attempts, different types of nanoparticles (metallic, magnetic or polymeric) have been introduced into the cells environment.[115–118] Particularly, gold nanoparticles have been widely studied in the field of nanomedicine for theranostic aspirations. These nanomaterials display interesting optical, electronic, and molecular-recognition properties not shown by bulk gold.[12,24,119,120] They are easily reproducible in a wide variety of shapes and sizes, and can be functionalized to perform specific functions, through the attachment of biologically active molecules, targeting sequences, imaging devices and biocompatible coatings.[121,122]

The targeting of fluorescent agents to cells and tissues by using AuNPs has emerged as a main focus in cancer research since nonspecific toxicity can be minimized and transportation efficiency can be enhanced.[123–127] However, AuNPs are well known to self-quench upon surface fluorescent tagging. Notwithstanding, under certain conditions, the fluorescence can be enhanced by the near-field of AuNPs, which is a subject of considerable interest.[13,128,129] Aiming the development of robust gold biotags, able to target the cells environment, and ultimately the nucleus, we investigated novel biocompatible coatings comprising oligomers of poly(ethylene

glycol) (PEG) and a fluorescent water-soluble oligoaziridine (OA). Although OA, was already investigated as a biosensor for fluorescence microscopic imaging of metal cations under physiological conditions,[130] we now demonstrate its efficient biotagging performance. To foster internalization features, while guarantying nanoparticle stability and avoiding unspecific interactions, a biocompatible coating based on homobifunctional maleimide poly(ethylene glycol) (MPM) units was chosen. The selection of MPM relied mainly on its biocompatibility and high reactivity.[131–134]

Using a convergent strategy we were able to synthesize stable PEG-oligoaziridine fluorescent water-soluble bilayered AuNPs through a simple and straightforward route. The cellular uptake of these novel gold nanoparticles was followed through fluorescence microscopy and their biocompatible profile was assured through the MTS assay. Morphological and spectral characterizations were also performed.

2.3. EXPERIMENTAL PROCEDURES

2.3.1 Materials

A549 non-small lung carcinoma cell line was purchased from ATCC. Sodium azide was acquired from Amresco. Fetal bovine serum (FBS) was purchased from Biochrom AG. Tris Base was obtained from Fisher Scientific. CellLight® Actin-GFP, BacMam 2.0 (GFP) was attained from Invitrogen, Life Technologies. Glass bottom dishes were dispensed by MatTek Corporation. Maleimide-PEG-Maleimide (MPM, Mw= 3.4 KDa) was bought from NANOCS. Amphotericin B, collagen solution, ethanol (EtOH), glutaraldehyde, Ham's Nutrient Mixture-F12, L-glutamine, penicillin G, phosphate-buffered saline (PBS), streptomycin, tetrachloroauric (III) acid ($HAuCl_4.3H_2O$), 3-(4,5-dimethylthiazol-2-yl)-5-(3-carboxymethoxyphenyl)-2-(4-sulfophenyl)-2H-tetrazolium reagent MTS, trisodium citrate and trypsin were purchased from Sigma Aldrich. The oligoaziridine biosensor (OA) was synthesized as described elsewhere.[130]

2.3.2 Synthesis of gold nanoparticles

The synthesis followed the Frens method.[135] Briefly, 100 mL of 0.01 % (w/v) $HAuCl_4.3H_2O$ were heated until reflux. Then, 1mL of trisodium citrate hydrate, 1 % (w/v) was added to the refluxing solution under constant stirring. After 25 sec, the slightly yellow solution turned faintly blue. Subsequently, the solution color changed to dark red, which was indicative

of the formation of monodisperse spherical particles. The solution was boiled for more 5 min to allow the complete reduction of the gold chloride. The AuNPs obtained were then supplemented with 0.05 % (w/v) sodium azide and stored at 4 °C. Gold nanoparticles produced by this method are referred as AuNPs. UV-Vis: λmax= 525 nm. IR (film) ν (cm^{-1}): 1575 (C=O), 1393 (COO), 1078 (C–O).

2.3.3 Coating of gold nanoparticles with the oligoaziridine biosensor

Different molar ratios of oligoaziridine (100:1, 500:1, 750:1, 1250:1, 2500:1, 5000:1) were added to the colloidal solution of AuNPs and vortexed at low speed, during 2 min. The samples were then ultracentrifuged at 14500 x g, during 20 min, at room temperature. The supernatant was then removed and the pellet was redispersed in deionized water for all the subsequent tests. The nanoparticles produced by this method are denoted as Au-OA. Oligoaziridine biosensor: UV-Vis: λmax= 370 nm. IR (film) ν (cm^{-1}): 1658 (C=C), 1362 (S=O), 1156 (S=O), 1038. Au-OA biotag: UV-Vis: λmax= 525 nm. IR (film) ν (cm^{-1}): 1650 (C=C), 1362 (S=O), 1148 cm^{-1} (S=O), 1030, 1077.

2.3.4 Coating of gold nanoparticles with homobifunctional maleimide poly(ethylene) glycol

The AuNPs produced according to the Frens method were capped with MPM and are denoted as Au-MPM. Different ratios of MPM (PEG:AuNPs) (500:1, 750:1, 1250:1, 2500:1, 5000:1, 10000:1) were added to 10 mL of AuNPs colloidal solution. The mixture was allowed to react for one hour under stirring.[134] Afterwards, the reaction mixture was collected to 1.5 mL eppendorfs and centrifuged at 13500 x g, for 20 min at room temperature. The supernatant was removed and the pellet was redispersed in Tris buffer (pH 7.4) and stored at 4° C, until further use. Au-MPM biotag: UV-Vis: λmax= 525 nm; IR (film) ν (cm^{-1}): 1629 (C=O), 1552 (COO), 1296 (C–N), 1137 (C–O–C); 1050, 1036.

2.3.5 Coating of Au-MPM with oligoaziridine biosensor

The oligoaziridine biosensor was also added to Au-MPM and the samples were ultracentrifuged using the protocol above described. The samples were then re-suspended in water and, again, different molar ratios of OA biosensor were added (100:1, 500:1, 750:1, 1250:1, 2500:1, 5000:1). The mixtures were stirred during 1 h in the dark and then re-centrifuged at 13500 x g,

for 20 min. The supernatant was removed and the pellet was redispersed in deionized water for subsequent analyses. The nanoparticles produced with this procedure are designated by Au-MPM-OA biotag. UV-Vis: λmax= 525 nm. IR (film) ν (cm^{-1}): 1650 (C=C), 1635 (C=O), 1362 (S=O), 1148 (S=O); 1030, 1077.

2.3.6 Biotags properties and characterization

The morphology of the nanoparticles was analyzed by Transmission Electron microscopy (TEM). Samples were visualized and recorded using Hitachi H8100 TEM itch ThermoNoran light elements EDS detector and digital image acquisition. Nanoparticle's size was determined by dynamic light scattering (DLS). Briefly, nanoparticles were diluted in 800 µL of ultrapure water.[136] Size measurements were then performed in a nano partica SZ-100 series instrument from Horiba scientific, in automatic mode and with a scattered light detection angle of 90°. Zeta potential quantification was carried out in the same nano partica SZ-100 series Horiba instrument using a zeta dip cell with a scattered light detection angle of 173°. Thermogravimetric analysis (TGA) was performed on a TGA-DSC–STA 449 F3. Samples, previously lyophilized, were placed in platinum sample pans and heated under an argon atmosphere at a rate of 10 °C/min to 700 °C.[137]

2.3.7 Biotags spectral properties

FTIR spectra were recorded in a Nicoletis 20 spectrophotometer (64 scans) from Thermo Scientific equipped with a Smart iTR auxiliary module. Fluorimetry assays were performed in a Perkinelmer LS 45 Luminescence Spectrometer. UV-Vis spectroscopy was recorded in an Infinite 200 from Tecan using a Corning 384 Flat Bottom Black Polystyrene Low Volume/Flat microplate, kindly provided by Corning Corporation. The test was performed in a scan method from 260 to 700 nm.

2.3.8 Cell culture and biotags transfection

Cell culture experiments were performed using of A549 cell line. Cells were cultured in Ham's Nutrient Mixture-F12 medium supplemented with 10 % v/v heat-inactivated FBS and antibiotic-antimycotic (penincilin G (100 U/mL)), spectromycin G (100 µg/mL) at 37°C, under 5 % CO_2 humidified atmosphere. *In vitro* transfection studies were carried out by seeding cells in glass bottom dishes, dispensed by MatTek Corporation , at a density of $12x10^3$ cells per well,

with 1 mL of Ham's F12K medium supplemented with 10 % FBS without antibiotic for 24 h.[115] Nanoparticles were lyophilized, sterilized, resuspended in Ham's F12K medium (2 mg/mL) and filtered with a syringe and a filter with a membrane pore of 200 nm, before being added to the cells. Cell's transfection with all types of nanoparticles herein produced was performed and was stopped over 4 h, by exchanging the culture medium by a complete Ham's F12K medium. Subsequently, cell growth was monitored using an Olympus CX14 inverted light microscope equipped with an Olympus SP-500 UZ digital camera. This last procedure was repeated for 2 days.

2.3.9 Fluorescence and Confocal Laser Scanning Microscopy

In order to evaluate the ability of nanoparticles to enter into the cells environment without losing their electronic properties, both fluorescence and confocal laser microscopy assays were performed after *in vitro* transfection. First, the glass bottom dishes containing transfected live cells were visualized using a Zeiss AX10 microscope (Carl Zeiss SMT Inc.) and analyzed with Axio Vision Real 4.6 software. Formerly, the cells cytoplasm was marked with CellLight® Actin-GFP, BacMam 2.0 (GFP), and then, confocal images were obtained with a Zeiss LSM 710 laser scanning confocal microscope (Carl Zeiss SMT Inc.) equipped with a plane-apocromat 40x/DIC objective. Data analysis of Confocal Laser Scanning Microscopy (CLSM) images was performed with Zeiss software (Axio Vs40 V4.5) and Imaris Bitplane (Vs7.6.1 Bitplane).

2.3.10 Evaluation of the biotags cytotoxic profile

An MTS assay was performed to evaluate nanoparticles biocompatibility according to the manufacturer instructions. Twenty four hours prior to the experiment the cells were seeded at a density of $12x10^3$ cells per well into 96-well plates with 200 μL of cell culture medium supplemented with 10 % FBS, without antibiotics. The cells were then incubated with nanoparticles formulations for 24 and 48 hours. All the formulations of nanoparticles were resuspended in pre-warmed culture medium containing 10 % FBS and then added to each well. A total of three replicates were considered for each formulation. The absorbance of the samples was measured at 492 nm using a microplate reader Anthos 2010. Wells containing cells in the culture medium without materials were used as negative control. Ethanol (EtOH) 96 % was added to wells containing cells as a positive control.[130]

2.4. RESULTS AND DISCUSSION

2.4.1 Particles synthesis and characterization

The particle design aimed the construction of bilayered, biocompatible and optical active gold nanoparticles. The first layer (PEG oligomer) was assembled into the AuNPs by the reaction of the alcohol from citrate with the MAL-PEG-MAL homobifunctional oligomer (Au-MPM). The reaction of alcohols with maleimide is reported in the presence of a catalytic amount of Au^{3+},[138] and the successful AuNPs PEGylation led us to conclude that indeed AuNPs (synthesized using a Au^{3+} precursor), must be involved in this step. Next, a second layer (OA fluorescent oligomer) was added by reacting OA with the terminal maleimide from Au-MPM (Au-MPM-OA). Following this strategy (see schematic synthesis in Figure 2.1) we were able to synthesize stable nanogold biotags avoiding elaborated synthesis and purification.

The MPM coating was confirmed by FTIR- ATR through the presence of the characteristic (slightly shifted) ether bands (1552, 1296, and 1137 cm^{-1}) (Figure 2.1A). Similarly, the OA coating was confirmed by the presence of sulfonamide bands (1658, 1362 and 1156 cm^{-1}) (Figure 2.1B). As expected, in the final formulation Au-MPM-OA, both bands from MPM and OA were identified (1650, 1362 and 1148 cm^{-1}), thus proofing the successful reaction between Au-MPM and OA.

After the synthesis different nanogold formulations were developed. The influence of OA (fluorescent biosensor) and PEG oligomers on the particles morphology and size was investigated using different molar ratios of OA and MPM (100:1, 500:1, 750:1, 1250:1, 2500:1, 5000:1, 10000:1),[139] leading to the production of Au-OA, Au-MPM and Au-MPM-OA formulations.

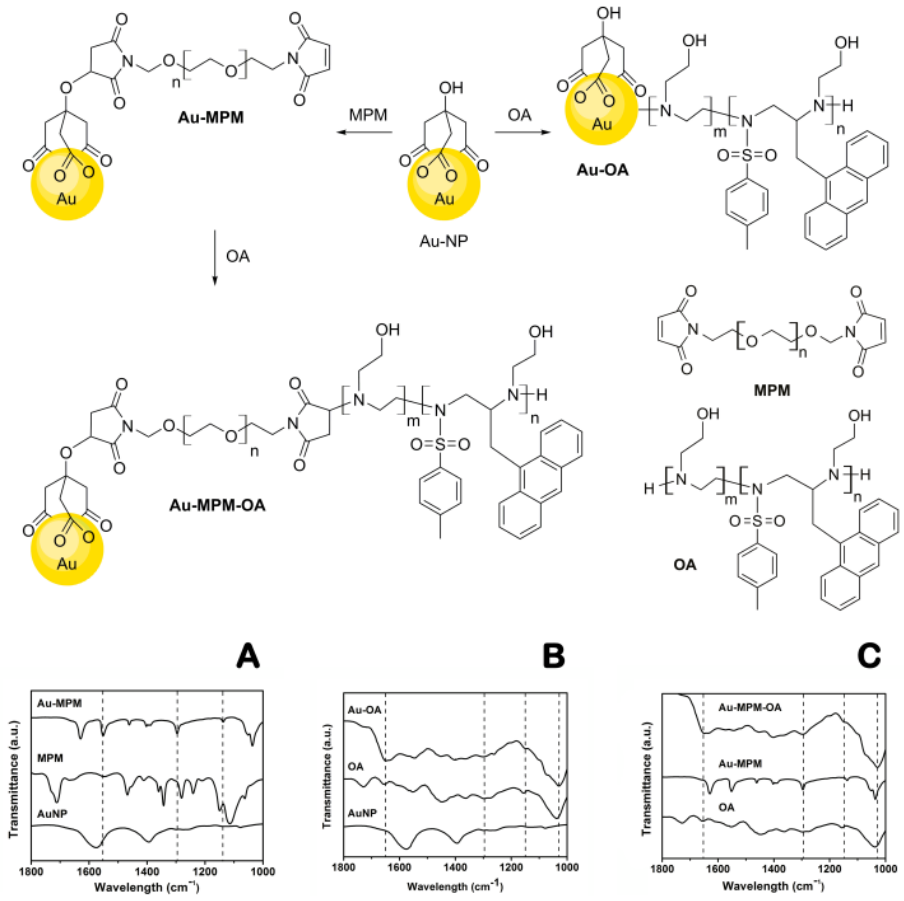

Figure 2.1-PEG-oligoaziridine bilayer coating of gold nanoparticles schematic synthesis (top) and the corresponding IR spectra (bottom) of (A) Au-MPM, (B) Au-OA; and (C) Au-MPM-OA.

The nanoparticles morphology was assessed by TEM. We found that the best molar ratios for OA:AuNPs and MPM:AuNPs were 750:1 and 5000:1, respectively. The produced biotags showed spherical and oval-like morphologies as it can be observed in Figure 2.2.

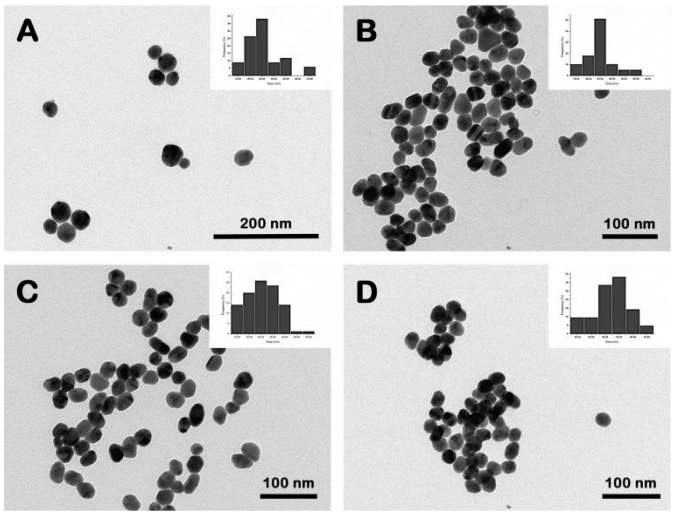

Figure 2.2-TEM images of the biotags (A) gold nanoparticles, (B) gold nanoparticles coated with oligoaziridine (Au-OA), (C) gold nanoparticles coated with MPM (Au-MPM) and (D) PEGylated gold nanoparticles coated with oligoaziridine (Au-MPM-OA). The insets show size measurements performed using the Image J software.

The nanoparticles were also characterized in terms of their ability to form stable colloidal formulations with appropriate physicochemical properties for intracellular applications. Dynamic light scattering was also performed to evaluate the nanoparticles size, and similar values were obtained using both methods. All formulations exhibited sizes well-suited for delivery into tumoral microenvironments. As expected, the AuNPs show sizes around 30 nm and a zeta potential of approximately -30 mV.[125,135] (see Figure 2.2A and Table 2.1) After coating with OA, the zeta potential tends to became positive, thus favoring cellular internalization due to electrostatic interaction between negatively charged proteoglycans and positively charged nanoparticles.[136] Our data showed that all the produced formulations have positive zeta potential values within the range of colloidal stability (between -40 to +40 mV).

Table 2.1-Particle size and zeta potential data for nanogold PEG-oligoaziridine coatings.

Nanoparticles	Particle size (nm)	PDI	Zeta potential (mV)
AuNP	28±1	0.369	-34±4
Au-OA[a]	30.7±0.5	0.371	18±1
Au-MPM[a]	28.4	0.379	-31±4
Au-MPM-OA[b]	28±1.5	0.396	20.4±2

[a]Au-MPM/OA biosensor 5000:1 ratio.

[b]Au-MPM/OA biosensor 750:1 ratio.

The amount of organic components on the AuNPs was assessed by thermal gravimetric analysis (TGA) (Figure A.1, Appendix A). The total mass loss was 6.67 %, 6.11 % and 4 % for Au-MPM, Au-OA and Au-MPM-OA, respectively. By combining the data from TGA and Inductively Coupled Plasma (ICP) analyses, the amount of Au and S in the nanoparticles was determined (see calculations in Appendix A) thus confirming a bilayered architecture (MPM/OA 1:1 ratio). The synthesized bilayered nanogolds showed a high colloidal stability that was corroborated by UV-Visible spectroscopy (Figure 2.3A) and by colorimetric analyses (Figure 2.3B). By comparing the absorbance intensity of the characteristic band of AuNPs (spectrum 1 in Figure 2.3A, λmax = 526 nm) of the formulations, we found that all coatings lower the intensity of this band (more significantly in case of Au-OA, spectrum 3 in Figure 2.3A). However, for the formulation Au-MPM-OA (750:1 ratio) the intensity is recovered (spectrum 8 in Figure 2.3A), demonstrating a synergistic effect between MPM and OA layers. For higher ratios (1250:1 and 2500:1) the variation in the absorption is negligible.

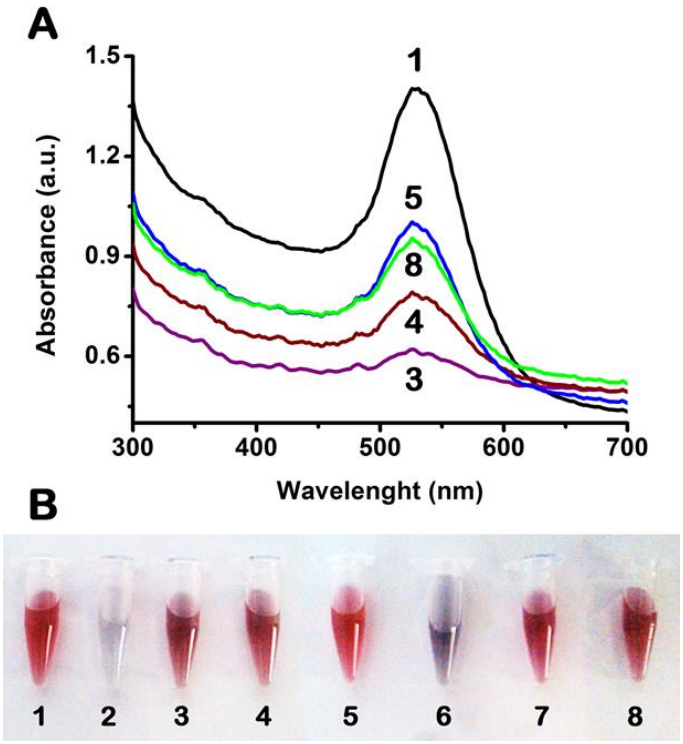

Figure 2.3-Colloidal stability of the biotags: (A) UV-Vis spectra and (B) colorimetric evaluation: (1) AuNPs, (2) Au-OA 2500:1, (3) Au-OA 1250:1, (4) Au-OA 750:1, (5) Au-MPM, (6) Au-MPM-OA 2500:1, (7) Au-MPM-OA 1250:1, (8) Au-MPM-OA 750:1.

The optical properties of the biotags were evaluated in aqueous media. Interestingly, biotags coating with OA leads to optical active nanoparticles, thus avoiding self-quenching events (Figure A.2, Appendix A).

2.4.2 Qualitative evaluation of biotags cellular uptake

In the present study, the A549 cell line was used as a model to study the cellular uptake of the OA biosensor, Au-OA and Au-MPM-OA nanogold formulations. Also an evaluation of the produced biotags was performed to conclude about their suitability for cell live imaging applications using microscopic fluorescence. Fluorescence (Figure 2.4) and CLSM (Figure 2.5) gave insights on cell internalization, without requiring any auxiliary reagents to 'force' their entry. The fluorescence images show that the OA biosensor (Figure 2.4A), as well as the synthesized nanogolds, Au-OA (Figure 2.4B) and Au-MPM-OA (Figure 2.4C), were able to enter into the cells environment. It should be stressed out that all of the images regarding internalization studies were taken with the same color ranges and contrast features.

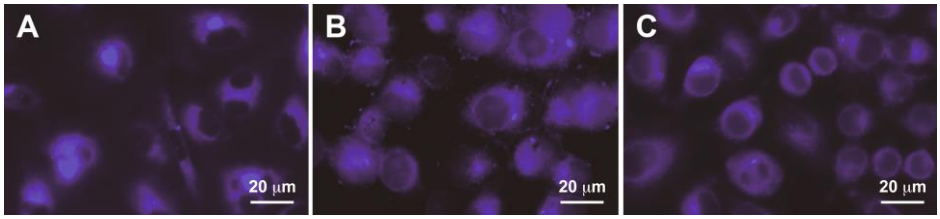

Figure 2.4-Fluorescence images of A549 cells transfected with (A) an oligoaziridine biosensor, (B) Au-OA and (C) Au-MPM-OA biotags. Original magnification x63.

CLSM images showing intracellular localization of Au-OA and Au-MPM-OA are displayed in Figure 2.5A and Figure 2.5B, respectively. These images show that biotags are located both within cell cytoplasm and nucleus, clearly demonstrating their potential application as imaging agent and/or as drug delivery agents when loaded with anti-cancer drugs. The high cellular internalization verified for both nanogold formulations can be easily rationalized from their physico-chemical properties such as size, zeta potential, morphology and hydrophobicity. When comparing the cellular uptake of the different nanogold formulations, we noticed that Au-MPM-OA exhibits a slightly higher internalization (Figure 2.5B and Figure 2.5D), a finding that was also corroborated by the analysis of Image J color histograms of the cell region (the artifacts/particles outside the cells were not taken into account, Figure A.3 in APPENDIX A). Co-localization histograms represented in Figure 2.5B and Figure 2.5D also show a higher amount of co-localized pixels for Au-MPM-OA particles. In fact, PEGylation is known to enhance materials integration within biological systems.[115,140] Thus, Au-MPM-OA are more likely to be uptaken by cancer cells.

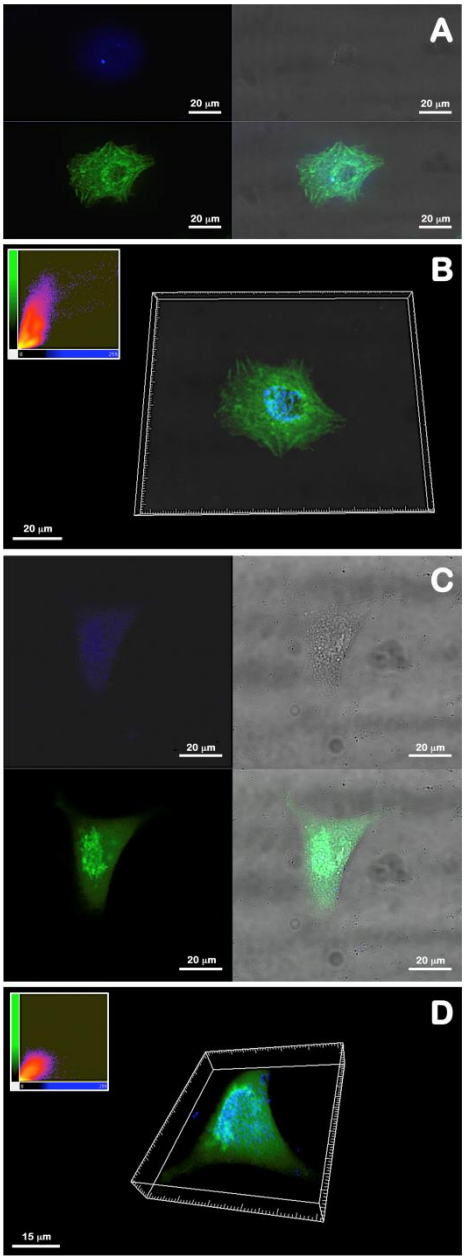

Figure 2.5-Cellular uptake of the biotags CLSM images of A549 cells transfected with (A) Au-OA and the respective 3D reconstruction (B); (C) A549 cells transfected with Au-MPM-OA and the respective 3D reconstruction (D). Green color – CellLight® Actin-GFP, BacMam 2.0; Blue color – Gold NanoProbe (GNP). Original magnification x40. Figures 2.5B and 2.5D were further processed using the *Imaris Bitplane* software.

2.4.3 Evaluation of the cytotoxic profile of the biotags

The cytotoxic profile was assessed after the cellular uptake took place. The MTS assay showed that cells in contact with the biotags showed higher cell viability than the positive control (K+) (ethanol) but lower than that of the negative control (K-) (culture medium), during the period of incubation (48 h). Although in literature there are different studies reporting contradic-

tory results regarding AuNPs cytotoxicity,[122,129] we found that the biotag precursors, as well as the gold nanoparticles *per se*, did not affect cell viability, being above 80 % for all samples. Besides, a significant difference in cell viability was obtained between the positive and negative control ($p < 0.05$), and cells exposed to the different precursors and biotags after 24 h ($p^* < 0.05$) and 48 h ($p\# < 0.05$) of incubation (Figure 2.6). Cell growth and adherence of the cells with internalized nanoparticles was also observed in the inverted microscopy micrographs (Figure A.4 in Appendix A).

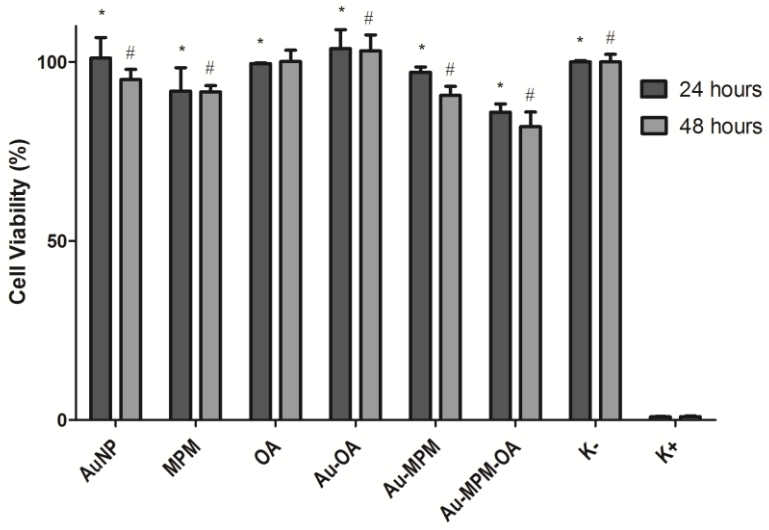

Figure 2.6-Cellular activities measured by the MTS assay after 24 h and 48 h in contact with the biotags and respective precursors. MPM= MAL-PEG-MAL; OA= Oligoaziridine biosensor (OA). Negative control (K-); Positive control (K+).

2.5. CONCLUSIONS

Gold nanoparticles coated with a PEG-oligoaziridine bilayer were fully investigated and found to be stable, biocompatible, optical active and water-soluble biotags, able to target the cell nucleus. Live cell assays were assured in a faster, accessible and precise manner, enabling the acquisition of 3D images well representative of AuNPs course within the cells environment. Particularly, the reported methodology makes use of a simple and convergent approach that allows straightforward coating of PEG and fluorescent oligoaziridine oligomers onto the AuNPs surface. The incorporation of a fluorescent oligoaziridine layer avoids major fluorescence self-quenching, the major limitation of AuNPs fluorescent tagging. Furthermore, the PEG layer confers not only the desired stability, but also a higher cellular internalization. We envisage that biotags tethering with specific antibodies or peptide sequences will be capable of selectively target cancer cells. Additional conjugation of these formulations with anti-cancer drugs will

permit their use in cancer therapy. Such features, allied to powerful tools such as photothermal microscopy, fluorescence microscopy and cancer imaging make these biotags, especially Au-MPM-OA, valuable tools for biotagging and cancer theragnosis.

CHAPTER 3. Nanogold POXylation: Towards always-on fluorescent lung cancer targeting

The contents of this chapter were submitted to a peer reviewed international journal:
A. Sofia Silva, Marta C. Silva, S P Miguel, Vasco D.B. Bonifácio, Ilídio J. Correia, Ana Aguiar-Ricardo

These results were presented as an oral presentation in the International Symposium on Nanoparticles/Nanomaterials and Applications, and awarded as the *Best Shot-Gun Presentation*, Costa da Caparica (Portugal), 20th – 22nd January 2014

Keywords: gold nanoparticles, fluorescent, oligo-oxazolines, laminin fragment, cell targeting

Personal contribution

A.Sofia Silva contributed to the design of the study, performed the majority of experimental work, co-interpreted the data and wrote the manuscript.

3.1 ABSTRACT

Biocompatible gold nanoparticles targeted with a laminin fragment were successfully engineered using fluorescent oligo-oxazolines produced in supercritical carbon dioxide. The architecture and properties of the POxylated constructs were fully characterized and confocal laser scanning microscopy measurements demonstrated a higher cellular uptake into A549 lung cancer cells.

3.2 INTRODUCTION

Gold nanoparticles can be engineered to exhibit diagnosis and therapy (theragnosis) features.[141,142] Despite cargo and release functions, at both extracellular and intracellular levels, gold-based nanodevices are also able to penetrate into deep tissue and undergo cellular uptake. Surface design also provides a stealth surface to prevent opsonisation, increasing residence time and enhancing therapeutic delivery at specific sites. Usually, this goal is achieved by coating AuNPs with hydrophilic Poly(Ethylene glycol) (PEG). However, some recent reports state that increasing amounts of PEG may lead to undesired hepatic accumulation leading to an inflammatory response trigger by the liver,[8,143] a fact that led pharmaceutical companies to investigate alternatives to PEGylation. Poly(ethyleneimine) (PEI) is reported as an useful hydrophilic cationic polymer for transfection enhancement, however its use in biomedical applications is limited due to its known cytotoxicity.[63,144,145] Related poly and oligo(2-alkyl-2-oxazolines) are another class of hydrophilic and biocompatible polymers regarded as versatile PEG alternatives. Importantly, they are easily eliminated by renal clearance and, opposing to PEG, their properties can be gradually fine-tuned over a broad range by side chain design enabling different biomedical applications. In particular, poly(2-ethyl-2-oxazoline), an already FDA approved indirect food additive (adhesive, Aquazol®), is of special interest since has been already conjugated with Ara-C, a low molecular weight drug,[8] and model proteins.[9] The synthesis of polyoxazolines is well established, either by microwave[10] or supercritical carbon dioxide ($scCO_2$)-assisted Cationic Ring-Opening Polymerization (CROP).[11] In the last decade, our group fully explored the properties of oligo(2-alkyl-2-oxazolines) (OOxs) produced by a clean $scCO_2$–assisted CROP,[12] and enlarged the scope of its applications by producing blue fluorescent low polydisperse oligomers.[146–148] It is known that the distance of the fluorophore to the AuNP core is crucial to avoid interactions of the electrons of the fluorophore with the plasmon field (typically > 10 nm), being the fluorescence almost completely quenched on the particle surface.[14]

Herein, we report the optical features of stable fluorescent AuNPs and its impact in the performance of cellular uptake into A549 lung cancer cells.

Since the surface chemistry is vital for cell-nanoparticles interactions we evaluated the coating effect of oligo-oxazolines end-terminated with cysteamine and a *N*-substituted PEI having pendant chromylium salts, obtained by post-functionalization of poly(2-ethyl-2-oxazoline). AuNPs were further tagged with a laminin fragment (YIGSR), known to bind to the overexpress β1 integrins of A549 non-small cell lung cancer.[149,150] Surprisingly, the nanoconstructs exhibit fluorescence, thus meaning that the OOxs carbamic acid starting end, responsible for coating fluorescence, is not affected by the GNPs plasmon field, and this polymer layer seems to ensure conservation of the optical properties.

3.3 EXPERIMENTAL PROCEDURE

3.3.1 Materials

A549 non-small lung carcinoma cell line was purchased from ATCC. Fetal bovine serum (FBS) was purchased from Biochrom AG. Tris Base was obtained from Fisher Scientific. CellLight® Actin-GFP, BacMam 2.0 (GFP) was attained from Invitrogen, Life Technologies. Glass bottom dishes were dispensed by MatTek Corporation. Amphotericin B, collagen solution, ethanol (EtOH), glutaraldehyde, Ham's Nutrient Mixture-F12, L-glutamine, penicillin G, phosphate-buffered saline (PBS), streptomycin, 3-(4,5-dimethylthiazol-2-yl)-5-(3-carboxymethoxyphenyl)-2-(4-sulfophenyl)-2H-tetrazolium reagent (MTS), trisodium citrate, trypsin, ethyl oxazoline monomer, boron trifluoride etherate ($BF_3.Et_2O$), cysteamine, Laminin fragment (Cys-Asp-Pro-Gly-Tyr-Ile-Gly-Ser-Arg) (YIGSR), anhydrous dimethylformadide (DMF) and dihydrogen phosphate were purchased from Sigma Aldrich. Gold in the form of tetra-chloroauric[III] acid trihydrate ($HAuCl_4.3H_2O$) and trisodium citrate hydrate were purchase from Alfaaesar.

3.3.2 Gold nanoparticles synthesis

AuNPs were synthetized according to the Frens method.[135] Briefly, 100 mL of 0.01 % (w/v) $HAuCl_4.3H_2O$ were heated to boiling. Then, 1mL of trisodium citrate hydrate 1 % (w/v) was added to the boiling solution under constant stirring. After 25 seconds, a slightly yellow solution turned faintly blue. Subsequently, the solution color changed to dark red, which is indicative of the formation of monodisperse spherical particles. The solution was boiled over 5 min, to allow the complete reduction of the gold chloride.[135]

3.3.3 Synthesis of differently end-capped oligo-oxazolines

Prior to particles' functionalization, the living OOXs were polymerized in a stainless-steel reactor and OEtOx was produced and $BF_3.OEt_2$ was used as the initiator. The monomer/initiator ratio used for the polymerization was [M]/[I]¼ = 12. The reactor cell was charged with the monomer, the initiator, a magnetic stirring bar, and then immersed in a thermostatized water bath at 60 ºC. Carbon dioxide was introduced in the reactor in order to achieve the desired reaction pressure (from 16 to 20 MPa). After 20 hours of reaction, the pressure was slowly released until the reactor reach room temperature. Inside the reactor, a viscous foam was obtained (OEtOx). At the end of the polymerization the living oligomer was end-capped either with water or cysteamine, generating OEtOx-OH (1) and OEtOx-SH (2), respectively. Post-functioalization of 1 with 2,4-dihydroxybenzaldehyde produced a polycationic oligo(ethyleneimine-*N*-chromylium salt), OEI-CS (3) Figure 3.1. Briefly, cysteamine termination was obtained through the addition of a tenfold excess of cysteamine, solubilized in anhydrous DMF, relatively to the initiator. The mixtures were kept at 70 ºC using an oil bath under stirring for 24 hours. The oily oligomer solubilized in dry DMF was purified by dialyses against pure milliQ water. The resulting mixture was dried under vacuum and the resulting oily polymer presented a yellow brownish color. For the synthesis of the oligo-oxazoline-N-chromylium PEI salt, the *living* oligo-oxazoline was initially capped with water (OEtOx-OH, 1),[148] (0.77 g, 7.8 mmol) and 2 4-dihydroxybenzaldehyde (1.07 g, 7.8 mmol) and $BF_3.OEt_2$ (4.0 mL) were added. The reaction mixture became red and was allowed to react for 24 h at room temperature. After this period, diethyl ether was added and the polymer precipitated as a dark red solid. The hygroscopic solid was washed several times with diethyl ether and dried under vacuum (quantitative yield). Oligomers 2 and 3 are both soluble in water and show a blue fluorescence at 408 nm (λ_{exc}=348 nm).[147] The oligomers were characterized by IR, ^{1}H NMR (Figure B.2, Appendix B) and Maldi-TOF (Figure B.3, Appendix B).

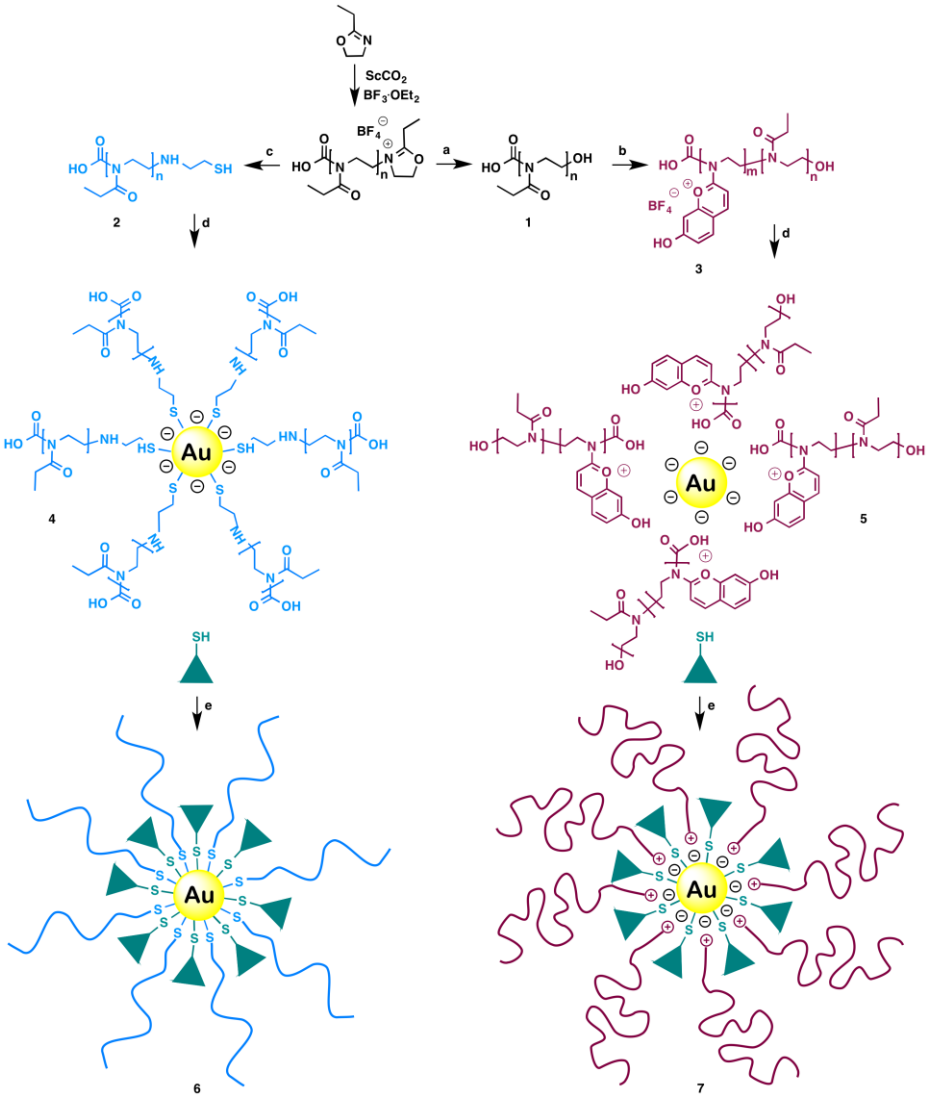

Figure 3.1-Scheme of synthesis of nanogold POxylated probes: (a) water, (b) 2,4-dihydroxybenzaldehyde, $BF_3.OEt_2$, (c) cysteamine, (d) gold nanoparticles and (e) YIGSR.

3.3.4 Gold nanoparticles functionalization

AuNPs were capped with (**2**) and (**3**) (AuNPs:OOx molar ratios of 1:5000 and 1:2500, respectively, at which no aggregation or flocculation occurs) producing Au-OEtOx-SH (**4**) and Au-OEI-CS (**5**), respectively. Afterwards, the mixtures were collected to 1.5 mL eppendorfs and centrifuged at 13500 X g, for 20 min, at room temperature. The supernatant was removed and the pellet was redispersed in milli-Q water. The resulting types of nanoparticles were further conjugated with the YIGSR: different ratios of a stocking solution were added to the Au-OOXs producing Au-OEtOx-SH-YIGSR (**6**) and Au-OEI-CS-YIGSR (**7**). The mixtures were allowed

to stir during 16 hours at room temperature under dark conditions. The resulting mixtures were centrifuged at 13500 X g and ressuspended in milli-Q water.[139]

YIGSR was quantified using RP-HPLC and a ubondapack C18 10µm 3.9 x 100 mm with a gradient of acetonitrile:water (0.05% TFA + 5% TFA respectively) at 220 nm based on standard curves ($R^2 > 0.99$). Briefly, the produced nanoparticles containing the oxazolines and the peptide sequence were centrifuged twice. The supernatant was removed, lyophilized and ressuspended in 1 mL of mili-Q water in order to recover possible traces of unbounded YIGSR.[151]

3.3.5 Nanogold poxylated particles: proprieties and characterization

The nanoprobes were characterized using various analytical techniques. The morphology of the nanoparticles was analyzed by Transmission Electron Microscopy (TEM). Samples were visualized and recorded using Hitachi H8100 TEM itch. ThermoNoran light elements EDS detector and digital image acquisition. Nanoparticle's size was determined by dynamic light scattering (DLS). Briefly, the end-capped nanoparticles were diluted in 800 µl of milliQ ultrapure water in a Zetasizer Nano ZS instrument (Malvern Instruments) kindly provided by PARALAB. Zeta potential quantification was carried out in the same Zetasizer Nano ZS instrument using a zeta dip cell. Thermogravimetric analysis (TGA) was performed on a TGA-DSC–STA 449 F3. Samples, previously lyophilized, were placed in platinum sample pans and heated under an argon atmosphere at a rate of 10 °C/min to 700 °C.[137]

FTIR spectra were recorded in a Nicoletis 20 spectrophotometer (64 scans) from Thermo Scientific equipped with a Smart iTR auxiliary module. Fluorimetry assays were performed in a Perkinelmer LS 45 Luminescence Spectrometer. UV-Vis spectroscopy was recorded in a PerkinElmer Lambda 25 UV/Vis Spectrometer with a slit width of 5 nm at a scan rate of 240 nm/min at 25 ºC, in a wavelength range from 350 to 750 nm, and then analyzed with PerkinElmer UV WinLab™ software. The test was performed in a scan method from 260 to 700 nm.

3.3.6 Cellular uptake

The proliferation of A549 cell line in the presence of Au-OOxs was evaluated by seeding the cells in 96-well plates at a density of 4×10^4 cells/well with nutrient mixture Ham-F12 supplemented with 10 % fetal bovine serum (FBS), for 24 h. After that, the medium was removed; the nanoparticles were ressuspended in Ham F-12 at a concentration of 200 µg/mL and placed in contact with cells for 4 h to allow nanoparticles internalization. After this period of time, cells

medium was replaced by Ham-F12 supplemented with FBS and antibiotics. Cell proliferation was evaluated at 24 and 72 h. Cell growth and adherence of the cells with internalized nanoparticles was monitored using an Olympus CX41 inverted light microscope equipped with an Olympus SP-500 UZ digital camera.

The uptake of the nanoprobes was assessed by confocal laser scanning microscopy (CLSM). A549 cell line was seeded and grown in Ham-F12 containing 10 % FBS, on glass-bottomed coverslips coated with collagen during 24 h. Afterwards, nanoparticles were placed in contact with cells for 4 h to allow nanoparticles internalization. After this period of time, cells medium was replaced by Ham-F12 supplemented with FBS and antibiotics. Then, the cells' cytoplasm was marked with CellLight® Actin-GFP, BacMam 2.0 (GFP).[11]

3.3.7 Evaluation of the cytotoxic profile

Briefly, $4x10^4$ cells/well were seeded in a 96-well plate and cultured with Ham-F12 at 37 ºC under a 5 % CO_2 humidified atmosphere. Then, 200 µg/mL of nanoparticles were added, and the mitochondrial redox activity of the viable cells was assessed through the reduction of the MTS into a water-soluble brown formazan product as previously described. Wells containing cells in the culture medium without materials were used as negative control. EtOH 96 % was also added to some wells, to be used as a positive control.[3,5]

3.4 RESULTS AND DISCUSSION

3.4.1 Nanoparticles characterization and cellular uptake

The nanoprobes were characterized using various analytical techniques. TEM analysis, showed that the nanoparticles is nearly round or oval and uniform and has a narrow diameter distribution around 30 nm (Figure 3. 2E and F).

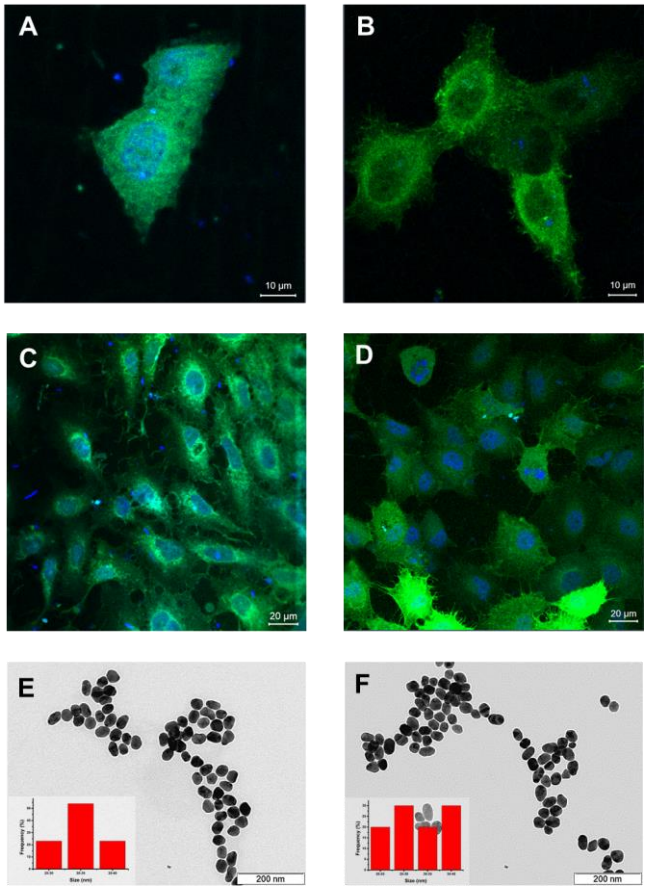

Figure 3. 2-Cellular uptake of nanogold POxylated probes. CLSM images show A549 cells transfected with (A) Au-OEtOx-SH; (B) Au-OEI-CS; (C) Au-OEtOx-SH-YIGSR; (D) Au-OEI-CS-YIGSR. Green color – CellLight® Actin-GFP, BacMam 2.0; Blue color – nanogold POxylated probes. Original magnification x40. Figures 3.2B and 3.2D. TEM images show (E) Au-OEtOx-SH-YIGSR; and (F) Au-OEI-CS-YIGSR nanoparticles. The insets show size measurements performed using the Image J software.

In fact, DLS measurements are consisted with these values and the zeta potential of the nanoprobes increase when laminin fragment is attached to Au-OEtOX-SH and when OEtOX-CHR is used as a grafting oligomer (Table 3.1).

Table 3.1-DLS and zeta potential measurements.

Sample	Size (nm)	Zeta Potential (mV)
AuNPs	27.7±1.1	-40
Au-OEtOx-SH	28.7±0.7	-30
Au-OEtOx-SH-YIGSR	29.2±1.8	-15
Au-OEI-CS	29.4±1.4	-9
Au-OEI-CS-YIGSR	31±1	-9

The uptake of the nanoprobes was assessed by CLSM. By comparing the results obtained for the differently coated systems, neutral Au-OEtOx-SH and cationic Au-OEI-CS (Figure 3.2A and B, respectively), a higher uptake was observed when a non-charged coating was used. Despite the charge effect, the data might be also explained with the higher concentration of OOxs chains attached to the GNP in the neutral system (AuNPs:OOx molar ratio of 1:5000), thus leading to an extra stabilization of the nanoparticles and improved passive targeting. As expected, an enhanced cellular uptake is verified when YIGSR is conjugated to the nanoconstructs. Interestingly, an enriched nuclear location is observed in the CLSM images (Figure 3.2 C and D). This higher internalization seems to be a result of the particles design: size, morphology, zeta potential and recognition active sites. Cell growth and adherence in the presence of the nanocarriers can be depicted in Figure B.1 (Appendix B).

The successful coating with OOxs or immobilization with YIGSR into the particles surface was also corroborated by a significative broadening of the characteristic UV-Vis band of AuNPs (λmax = 530 nm) (Figure 3.3A). Increased molar ratios and consequently increased number of molecules attached to AuNPs lower the intensity of this band. Still, the AuNPs herein depicted did not show signs of aggregation or flocculation (Figure 3.3A and B). The fluorescence properties of the produced particles were confirmed in aqueous media under ultraviolet irradiation of 350 nm light (Figure 3.3C and D).

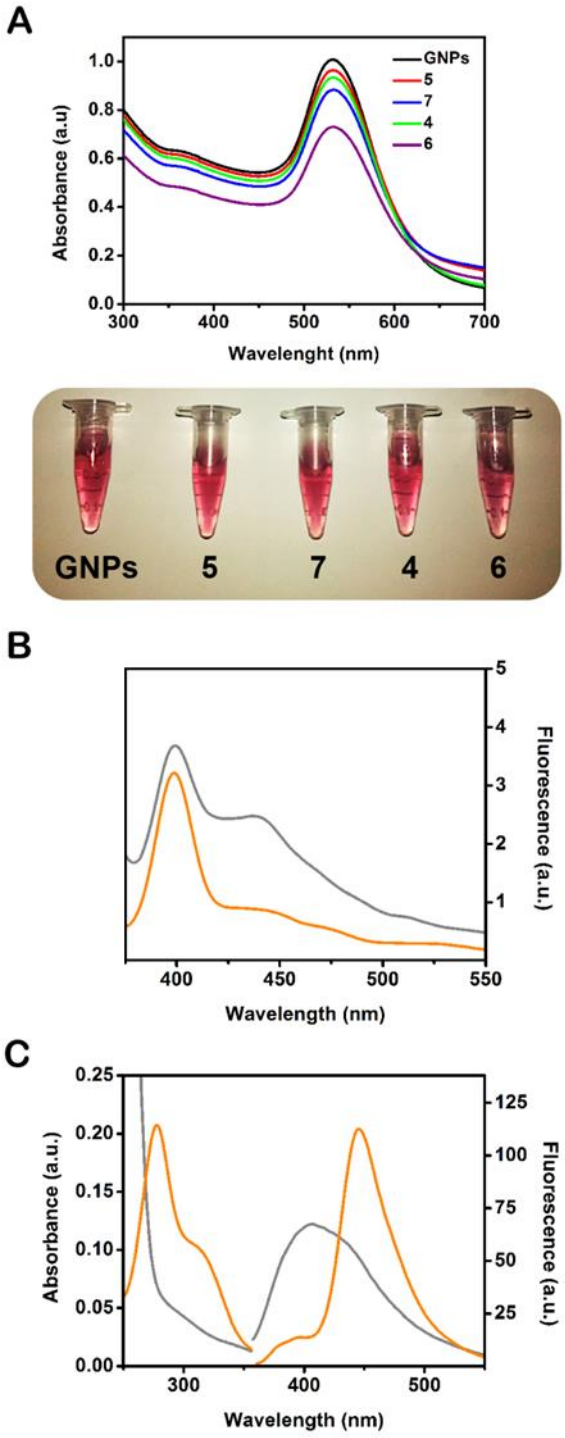

Figure 3.3-Colloidal stability and optical properties of nanogold POxylated probes and intermediates: (A) absorbance spectra (top) and colorimetric evaluation (bottom) of AuNPs s, **4**, **5**, **6** and **7**; (B) fluorescence spectra of **4** (grey) and **5** (orange); (C) absorbance and fluorescence spectra of **2** (grey) and **3** (orange). Studied compounds: gold nanoparticles (AuNPs), OEtOx-SH (**2**) and OEI-CS (**3**), Au-OEtOx-SH (**4**), Au-OEI-CS (**5**), Au-OEtOx-SH-YIGSR (**6**) and Au-OEI-CS-YIGSR (**7**)**.**

The interactions between OOx's and YIGSR, with AuNPs were also proven by FTIR-ATR spectroscopy as shown in Figure 3.4. Specifically, the S-H stretch of laminin fragment at 2610 cm^{-1} is shifted to 2545 cm^{-1} in Au-OEtOx-SH-YIGSR spectrum (b, Figure 3.4A). The characteristic peak of OEtOx-SH at 1628 cm^{-1} is slightly shifted in Au-OEtOx-SH to 1598 cm^{-1} and then, due to the interaction of YIGSR with the produced particles, to 1620 cm^{-1} in Au-OEtOx-SH-YIGSR and is related with N-H stretch. The latest particles also present another shifted peak at 1656 cm^{-1} that is indicated as a C=N stretch (c, Figure 3.4A). Other specific peak representative of the C-N stretch of the terciary amine is demonstrated in the spectra of Au-OEtOx-SH, YIGSR and Au-OEtOx-SH-YIGSR at 1393, 1398 and 1393 cm^{-1}, respectively (d, Figure 3.4A). In turn, the amide characteristic peak of OEI-CS at 1614 cm^{-1} also appears in Au-OEI-CS and is slightly shifted (1618 cm^{-1}) to higher values in Au-OEtOx-CS-YIGSR (a, Figure 3.4B). The YIGSR attachment to Au-OEI-CS also deviates the C-N stretch of the tertiary amine in (1356 cm^{-1}) to upper values in Au-OEI-CS-YIGSR (1360 cm^{-1}). The same is observed in the C=C-C aromatic string: 1394 cm^{-1} in Au-OEI-CS, 1397 cm^{-1} in laminin fragment and 1405 cm^{-1} in Au-OEI-CS-YIGSR (b, Figure 3.4B).

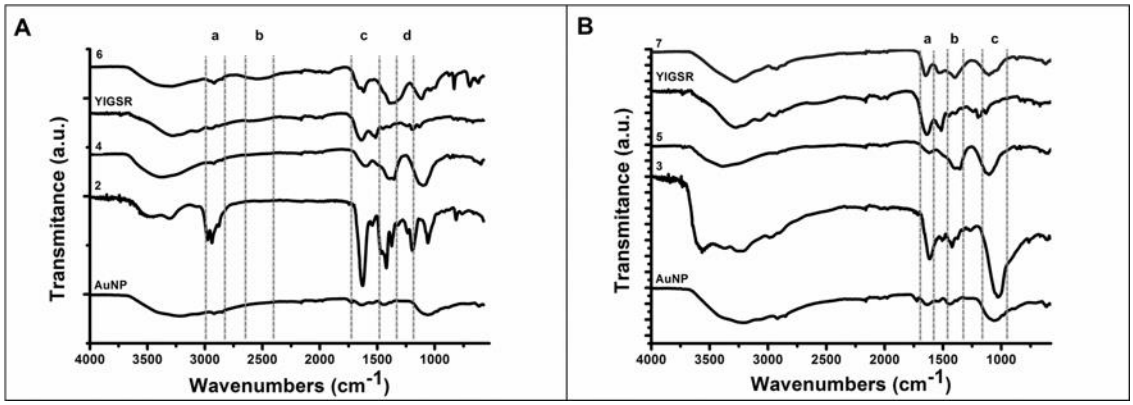

Figure 3.4-FTIR-ATR spectra of nanogold POxylated probes and intermediates: synthetic peptide (YIGSR), oligomers OEtOx-SH (**2**) and OEI-CS (**3**), AuNPs, Au-OEtOx-SH (**4**), AuOEI-CS (**5**), Au-OEtOx-SH-YIGSR (**6**) and Au-OEI-CS-YIGSR (**7**). Regions a, b and c correspond to the characteristic bands of the materials**.**

The amount of organic components on the AuNPs was assessed by thermal gravimetric analysis (TGA) and is depicted in Figure 3.5. The total mass loss was 8.06 % and 3.20 % for Au-OEtOx-SH-YIGSR and Au-OEI-CS-YIGSR, respectively. By combining the data from TGA analyses and HPLC peptide quantification, the amount oligomers and YIGSR were quantified (see calculations in Appendix B).

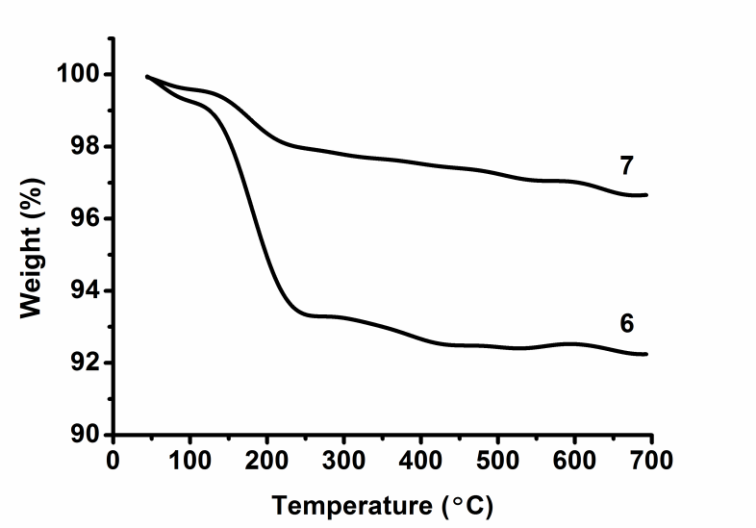

Figure 3.5-TGA curves of Au-OEtOx-SH-YIGSR (**6**) and Au-OEI-CS-YIGSR (**7**).

3.4.2 Evaluation of the cytotoxic profile of the nanogld POXylated particles

Particles biocompatibility (when no drug is used) was accessed by evaluating the metabolic activity of A549 cell line. Briefly, 4 x 10^4 cells/well were seeded in a 96-well plate and cultured with Ham-F12 at 37 ºC under a 5 % CO_2 humidified atmosphere. Then, 200 µg/mL of nanoparticles were added, and the mitochondrial redox activity of the viable cells was assessed through the reduction of the MTS into a water-soluble brown formazan product as previously described. Wells containing cells in the culture medium without materials were used as negative control. EtOH 96 % was also added to some wells, to be used as a positive control.[130] As demonstrated in Figure 3.6, the particles and the oligomers have proved to be biocompatible as cell viability was always above 80 % and even higher after 72 hours. Besides, a significant difference in cell viability was obtained between the positive and negative control ($p < 0.05$), and cells exposed to the different precursors and the nanoparticles after 24 h ($p^* < 0.05$) and 72 h ($p\# < 0.05$) of incubation.

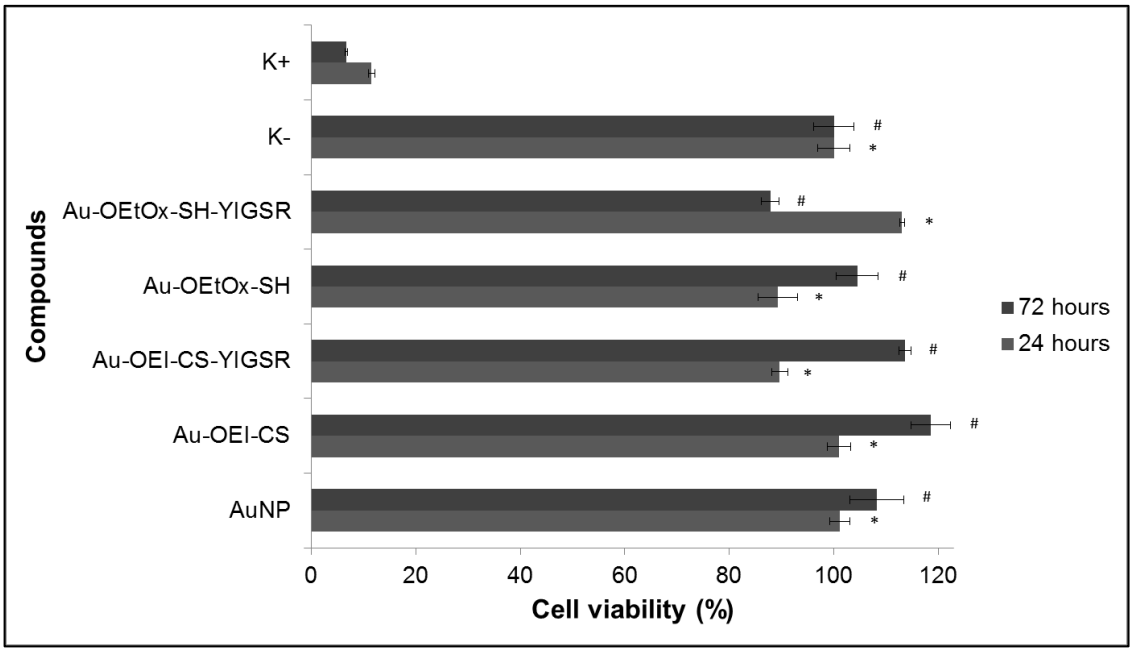

Figure 3.6-Cellular activities measured by MTS assay after 24 h and 72 h in contact with engineered AuNPs and respective precursors. Negative control (K-): live cells (no particles added); Positive Control (K+): dead cells (with 96 % ethanol).

3.5 CONCLUSIONS

In summary, stable, biocompatible and laminin fragment conjugated AuNPs were successfully engineered using fluorescent oligo-oxazolines (PEG alternatives) produced by a $scCO_2$-assisted protocol. Besides avoiding PEG hepatoxicity, nanogold POXylation circumvents grafting with expensive probes and particles fluorescence quenching by the surface plasmon resonance effect. The nanoconstructs have an ideal size for intracellular delivery and the additional conjugation with the laminin fragment strongly increased particles uptake by A549 cell line. Due to their optical and targeted capabilities, future conjugation with therapeutic drugs is envisaged for theragnostic applications, thus fostering efficient, greener, low cost, multifunctional nanocarriers for cancer treatment.

CHAPTER 4. Aerosolizable gold nano-in-micro dry powder formulations: New prospects for lung cancer theragnosis

The contents of this chapter were submitted to a peer reviewed international journal:
A. Sofia Silva, A. M. Sousa, Renato Cabral, Marta C. Silva, S P Miguel, Vasco D.B. Bonifácio, T. Casimiro, Ilídio J. Correia, Ana Aguiar-Ricardo

These results were presented as a poster presentation the International Symposium on Nanoparticles/Nanomaterials and Applications, Costa da Caparica (Portugal), 20th – 22nd January 2014; and as an oral presentation in the XX Encontro Luso-Galego de Química, Porto (Portugal) 26th – 28th November 2014

Keywords: Lung cancer, gold nanoparticles, oligo-oxazolines, nano-in-micro, SASD

Personal contribution

A.Sofia Silva contributed to the design of the study, performed most of the experimental work, co-interpreted the data and wrote the manuscript.

4.1 ABSTRACT

Lung cancer is the most common and prominent cause of cancer death worldwide. The lack of locally and effective deliveries of therapeutic biomolecules to the deep lungs are the major causes of such low survival rates. To address this problem, nanotechnology and pulmonary delivery have been combined to generate effective delivery systems, able to target the deep lungs and exert a positive therapeutic effect in lung cancer regression.

In such attempt, gold nanoparticles (AuNPs), which have been widely investigated as carriers and biosensors for lung cancer treatment, were conjugated with micronization technologies in order to produce respirable microparticles with theragnostic abilities. AuNPs were previously functionalized with "green" biocompatible and fluorescent coatings, and further conjugated with specific sequences for a targeted delivery. The micronization process was achieve using supercritical assisted spray drying (SASD), a process based on sustainable supercritical CO_2 technology. Nano-in-micro formulations comprising a chitosan matrix were successfully produced resulting in clean ultrafine dry powders with adequate aerodynamic sizes (3.2-3.8 μm) and morphologies and excellent fine particle fraction (FPF) (25.8 - 42.4 %). The optimal biodegradation and release profiles enabled a sustained and controlled release of the nanoparticles embedded opening new prospects for future lung theragnosis through the pulmonary route.

4.2 INTRODUCTION

With the significant increase of lung cancer incidence in the past 50 years, among both women and men, there has been a huge demand for the development of new strategies to address this health problem. Due to the limitations associated with the conventional treatment of several diseases, novel pulmonary therapeutics have been vastly investigated as it enables to target the drug delivery directly to the lungs for both local and systemic treatments. Such type of treatment allows for sustained release, reduced therapeutic dose and improved patient compliance. However, the design of inhaled carriers with suitable properties for an accurate deep lung deposition and effective delivery are two of the major challenges that need to be overcome. Respirable formulations should comprise aerodynamic sizes ranging from 1 to 5 μm (dry) in order to successfully reach the lungs, swell upon deposition in the moist lung, and provide a sustained controlled drug release through the polymeric matrix. Such features enable not only a proper delivery of the carriers, as also the avoidance of macrophage uptake.[3,19,32,46,47,152,153]

Nanoparticles have been foreseen as effective platforms to provide a controlled release of drugs or other biomolecules in the lungs. Due to their nanometric scale, nanoparticles can penetrate into the deep tissue and then suffer cellular uptake. Moreover, innovative designs of nanoparticles can allow for the tailoring of multifunctional airway targeting nanocarriers enabling the integration of multiple functions, such as cell targeting, ultra-sensitivity imaging and therapy, all into one system.[152–155]

However, nanoparticles are in a size range which is not suitable for deep lung delivery and can be easily exhaled or mucociliary cleared out before reaching the underlying epithelia.[9,16,42] Therefore, the major challenge for pulmonary delivery of nanoparticles is to find a proper carrier system. Increased effectiveness of an inhalation treatment may be achieved by the quick dissolution of powder particles in the airway mucus and rapid diffusion to the destination tissue.[4] Hence, novel systems incorporating nanoparticles into swellable and respirable micro-scale structures have been engineered to overcome the issues of storing and delivering the drugs and other biomolecules to the lungs. Micro and nano technologies are enabling the design of new materials and methods with enormous impact on medical technology, greatly improving the performance of many existing drugs and enabling the use of entirely new therapies. From all the formulations available for inhalation, dry powders are usually preferred as they exhibit the most suitable behavior for pulmonary delivery such as stability and bioavailability of active ingredients, when compared to their aqueous counterparts. [29,30]

In this contribution, new nano-in-micro platforms were developed for controlling pulmonary delivery and combine both the benefits of multifunctional nanoparticles and the respirable microspheres. The developed systems comprised of targeted and always-on fluorescent gold nanoformulations, already described in our recent works, embedded in a chitosan (CHT) polymeric matrix. The innovative design of our gold nanoprobes (GNP) allow for the integration of both cell targeting (through a laminin fragment receptor known to bind to the overexpress β1 integrins of A549 non-small cell lung cancer[149,150]) and imaging (through the gold core to more advanced imaging techniques[156] and through the conjugation with oligo-oxazolines for fluorescent microscopy purposes[146–148]) for lung cancer screening. In fact, surface functionalized AuNPs have been extensively exploited to face the urgent need to further develop novel multifunctional nanosystem theragnosis of lung complications.[7,8]

CHT is a natural biopolymer obtained through the alkaline N-deacetylation of chitin.[152,157] Although it is not yet approved by FDA for any drug delivery product, it has several desirable advantages, including biodegradability, non-toxicity and biocompatibility. CHT is also pH re-

sponsive and commonly used for smart drug controlled released and different delivery systems have been engineered using supercritical carbon dioxide ($scCO_2$)-assisted processes.[158–160]

These properties together with the mucoadhesive features and ability to improve drug absorption in lung tissues show that CHT is a promising excipient for dry powder inhalation.[158,161,162]

In this study, CHT bearing different formulations of GNP (CHT-GNP) were synthesized in a laboratory scale using SASD apparatus. The resulting micronized powders were fully characterized and evaluated as novel biodegradable systems that confer a controlled and sustained release of the GNP entrapped. The optimal aerodynamic features and performances, nearly match the DPIs currently available on the market. Furthermore, the conjugation of targeted and always-on fluorescent gold nanoformulations with a biodegradable and biocompatible excipient enabled the production of inhaled systems able to interact with cancer cells, bringing new insights for lung cancer screening and treatment.

4.3 EXPERIMENTAPROCEDURE

4.3.1 Materials

Gold in the form of tetra-chloroauric[III] acid trihydrate ($HAuCl_4.3H_2O$) and trisodium citrate hydrate were purchase from Alfa Aesar. Dissodium hydrogen phosphate sodium and sodium chloride was purchased from AppliChem Panreac. Acetic acid glacial (99.7 % purity) was purchased from Carlo Erba Reagents. Ethanol absolute anhydrous (99.9 % purity) was purchased from Scharlau. Ethyl oxazoline monomer, boron trifluoride etherate ($BF_3.Et_2O$), cysteamine, anhydrous dimethylformamide (DMF) dihydrogen phosphate trisodium citrate hydrate, Laminin fragment (Cys-Asp-Pro-Gly-Tyr-Ile-Gly-Ser-Arg) (YIGSR), and lysozyme chloride from Grade VI: from chicken egg white were purchased from Sigma-Aldrich. Chitosan (viscosity 5-20 mPa.s, 0.5 % in 0.5 % acetic acid at 20 °C) was purchased from Tokyo Chemical Industry. Hydranalcoulomat AD from Sigma-Aldrich was used in Karl Fischer. All components were used as received without any further purification. Industrial carbon dioxide (purity ≥ 99.93 %) from Air Liquid (Portugal) was used.

4.3.2 Nanoparticles formulation

The nanoparticles production was already described in CHAPTER 3. Briefly, AuNPs were synthetized according Frens's:[135] 100 mL of 0.01 % (w/v) $HAuCl_4.3H_2O$ were heated to boiling. Then, 1 mL of trisodium citrate hydrate 1 % (w/v) was added to the boiling solution under constant stirring. After 25 seconds, a slightly yellow solution turned faintly blue. Subsequently, the solution color changed to dark red, which is indicative of the formation of monodisperse spherical particles. The solution was boiled over 5 min, to allow the complete reduction of the gold chloride.[135] Afterwards, the nanoformulations were grafted with "green" oligomers synthetized using $scCO_2$, OOxs. OOxs were polymerized in a stainless-steel reactor and OEtOx was produced and $BF_3.OEt_2$ was used as the initiator. The monomer/initiator ratio used for the polymerization was [M]/[I]¼ = 12. The reactor cell was charged with the monomer, the initiator, a magnetic stirring bar, and then immersed in a thermostatized water bath at 60 ºC. Carbon dioxide was introduced in the reactor in order to achieve the desired reaction pressure (from 16 to 20 MPa). After 20 hours of reaction, the pressure was slowly released until the reactor reach room temperature. Inside the reactor, a viscous foam was obtained (OEtOx). At the end of the polymerization, the living oligomer was end-capped either with cysteamine or water, generating OEtOx-SH (**1**) and OEtOx-OH (**2**), respectively. Post-functioalization of **2** with 2,4-dihydroxybenzaldehyde produced a polycationic oligo(ethyleneimine-N-chromylium salt), OEI-CS (**3**). AuNPs were capped with OEtOx-SH (AuNP:OOx molar ratio 1:5000) and OEI-CS (AuNP:OOx molar ratios 1:2500) producing Au-OEtOx-SH and Au-OEI-CS, respectively. Afterwards, the mixtures were collected to 1.5 mL eppendorfs and centrifuged at 13500 x g, for 20 min, at room temperature. The supernatant was removed and the pellet was redispersed in milliQ water. Further conjugation of the produced particles with a YIGSR, known to bind to the overexpress β1 integrins of A549 non-small cell lung cancer,[13,163] was also performed, producing Au-OEtOx-SH-YIGSR and Au-OEI-CS-YIGSR. The mixtures were allowed to stir during 16 hours at room temperature under dark conditions. The resulting mixtures were centrifuged at 13500 x g and ressuspended in milliQ water.[11]

4.3.3 SASD process and apparatus: Production of chitosan microparticles

Dry powder formulations were prepared using SASD, in which solutions of CHT (0.06 % w/v) and nanoformulations differently functionalized (9 % v/v) were prepared in 1 % acid water and 18.6 % (v/v) of ethanol and homogenised under stirring. Liquefied CO_2 is pumped with a high-pressure liquid pump (HPLC pump K-501, Knauer), which is then heated and sent to the static mixer (model 37-03-075, Kenics-Chemineer, 4.8 mm ID x 191 mm L, 27 helical mixing elements). The casting solution containing both nanoparticles and chitosan was pressurized

through a high pressure pump (HPLC 305, Gilson) to the static mixer that promotes a near-equilibrium mixing of $scCO_2$ and the liquid solution. Pressure is measured with a Setra pressure transducer (0.1 psig stability). The solution was then sprayed through a 150 μm diameter nozzle into a thermostated aluminum precipitator (± 0.1 ºC), operating at near atmospheric pressure, where particles are formed by drying the droplets using a heated air flow (70 °C). The formed particles exit the precipitator from the bottom and enter into a cyclone where they are separated from the gas stream and collected in a reservoir and in a filter bag (FSI, nylon mono-filament, 50 μm).[164] T_{mix} = 70 °C; T_{preci} = 90°C; p_{CO2} = 10 MPa.

4.3.4 Morphological and physical-chemical characterizations

Particle size analysis (sieve and Feret's diameter) was determined using an optical particle analyzer system (Morphologi G3 Essentials, from Malvern Instruments Ltd). The particles were characterized by the volume mean diameter (D_v) and the relative width of the distribution (span), calculated as follows:

$$Span = \frac{D_{v,90} - D_{v,10}}{D_{v,50}} \qquad \text{Equation 4.1}$$

where $D_{v,90}$, $D_{v,10}$ and $D_{v,50}$ are the diameters at 90 %, 10 % and 50 % cumulative volume. To observe morphology, the microparticles were imaged via scanning electron microscopy (SEM) (Hitachi, S-2400 instrument) with an accelerating voltage set to 15 kV and various amplifications. All the samples were mounted on aluminum stubs using carbon tape and were gold coated priori analysis.[165]

FTIR spectra were recorded in a Nicoletis 20 spectrophotometer (64 scans) equipped with a Smart iTR auxiliary module (ThermoScientific).

X-ray powder diffraction (XRD) analysis was performed in a RIGAKU X-ray diffractometer (model Miniflex II). Samples were placed in a holder and analyzed through CuKα radiation (30 KV/15 mA), with a 2θ angle ranging between 2° and 55° with a scan rate of 1°/min.

Moisture content of each formulation was accessed using Karl Fischer assay (Metrohm). 1.5 mg of powder were accurately weighted and introduced in the reaction cell. Moisture content was determined by subtracting the background signal.[36,166]

4.3.5 Entrapment Efficiency

The entrapment efficiency was determined by measuring the amount of Au atom (mg/L) using Inductively Coupled Plasma-Atomic Emission Spectrometer (ICP-AES) from Horiba

Jobin-Yvon (model Ultima). Briefly, powder samples (20 mg) were dissolved in 1 mL of *aqua regia* solution overnight. GNP precursors from each sample were used as controls. Based on the ICP results it was possible to calculate the amount of Au (in mg) entrapped within the microcarriers. The entrapment efficiency (E%) of Au atom was calculated as follows:

$$E\% = \frac{m_r}{m_i} \times 100 \qquad \text{Equation 4.2}$$

where m_r is the amount of Au remaining within the particles and m_i is the Au amount loaded into the casting solution. This percentage matches the percentage of the whole GNP entrapped.

4.3.6 *In* vitro aerosolization study

An *in vitro* dry powder aerosolization study was carried out for the nano-in-micro formulations using a seven stages Andersen Cascade Impactor (ACI) (Coopley Scientific). In a typical procedure 30 mg of powder were loaded into 5 hydroxypropylmethylcellulose capsules (Aerovaus). The capsules were individually placed in a handheld, dry powder, breath activated inhaler device (PlastiApe device HR model 7), previously weighted, which is coupled to the ACI device. The 7 metal plates within the cascade impactor were covered with pre weighted glass microfiber filters (MFV1 diameter 80 mm, Filter Lab). The DPI punctures the capsule prior to the inhalation and a high capacity pump is actuated to simulate an inspiration: air flow rate 60 L/min during 4 s, according to the European pharmacopeia.[167] After the dispersion, the filters and the dry powder inhalers (DPI) were weighted again. The emitted dose (ED %), which corresponds to the total loaded powder mass exiting the capsules and inhaler, was determined gravimetrically and can be expressed as follows:

$$\mathrm{ED}(\%) = \frac{\mathrm{m_{full}} - \mathrm{m_{empty}}}{\mathrm{m_{powder}}} \times 100 \qquad \text{Equation 4.3}$$

where m_{full} and m_{empty} are the weights (mg) of the capsule before and after simulating the inhalation and m_{powder} is the initial weight (mg) of the powder in the capsule.

The FPF was determined by the interpolation of the percentage of the particles with less than 5 μm diameter emitted from the capsules in each ACI experiment. The Mass Median Aerodynamic Diameter (MMAD) was determined as the particle diameter corresponding to 50 % of the cumulative distribution. The Geometric Standard Deviation (GSD) was determined by the following equation:

$$GSD = \sqrt{\frac{d_{84}}{d_{16}}} \qquad \text{Equation 4.4}$$

where d_{84} and d_{16} are the diameters corresponding to 84 % and 16 % of the cumulative distribution, respectively.

4.3.7 *In vitro* cumulative release studies and nanoparticles stability

The release of GNP from the microspheres was evaluated at two distinct pHs: 7.4 and 6.8, pH of healthy cells and pH of lung cancer cells, respectively. Approximately 20 mg of the powders were transferred to a special membrane size cut off 1 μm, and incubated in 1.5 mL of different pH solutions in a shaking (35 rpm) water bath at 37 ºC. Then, the samples were centrifuged at 14500 x g for 20 min and the supernatant was removed. Afterwards, 30 μL of the correspondent buffer solutions were added to resuspend the pellet. The samples were placed in a 384 Well Black with clear flat bottom polystyrene and read UV-Vis spectrophotometer microplate reader. From the absorbance obtained and from the previous ICP results (initial amount of Au or nanoformulations entrapped) it was possible to calculate the amount of nanoparticles (in mol and in mg) being released from the microcarriers. UV-visible spectroscopy was recorded in an Infinite 200 from Tecan using a corning 384 flat bottom black polystyrene low volume/flat microplate, kindly provided by Corning Corporation. The test was performed in a method from 260 to 700 nm.

Nanoparticles release from swelling-controlled systems was modelled by the Korsmeyer-Peppas equation as follows:

$$\frac{M_t}{M_\infty} = kt^n \qquad \text{Equation 4.5}$$

where M_t/M_∞ is the fraction of the drug release at time t, *k* is the rate constant and *n* is the diffusional exponent. The *n*-value is obtained from the slope of the Korsmeyer-Peppas plot and represent different release mechanisms. For spherical geometries: n = 0.43 for Fickian diffusion; 0.43 < n < 0.85 for anomalous non-Fickian diffusion; n = 0.85 for Case-II transport.[168,169]

4.3.8 *In Vitro* Biodegradation Studies

An *in vitro* biodegradation study of the microparticles was carried out in the presence of lysozyme. A solution of lysozyme in PBS (pH 7.4) was prepared (0.2 mg/mL) and 20 mg of microparticles were transferred to eppendorf tubes and incubated in 1.0 mL of lysozyme solu-

tion in a shaking (100 rpm) water bath at 37 °C for 30 min. Then, the samples were centrifuged at 13,500 rpm for 8 min and the supernatant was removed. The weights of the swollen microparticles (W_0) were determined. Then 1 mL of fresh lysozyme solution was added to the swollen microparticles. At certain intervals starting from determination of W_0, the steps of centrifugation and weighing were repeated and the final weights (W_t) of microparticles at these intervals were determined. The percent weight remaining of the samples due to enzymatic degradation was determined according to the following equation:

$$Wr\% = 100 - \frac{W_0 - W_t}{W_0} \times 100 \qquad \text{Equation 4.6}$$

where W_0 is the weight of sample after 1 h swelling in lysozyme solution and W_t is the weight of the sample after incubation with lysozyme for a given time t.[152]

4.3.9 Confocal Laser Microscopy (CLSM): nano-in-micro cell interactions with cells environment

Cell culture experiments were performed using of A549 cell line. Cells were cultured in Ham's Nutrient Mixture-F12 medium supplemented with 10 % v/v heat-inactivated FBS and 1 % of antibiotic-antimycotic (penincilin G (100 U/mL)), spectromycin G (100µg/mL)) at 37 °C, under 5 % CO_2 humidified atmosphere.[155]

Microparticles' interactions with cells and consequent nanoparticles' release and cellular uptake were qualitatively assessed using a Zeiss LSM 710 laser scanning confocal microscope (Carl Zeiss SMT Inc.) equipped with a plane-apocromat 40 x/DIC objective. Priori to cellular incubation with the nano-in-micro formulations, cells cytoplasm was marked with CellLight® Actin-GFP, BacMam 2.0 (GFP). Immediately afterwards, cells were seeded in glass bottom dishes cells dispensed by MatTek Corporation (Ashland), at a density of 4 x 10^3 cells/cm^2 per well in Ham's Nutrient Mixture-F12 medium supplemented with 10 % v/v heat-inactivated FBS. Twenty four hours later, nano-in-micro formulations (1 mg/mL) were added. After 4 h, microparticles interactions with cells were qualitatively evaluated. Nano location within the microparticles was also assessed using CLSM. Data analysis of CLSM images was performed with Zeiss software (Axio Vs40 V4.5) and Imaris Bitplane (Vs7.6.1, Bitplane).Cellular uptake for the nanoparticles alone was also investigated in our previous works (CHAPTER 3).

4.3.10 Evaluation of the cytotoxic profile

An MTS assay was performed to evaluate nano-in-micro formulations biocompatibility. Twenty four hours prior to the experiment the cells were seeded at a density of $4x10^3$ cells per well into 96-well plates (Orange Scientific) with 200 µL of cell culture medium supplemented with 10 % FBS and 1 % of antibiotic-antimycotic (penincilin G (100 U/mL), spectromycin G (100 µg/mL)). Formerly, 1 mg/mL of microparticles were added to wells and incubated with cells at 37 °C in a 5 % CO_2 humidified atmosphere, for 3 days.

After 1 and 3 days of incubation, the culture medium was removed and replaced by a mixture of 100 µL of fresh culture medium and 20 µL of MTS/PMS (phenazine methosulfate) reagent solution. A total of three replicates were considered for each formulation. The absorbance of the samples was measured at 492 nm using a microplate reader Anthos 2010 (Biochrom). A similar procedure performed for the nanocarriers was previously reported in CHAPTER 3. Wells containing cells in the culture medium without materials were used as negative control. Ethanol (EtOH) 96 % was added to wells containing cells as a positive control.[130]

4.3.11 Statistical Analysis

All statistical analysis, unless noted, (GraphPad, Prism and Origin) were performed using one-way ANOVA analysis of variance following the Bonferroni post-hoc test with a significant set at $p<0.05$.

4.4 RESULTS AND DISCUSSION

4.4.1 Microparticles morphology and physical-chemical characterization

The volume mean diameter (D_{v50}) represents 50 % of a cumulative distribution of microparticles' diameter and it can provide an appropriate estimation of particle size for dry-powder inhalation purposes. Microparticles produced by SASD technology have no significant differences between the volume mean diameters, ranging from 3 to 4 µm ideal for inhalation devices. Similar span values were obtained for all types of chitosan microparticles herein engineered, with the exception of CHT-Au, indicating that they have the same distribution width (Figure 4.2). The production yield of the nano-in-micro formulations achieved for this process was between 57 to 75 %. All is displayed in the Table C.1 in Appendix C.

The entrapment of produced gold nanoprobes, was determined through ICP analysis. Briefly, approximately 20 mg of powders were degraded in fresh aqua regia and gold atom (Au) content was measured and compared to the amount of Au existing in each GNP precursor (measurements performed priori to GNP encapsulation). The results are also displayed in Table 4.1. GNP's entrapment values vary among the samples being the highest value 51.8%. Such result implies that the remaining GNPs were lost during powder formation, either by leaving the system with the CO_2 flow or by degradation. Interestingly, the addition of laminin fragment (YIGSR) to the nanoparticles increases their encapsulation into the micropowders. Further calculation and measurements are displayed in Table C.2 (Appendix C).

Table 4.1-Nano-in-micro formulations, physical characteristics.

Sample	**$D_{v,50}$ (μm)**	**Span**	**Encapsulation Efficiency (%)**	**Moisture Content (%)**
CHT	3.6	1.3	-	15.4
CHT-Au	3.2	2.9	34.7	14.8
CHT-Au-OEI-CS	3.7	1.7	17.2	12.4
CHT-Au-OEI-CS-YIGSR	3.4	1.7	51.8	16.2
CHT-Au-OEtOx-SH	3.8	1.4	38.6	14.9
CHT-Au-OEtOx-SH-YIGSR	3.4	1.7	46.5	12.5

All CHT-AuNP microparticles produced under the specified conditions are spherical, with mean diameters between 3.2 and 3.8 μm and have smooth surface as shown in SEM images in Figure 4.1.

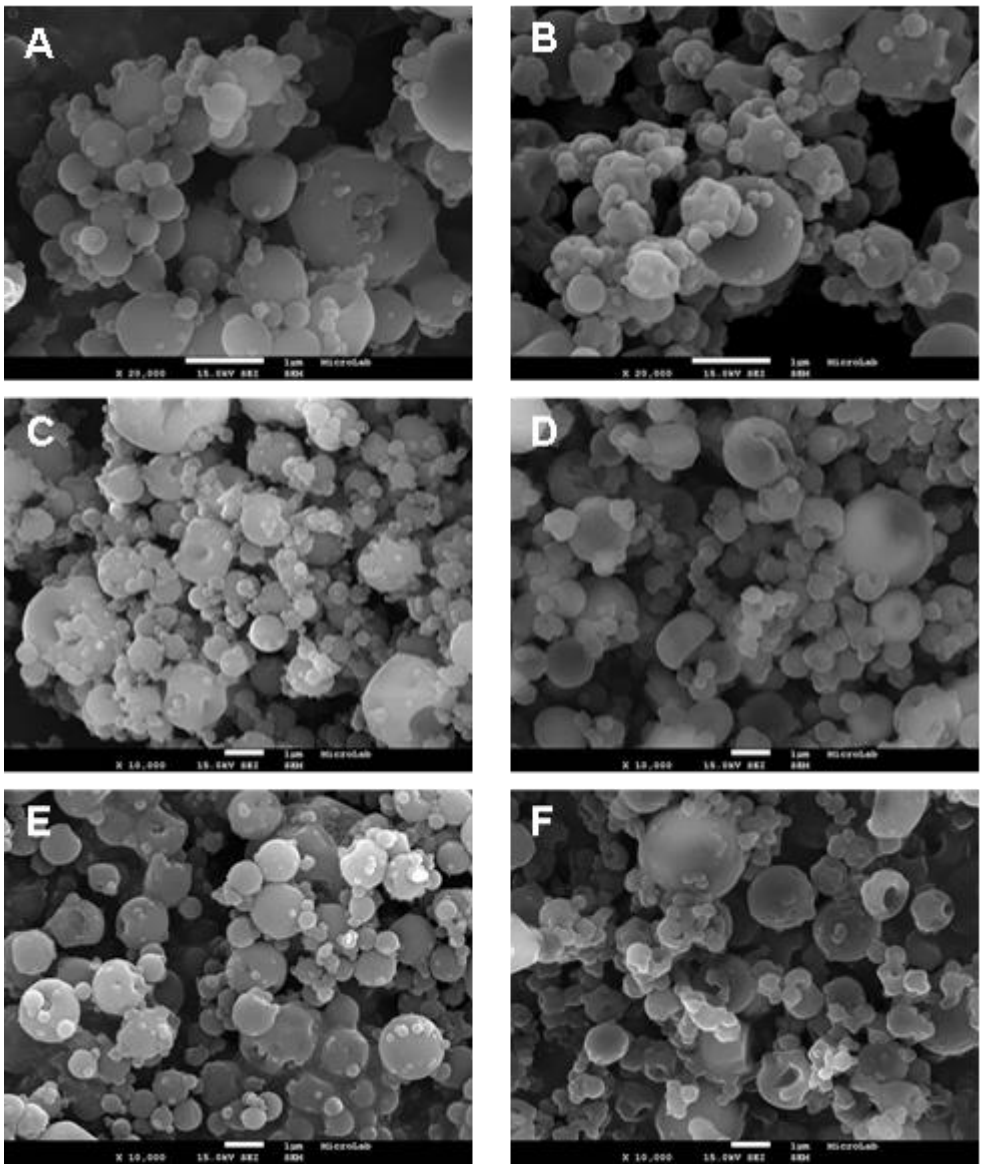

Figure 4.1-SEM images of the produced microparticles: (A) CHT; (B) CHT-Au (x 20 000); (C) CHT-Au-OEtOx-SH; (D) CHT-Au-OEtOx-SH-YIGSR; (E) CHT-Au-OEI-CS; (F) CHT-Au-OEI-CS-YIGSR (x 10 000).

The moisture content of each formulation was accessed through the Karl Fisher assay and found to be in the range of 12.4 – 16.2 %. The XRD patterns for all the formulations are displayed in Figure C.1 (Appendix C). Figure C.1A shows the crystallinity pattern of nude AuNP.[170] Upon co-atomization with CHT, no crystalline peaks are presented in all the formulations (Figure C.1B) with the exception of CHT-Au-OEI-CS. This particular pattern shows both the broadening at 20º, characteristic of processed CHT, and the characteristic peaks of AuNP. Slight deviations may be a result of nanoparticles interactions with the polymeric chains involving the nanosystems (either CHT or OEI-CS). The low encapsulation efficiency demonstrated

by this particular formulation may be a consequence of such interactions resulting in a pronounced crystalline arrangement. All the other CHT-GNP formulations do not show any crystalline pattern, exhibiting only the amorphous state of processed CHT (broadening at $2\theta = 20^{o}$). The importance to have an amorphous carrier for lung delivery applications has been widely reported in the literature. Such amorphous state is responsible not only for stabilizing the Active Pharmaceutical Ingredient (API), but it also increases the dissolution rate and it has high water adsorption capacity, contributing for a sustained release and rapid cellular absorption. On the other hand, the API is usually preferred in a crystalline form, since it maintains the bioavailability of the drug, maximizing its efficiency and minimizing the required dosage.[32,153]

FTIR-ATR spectra of the powders were also acquired and can be found in Figure C.2 (Appendix C). The resemblance between the acquired spectra, either for CHT or CHT-GNP powders is evident and can be explained by the large amount of chitosan in comparison to the engineered nanoparticles. In turn, FTIR-ATR spectra of the nanoformulations were already discussed in our previous chapter.

4.4.2 *In vitro* aerosolization study

The powder aerosolization characteristics of the CHT-GNP formulations were assessed *in vitro* using a dry powder breath activated inhaler device with the aid of an Anderson Cascade Impactor. The percentage of powders deposited on each stage of the ACI, inhaler, capsule and induction port was calculated gravimetrically and is plotted on Figure 4.2.

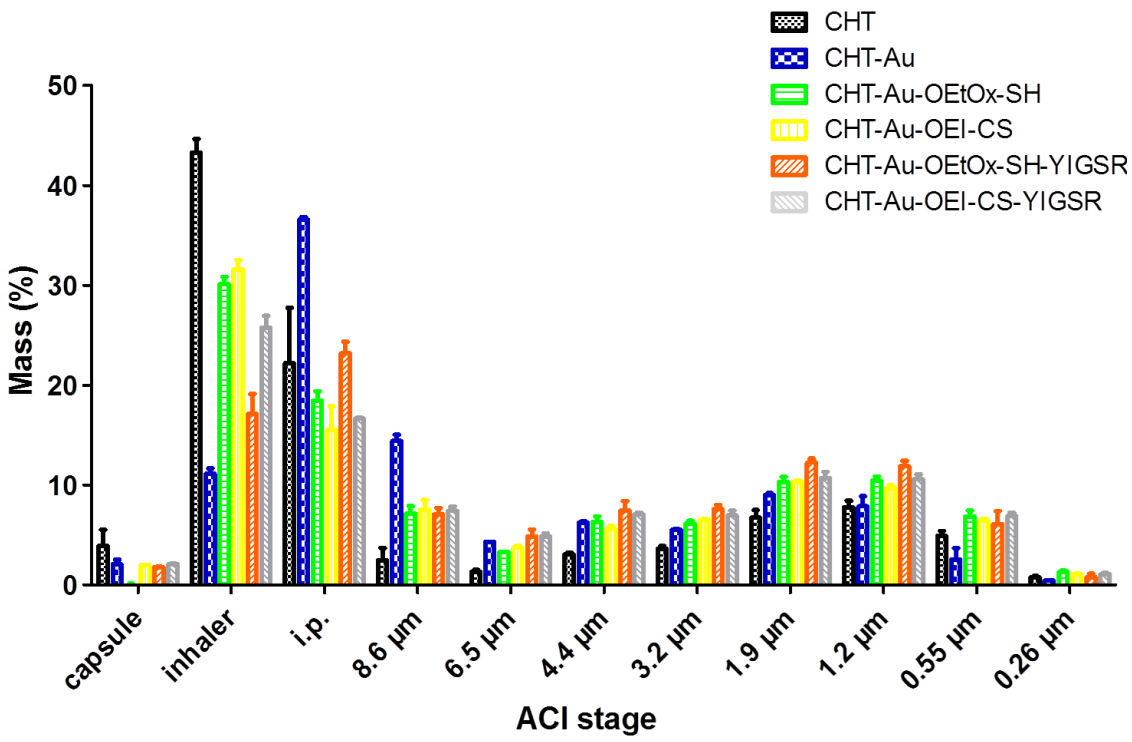

Figure 4.2-Powder dispersion among the different micronized powders by ACI.

Cascade impaction measurements displayed on Table 4.2 were obtained through dispersion of 4 consecutive capsules (n = 3). The emitted dose (ED) which comprises the amount of powder that fluidize through the inhaler varied between 66 ± 2 % and 86.8 ± 0.3%. It was also found for these formulations that the FPF, the respirable fraction that is most likely to deposit in the deep lung, was 26 ± 2 % to CHT and between 32.8 ± 0.4% and 47 ± 2 % for all CHT-GNP formulation, matching almost the already marketed DPIs currently available.[152,153] In Figure 4.2 it can be seen that the majority of the powder is lost in the induction port, which simulates the upper airways. Such event may be due to the formation of turbulent eddies in this area, humidity or chitosan mucoadhesive property. The Au content (mg) in each stage of the ACI for each different formulation was also assessed and its distribution is depicted in Figure C.3, (Appendix C). The obtained Au dispersion among the different stages is in accordance with the cascade impactor measurements displayed on Table 4.2.

Table 4.2-Cascade Impactor Measurements.

Sample	ED (%)	FPF (%)	MMAD (μm)	GSD
CHT	75±2	26±2	1.40±0.04	2.9±0.1
CHT-Au	86.8±0.3	32.8±0.4	3.2±0.1	2.8±0.1
CHT-Au-OEI-CS	66±2	41±1	1.5±0.1	3.3±0.1
CHT-Au-OEI-CS-YIGSR	72.2±0.1	47±2	1.8±0.07	3.1±0.1
CHT-Au-OEtOx-SH	70.2 ± 1	42±3	1.3±0.2	3.3±0.1
CHT-Au-OEtOx-SH-YIGSR	81±1	47±2	1.8±0.2	2.9±0.1

4.4.3 Statistical analysis of the cascade impactor measurements

The obtained cascade impactor measurements were analyzed using Graph Pad, performing a one-way analysis of variance (ANOVA) with a Bonferroni's multiple comparison test for a significance level of 5 %. The incorporation of nude AuNP into CHT microspheres causes a significant difference ($p < 0.001$ ***) in the mass median aerodynamic diameter of the particles for higher values. However, the formulations containing Au-OEI-CS or Au-OEtOx-SH decreases again the MMAD to similar values to the ones presented for CHT microspheres not showing, therefore, any significant difference with CHT or among each other, but presenting a high significance when compared to CHT-Au ($p < 0.001$ ***). New incorporations of the GNP containing YIGSR increase again the MMAD. For instance, there is a high significant difference between CHT-Au-OEtOx-SH-YIGSR with CHT ($p < 0.01$ **), CHT-Au-OEtOx-SH, CHT-Au ($p < 0.001$ ***), but there is no significant difference with CHT-Au-OEI-CS-YIGSR. This last one formulation also shows a significant difference with CHT-Au ($p < 0.001$ ***), CHT ($p < 0.05$ *) but no significant difference with CHT-Au-OEI-CS. The differences noticed may be a result of the oligomers interaction with YIGSR and they together interaction with CHT.

A similar trend is observed for the ED of the particles. There is a significant difference between CHT microparticles and all the formulations with an exception of CHT-Au-OEI-CS-YIGSR. The encapsulation of AuNPs in CHT microspheres increases the ED of the powders. However the addition of the oligomers decreases such emitted fraction, which increases again with the grafting of YIGSR in the nanoformulations, to values similar to the ones observed for CHT only (the significance value for CHT-Au-OEtOx-SH-YIGSR is $p < 0.05$ *).

The incorporation of AuNP does not show any statistical significance of powders' FPF. However, the addition of the oligomers and peptide sequence significantly increases the FPF of the powders ($p < 0.001$ ***).

The geometric standard deviations (GSD) of the engineered powders shows a significant difference between CHT and CHT-Au-OEtOx-SH ($p < 0.001$ ***) and CHT-Au-OEI-CS ($p < 0.05$ *) for higher values of this parameter. The incorporation of the YIGSR lowers again the GSD of the powders, existing therefore no statistical significant difference between the complete formulations and the CHT microparticles.

4.4.4 *In vitro* cumulative release studies

The cumulative release profile of the nanoparticles from the microformulations is depicted in Figure 4.3. Two different pHs were used in this particular study: physiological pH (7.4) and a more acidic pH to mimic the lung-lining fluid of a lung cancer situation (6.8). For this *in vitro* release study only 3 formulations were investigated: CHT-Au, as a control sample; and both CHT-Au-OEtOx-SH-YIGSR and CHT-Au-OEI-CS-YIGSR since they are the more completed formulations and the ones of interest in cellular applications. The release profile was monitored by measuring the amount (mg) of the Au atom released from the microsystems. Briefly, the amount of particles released was monitored through a UV-Vis spectrophotometer microplate reader. The characteristic UV-Vis spectra (with the AuNP characteristic peak) were observed in all time points taken, allowing for a monitoring of GNP stability (data not shown). Based on the peak absorbance of the released particles ($\lambda = 530$ nm), and the amount of gold of the initial solution (corroborated either through UV-Vis and ICP) a calibration curve was created and all the concentrations, and therefore masses, released along the time were acquired and compared to the total amount of Au atom existing in the same amount of each powder (measured through ICP).

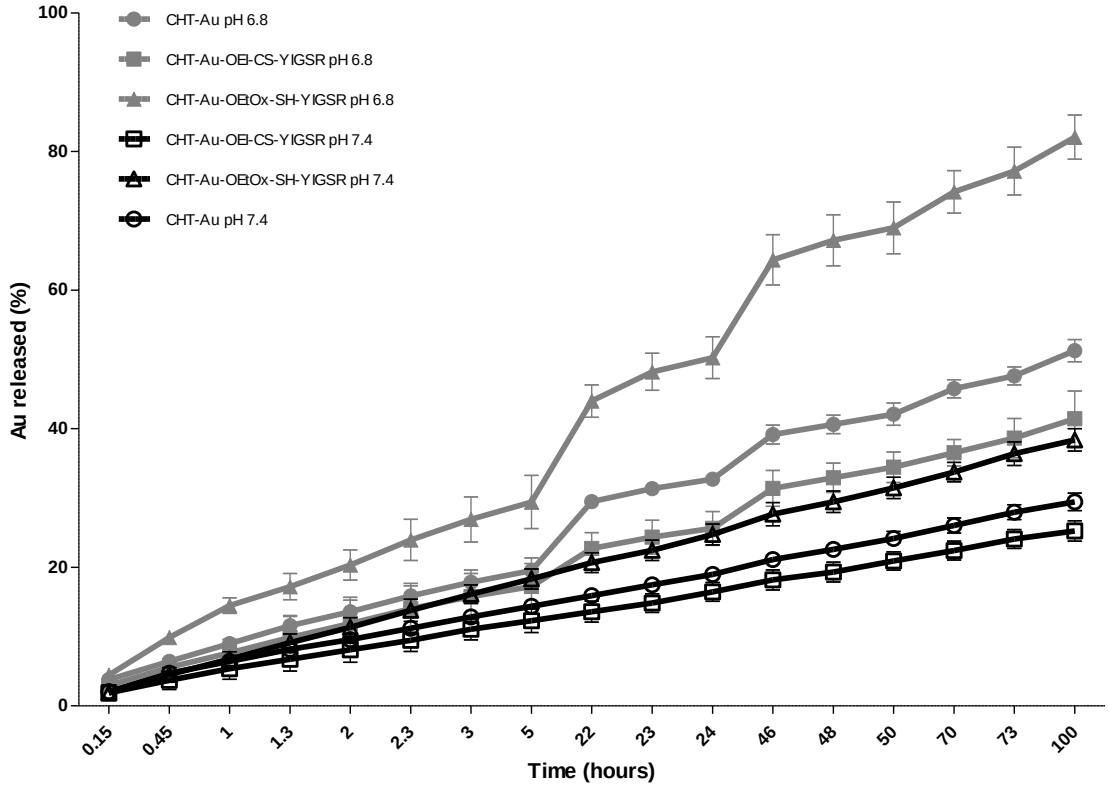

Figure 4.3-Au release profile from CHT microspheres at two distinct pHs (6.8, full symbols and 7.4, open symbols).

As shown in the figure, the release profile for pH 7.4 is similar among all samples and the amount of gold released was varied between 25 to 29 %. As for pH 6.8, the amount of gold released during the 4 days presents different values for the different formulations: 55 % for CHT-Au; 44 % for CHT-Au-OEI-CS-YIGSR; and 90 % for CHT-Au-OEtOx-SH-YIGSR. The different Au release profiles may be explained by the different polymeric arrangement of the nanoformulations, which results in different nano-in-micro interactions. For instance, the aromatic groups in OEI-CS may contribute to a more hydrophobic character of the oligomer which leads to a slower release when compared to OEtOx-SH and even nude AuNP.

CHT pKa is known to be around 6.5. Therefore, at pH 6.8, CHT amino groups are partially protonated turning the powders matrix more hydrophilic than at pH 7.4 where the amino groups are mainly deprotonated. Such effect on CHT amino groups appears to cause a faster release at pH 6.8 than at pH 7.4.

The diffusion mechanism of the nanoparticles through the microcarriers was evaluated by fitting the obtained data with Korsmeyer and Peppas equation, as displayed in Figure C.4 (Appendix C). Based on the diffusion exponent (n) of all the formulations (between 0.33 and

0.41) the release of the nanoparticles from the micropowders occurs through Fickian diffusion.[169]

4.4.5 *In* vitro biodegradation study

The *in vitro* enzymatic degradation study of the developed formulations was carried out in PBS, pH 7.4 in the presence and absence of 2 mg/mL lysozyme as already described in the literature.[152,171] In this study, the remaining weight percentage of the microparticles as a function of time was determined and taken as a measure of degradation. Figure 4.4 shows the degradation profiles of the three chosen formulations in the two mediums mentioned.

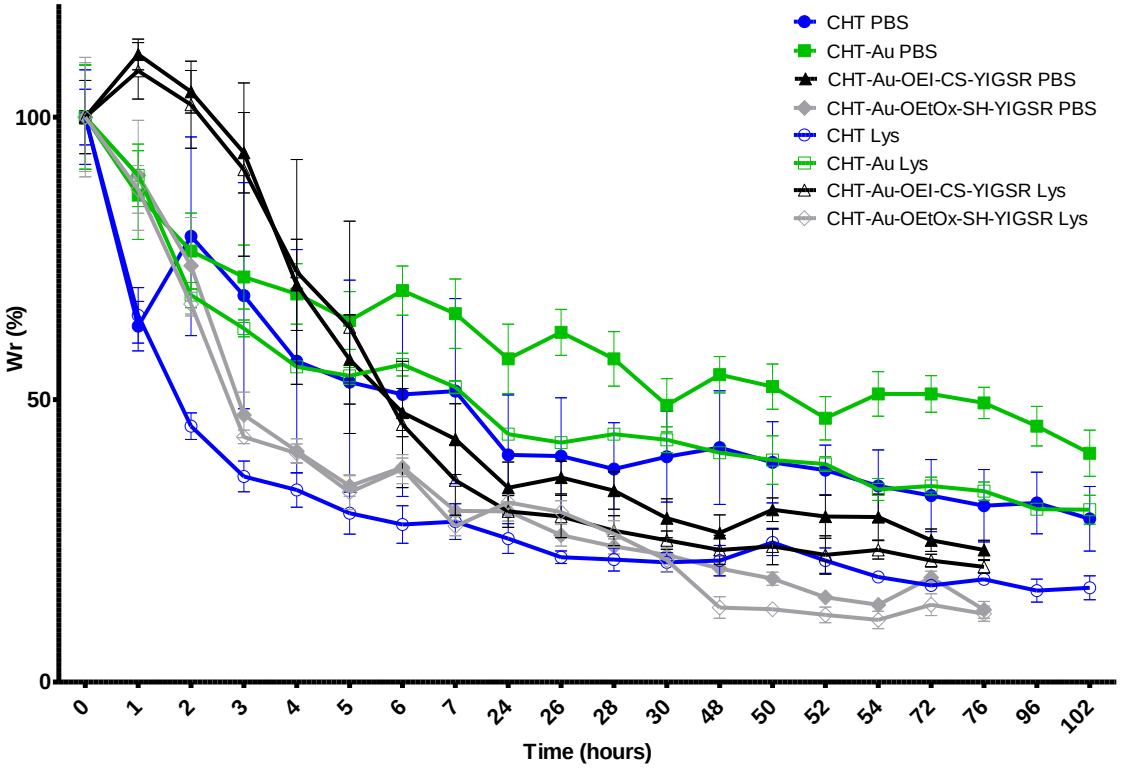

Figure 4.4-Degradation profile of micronized powders, in the presence of lysozyme (Lys) and absence (PBS).

The degradation rate in the presence of lysozyme is higher than in PBS for formulations CHT and CHT-Au. Lysozyme reacts with CHT, hydrolyzing the glycoside bonds between the glucosamine and acetylglucosamine units.[172] CHT-Au formulation is the less degradable formulation. Nude AuNPs (with no coating) incorporation tends to reduce the degradation rate which

may be attributed to a steric hindrance stabilized that tend to hinder the diffusion of the enzyme through the matrix of the microspheres and consequently retarding their degradation. On the other hand, Au-OEtOx-SH-YIGSR and Au-OEI-CS-YIGSR encapsulation into CHT microspheres seems to be similar in both PBS and Lys and the degradation rate increases to more than 80 %. It is hypothesized that oligomers and peptide encapsulation may cause a similar degradation trend in both media.

4.4.6 Nano-in-micro: Nano location within microspheres and powders interaction with cells environment

To address nanoparticles location within the microsphere and the powder formulation interaction with cells environment, CLSM was used.

The whole microsphere was placed on glass-bottomed coverslips containing culture media. The particles were immediately visualized under CLSM and their images can be depicted in Figure 4.5. Chitosan autofluorescence in DAPI region enabled the localization of whole particles (Figure 4.5A). Oligo-oxazolines (OOxs) are also fluorescent in the blue region. However, based on both systems own fluorescence it was possible to separate both channels using Zeiss confocal software and no channel's overlapping was observed (λ_{exc} of the laser = 405 nm; λ_{emm} for OOx = 435 nm; λ_{emm} for CHT autofluorescence = 495 nm). As already discussed in CHAPTER 3 the distance placement of the carbamic moiety in OOx (responsible for its fluorescence) enables the creation of new GNP non-quenched by the gold core. Due to this extraordinary feature, these new GNP were encapsulated within CHT microspheres and their always-on fluorescence was confirmed through CLSM (Figure 4.5B and D). Respective 3D reconstructions are displayed in Figure 4.5C and E, respectively. No 3D reconstruction of CHT microspheres was possible due to the photobleaching of CHT autofluorescence that occurs over time.

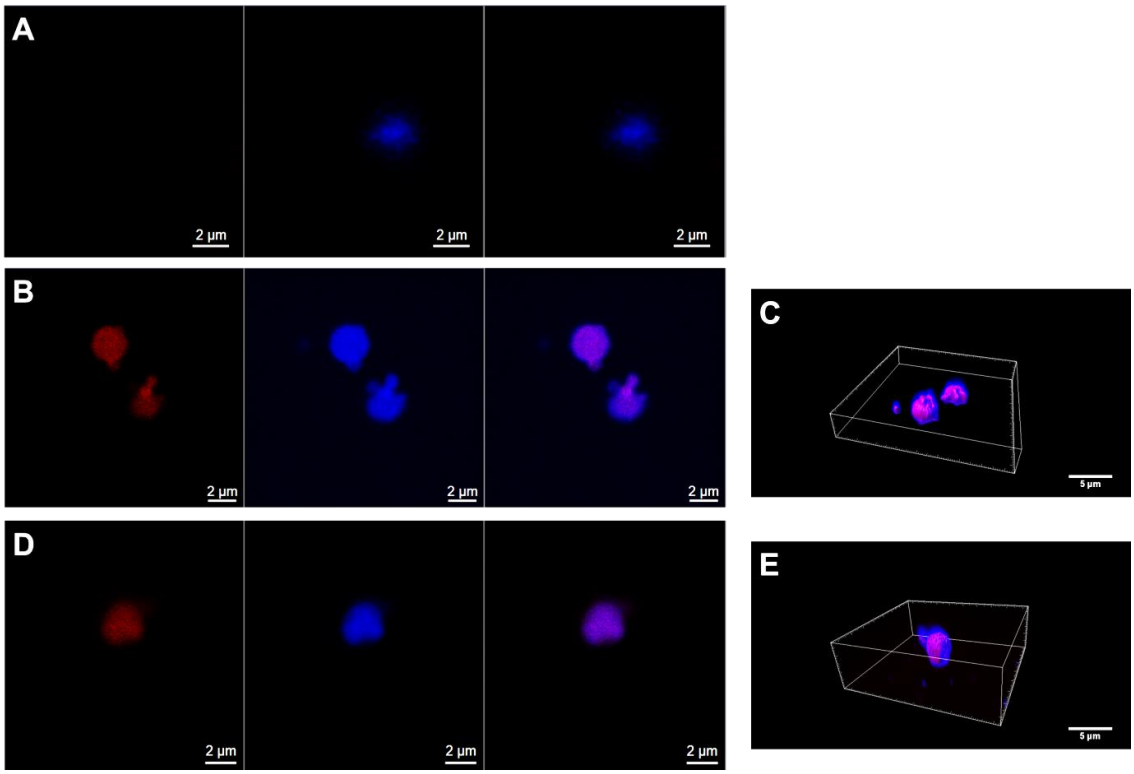

Figure 4.5-CLSM images of the produced microspheres: (A) CHT, (B) CHT-Au-OEtOx-SH-YIGSR and (D) CHT-Au-OEI-CS-YIGSR microspheres. 3D reconstructions of B and D are displayed in (C) and (E), respectively.

The CHT-Au-OEtOx-SH-YIGSR and CHT-Au-OEI-CS-YIGSR formulations were also placed in contact with cells environment (Figure 4.6A and B, respectively). As it can be seen, the engineered formulations were able to adhere to cells surface. The ability for such nanoparticles to enter successfully to cells environment was already discussed in CHAPTER 3.

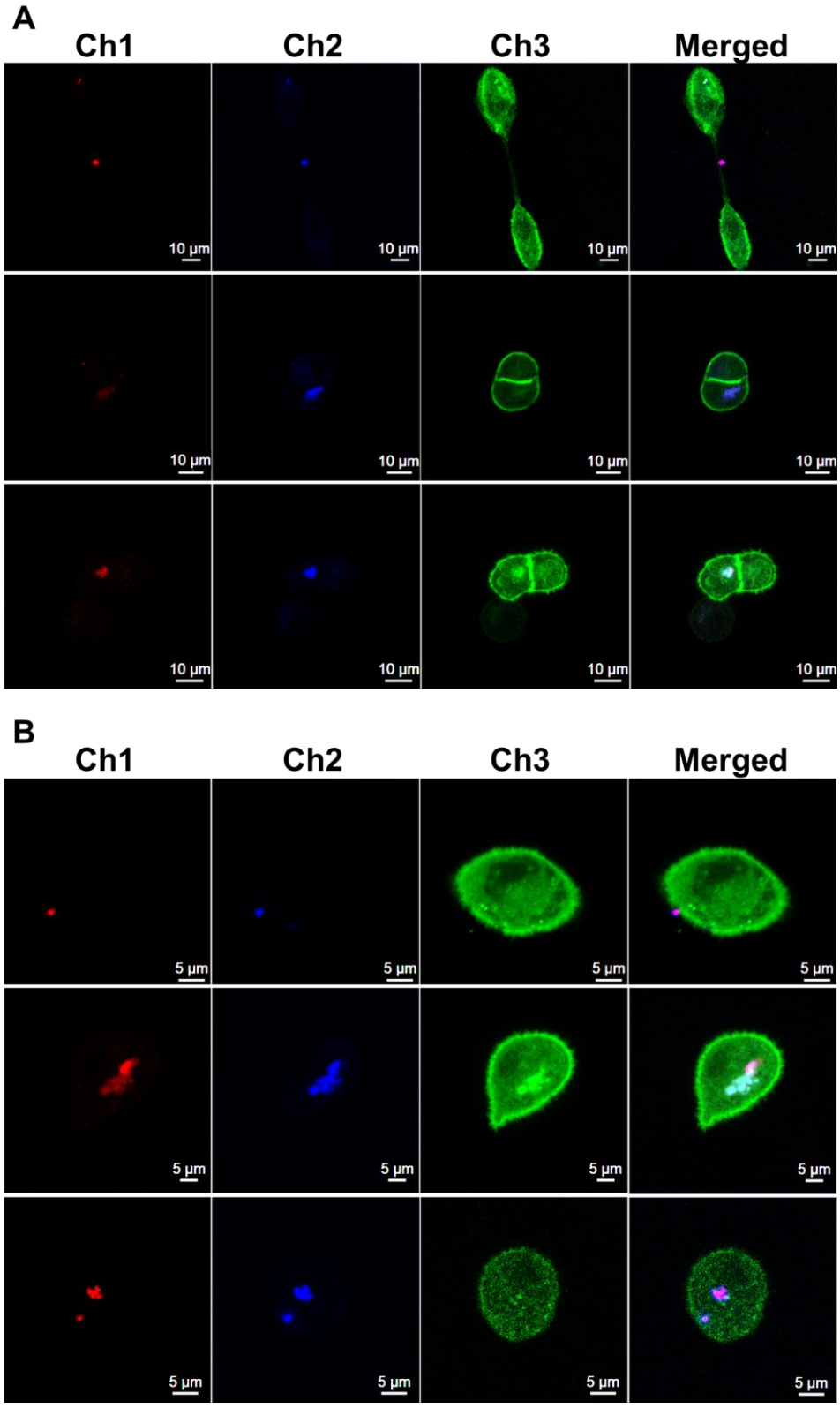

Figure 4.6-CLSM of A549 cell line incubated with 1 mg/mL of micronized powders: (A) CHT-Au-OEtOx-SH-YIGSR and (B) CHT-Au-OEI-CS-YIGSR. Ch1 – channel 1, red: GNP (λ_{emm} = 435 nm); Ch2 – channel 2, blue: CHT autofluorescence (λ_{emm} = 495 nm); Ch 3 – channel 3, green, A549 cell line marked with CellLight® Actin-GFP; Merged: channels overlapping.

4.4.7 Metabolic activity of A549 cell line in the presence of the microspheres

The cytotoxic profile was assessed through an MTS assay (Figure 4.7). Cells in contact with the microparticles showed higher cell viability than the positive control (K+) (ethanol) and similar or slightly above (108 %) the negative control (K-) (culture medium) during the period of incubation (72 h). Nanoparticles and the oligomers used for their synthesis have already proved to be biocompatible in CHAPTER 3. Their incorporation into chitosan microspheres do not seem to alter their biocompatibility, as cell viability is above 80 % for all samples. Besides, a significant difference in cell viability was obtained between the positive and negative control ($p < 0.05$*), and cells exposed to the different microsystems after 24 h ($p < 0.05$*) and 72 h ($p < 0.05$*) of incubation.

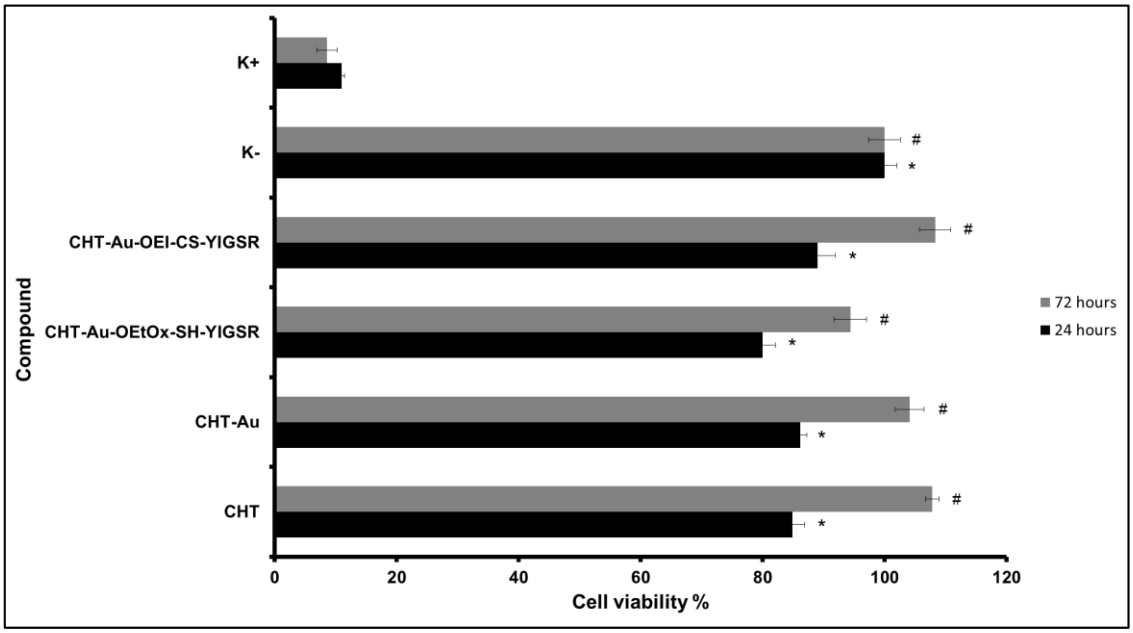

Figure 4.7- Metabolic activity of A549 cell line measured by MTS after 24and 72 h in contact with the micronized powders. Positive control (K+); Negative control (K-).

4.5 CONCLUSIONS

In the present work, CHT-GNP microparticles were successfully engineered through sustainable methodologies in a lab scale SASD apparatus. The obtained micronized powders exhibit appropriate morphological characteristics, as well as adequate aerodynamic and delivery performances. The sustained release profile observed at both pHs showed that CHT is a suitable carrier to be used in lung cancer situations through pulmonary delivery. Upon contact with lung cancer cells, the developed formulations adhere to cell membranes which, in turn, will promote a proper release of the nanosystems. The targeted and fluorescent character of the GNP as well as the core material, enable the use of such formulations in lung cancer imaging. Future integration of drugs into the GNP makes these nano-in-micro formulations potential candidates for sustained pulmonary delivery of theragnostic devices.

CHAPTER 5. Micronized Layer-by-Layer nanovehicles for siRNA delivery to the lungs: A novel approach for lung cancer therapy

The contents of this chapter are being prepared for submission to a peer reviewed international journal:

A.Sofia Silva, Kevin E.Shopsowitz, Santiago Correa, Stephen W. Morton, Erik C. Dreaden, Teresa Casimiro, , Ana Aguiar-Ricardo, Paula T. Hammond

Keywords: Layer-by-layer nanoparticles, siRNA, pulmonary delivery, micronized systems, SASD

Personal contribution

A.Sofia Silva contributed to the design of the study, performed most of the *in vitro* experiments, co-performed the *in vivo* experiments, co-interpreted the data and wrote the manuscript.

5.1 ABSTRACT

Lung adenocarcinoma is a subtype of the most common type of lung cancer, non-small cell lung cancer (NSCLC), and is currently associated with frequent mutations in KRAS and TP53 genes.

In an attempt to develop reliable systems that can silence at least one of this mutated genes, novel micronized layer-by-layer (LbL) nanovehicles comprising a nanolayer of siRNA for KRAS gene silencing were successfully engineered. The micronization was addressed using sustainable methodologies that make use of supercritical carbon dioxide ($scCO_2$) like Supercritical Assisted Spray Drying (SASD) technology. Due to its extraordinary properties like biocompatibility, biodegradability and mucus adhesion, chitosan (CHT) was elected as the carrier system for the siRNA LbL nanoparticles. Gene silencing of KRAS gene (using both nano and nano-in-micro systems), cell adhesion of the microsystems and cellular internalization by the nanoparticles, adequate release profiles and aerodynamic properties for pulmonary administration were achieved. *In vivo* biodistribution of the produced siRNA powders in healthy mice was also assessed and showed an alveolar distribution of the produced formulations. These results strongly suggest that the combination of LbL and SASD technologies for the production of siRNA powders provide a potential strategy to deliver siRNA to the lungs and address gene therapy in lung adenocarcinomas.

5.2 INTRODUCTION

Small interfering RNAs (siRNAs) consist of 21-23 nucleotides that can interfere with the expression of specific genes in mammalian cells. These bioactive molecules have potential applications in several untreatable and lethal diseases, like cancer and viral infections, and senescence-associated diseases. Some clinical trials have already been performed by making use of siRNA to knockdown particular proteins expression in these diseases. Notwithstanding, the delivery of functional siRNA to target cells is still a major challenge that needs to be carefully addressed. Nucleotides *per se* are not suitable for systemic administration due to their poor pharmacokinetics properties. Naked siRNA is rapidly degraded by endonucleases present in the bloodstream. Moreover, efficient intracellular delivery of siRNA across biological barriers and targeted cells is not straightforward since cells lack of efficient mechanisms to uptake nucleotides due to siRNA large size and highly anionic character. [22,26,173,174]

To overcome these barriers, a multitude of new formulations that compact siRNA into nano-sized systems suitable for cellular internalization have been widely investigated for *in*

vitro and *in vivo* applications. [26] LbL nanoparticles that use the mechanism of sequential deposition of adsorbed polyelectrolytes with complementary functionality (e.g. charge) to build a stable film with high siRNA content represent one of the more exciting drug delivery platforms to effectively carry the nucleotide to the target site and release it in a sustained manner. Such local and controlled delivery are of major clinical importance since they circumvent the undesired side effects that may result from high systemic therapeutic doses, like nonspecific tissue accumulation. [175,176]

Lung cancer for instance (including both NSCLC and small cell lung cancer (SCLC)), is the most common and leading cause of cancer death in both men and women worldwide and is an attractive cancer type for local and systemic siRNA delivery treatment. [1,2,177] The most common NSCLC subtype is lung adenocarcinoma, which is associated with frequent mutations in KRAS (~20-30%) and TP53 (~50%). Hence, targeted inhibition of KRAS expression and stimulation of TP53 effector functions are attractive therapeutic strategies for this particular lung cancer. KRAS is reported to be promising target for siRNA based therapy. In fact, Xue and collaborators have already demonstrated that oncogenic RAS can play a crucial role in tumor maintenance and that siRNA can effectively inhibit this gene. [177]

Effective siRNA delivery to the lungs can be achieved through pulmonary administration. Such local delivery enables the administration of reduced siRNA doses compared to systemic delivery, decreasing possible side effects and improving patient compliance. In fact, recent reports in literature describe the pulmonary delivery of siRNA for efficient gene silencing in the lungs.[2,26,178] Therefore, pulmonary administration of siRNA is becoming desired as new therapeutic platforms for lung diseases, like cancer.

The design of proper inhalable siRNA formulations is of extremely importance. Besides ideal aerodynamic diameter (1-5 μm), particles morphology and flowability properties, the integrity of siRNA must also be preserved in order to achieve an efficient pulmonary siRNA therapy. $ScCO_2$-assisted processes for the production of dry powder formulations have been successfully implemented. Moreover, some reports already describe the successful application of such technology to produce powders of nucleic acids, like siRNA for inhalable gene delivery.[26,173,179]

Therefore, in an attempt to produce dry powder formulations of siRNA targeted for KRAS mutation in lung adenocarcinoma, inhalable systems were engineered on a laboratory scale using SASD. CHT, as a natural polysaccharide generally accepted as biocompatible and biodegradable, was chosen as a carrier microsystem. For controlled release of the siRNA and to guarantee that it remains stable until it reaches the desired site of action, LbL nanosystems were

used as siRNA film carriers. Mesoporous silica nanoparticles (MSN) were used as the assembly core (due to their biodegradable and biocompatible features and ability to serve as a reservoir to other biomolecules of interest), poly-L-arginine (PLA) as a polycation and hyaluronic acid (HA) as the polyanion in the outermost of the nanoparticle to provide a targeted platform to the cell line in the study (due to the biding of HA to cells' CD44 receptors overexpressed).[180] Such constructs will enable a specific binding and controlled siRNA release, once CHT is degraded by the airway mucus and lining fluid enzymes.

The produced combined formulations were fully characterized in terms of their morphological properties, gene silencing and biocompatibility abilities, and aerodynamic features. *In vitro* release profiles were also investigated followed by an *in vivo* biodistribution proof-of-concept assay of the produced powders in healthy mice.

5.3 EXPERIMENTAL PROCEDURE

5.3.1 Materials

Stable tdTomato expressing KP derived lung adenocarcinoma lines (KP cells) were previously synthetized in Tyler's lab by following the protocol described by Wen and co-workers[177] KRAS 1211 modified siRNA (5'-UAAAGUCUAGGACACGCUGUUUU-3') was purchased from Dharmacon. AllStars negative Alexa Fluor 488 siRNA (AF 488 siRNA) was purchased from Qiagen. Silencer Negative Control siRNA (NC siRNA), NucBlue® Live ReadyProbes® Reagent (Hoechst 33342) and Lipofectamine® 2000 Transfection Reagent were purchased from ThermoFisher Scientific. Corning 384 flat bottom black polystyrene low volume/flat microplate were kindly provided by Corning Corporation. QuantiGene RNA assay and KRAS and MRPL53 reference genes were purchased from Affymetrix. RNA ladder were purchased from NEB. Hollow fiber module 300 kDa modified polyethersulfone (*m*PES) were purchased from Spectrum Labs. Hyaluronic acid (HA, 40 kDa) was purchased from Lifecore Biomedical. CellTiter Glo kit was purchased from Promega. Heparin sodium (PH-3005) was purchased from Celsus laboratories. Dulbecco's modified eagle's medium F12 (DMEM F12), fetal bovine serum (FBS) and penicillin/spectromycin were purchased from Media Tech. Ribogreen assay and RNAse free water were purchased from Life Technologies. IR-780 iodide dye, poly-L-arginine (PLA, 5-15 kDa), hyaluronidase from bovine testes type VIII (Hdase), proteinase K from Tritirachium album (Pkase), lysozyme chloride from Grade VI: from chicken egg white, ttraehtyl orthosilicate (TEOS), trimethylamine, cetyltrimethylammonioum bromide (CTAB), methanol, phosphate buffer saline, dibasic sodium phosphate, citric acid and sodium citrate were purchased from Sigma-Aldrich. Optimum cutting temperature (O.C.T.) fixing agent was

purchased from Sakura Finetek. Acetic acid glacial (99.7 % purity) was purchased from Carlo Erba Reagents. Ethanol absolute anhydrous (99.9 % purity) was purchased from Scharlau. Chitosan (viscosity 5-20 mPa.s, 0.5 % in 0.5 % acetic acid at 20 °C) was purchased from Tokyo Chemical Industry. Hydranalcoulomat AD was also from Sigma-Aldrich and was used in Karl Fischer. Dry powder insufflator was purchased from Penn Century. All components were used as received without any further purification. Industrial carbon dioxide (purity ≥ 99.93 %) from Air Liquid was used.

5.3.2 Preparation of IR-780 loaded mesoporous silica nanoparticles (MSN)

MSNs were synthesized by adapting the several methods described in the literature for the synthesis of this type of nanoparticles.[181,182] Briefly, 4.2 mmol of CTAB and 2.3 mmol of triethanolamine were mixed with 100 mL of H_2O and heated at 80 ºC for 1 h (until dissolved). Then, 70 mmol of TEOS were quickly added and the solution was stirred for another 1 hour. The particles were isolated by high speed centrifugation (30,000 x g, 30 min) and washed once with water and once with methanol (MeOH). Particles were resuspended in 200 mL of MeOH followed by the addition of 2 mL of 12 M HCl. The suspension was refluxed at 80 ºC for 14 h and the particles were recovered by centrifugation (30,000 x g, 30 min), followed by two washes with methanol.

IR-780 iodide is a near-infrared (NIR) fluorescence dye with great importance in theragnosis. [183] In this study, this dye was loaded into MSN to monitor nanoparticles entrapment efficiency into CHT microspheres. IR-780 dye loading was accomplished by using the solvent evaporation method with slight modifications. To load the dye in the pores of the particles, 90 mg of MSN were soaked in a concentrated solution of the dye (2 mg/mL in MeOH), with the aid of an ultrasonic bath, and the procedure was repeated 3 times. The solvent used for the dye dissolution was evaporated after each impregnation, under reduced pressure, in order to accomplish a more complete dye pore filling and improve the loading efficiency of the nanocarriers.[182] After the last procedure, the particles were washed with 500 µL of ultrapure water to remove the IR-780 dye not loaded into the MSNs. The particles were recovered by high speed centrifugation (30,000 x g, 15 min). The resulting particles were recovered and dried under reduced pressure overnight. The amounts of loaded and unloaded dye were quantified by measuring particles and their supernatant fluorescence in a microplate reader (Infinite 200 from Tecan,) and compared against a calibration curve.

5.3.3 siRNA Layer by Layer (LbL) assembly nanoparticles

The nanoparticle LbL assembly was developed on the basis of the previously established methods, with slightly modifications. [25,180]

For LbL assembly, 5 mg of MSN_IR-780 were redispersed in 10 mL of PBS 0.2X. A solution of 1.5 mg/mL of the polycation PLA (5 – 15 kDa) in RNAse free water, was added dropwise to the nanoparticles dispersion, under stirring. The solutions were allowed to mix for 30 sec more in an ultrasonic bath, followed by purification in a bench scale tangential flow filtration (TFF) development systems with data acquisition and pressure indicator (Spectrum Labs KrosFlo® Researcher II). Such filtration process was performed using a 300 kDa modified polyethersulfone hollow fiber module (Spectrum Labs MidiKros® D02-E300-05-N) at a flow rate of 200 mL/min (no pressure applied). A total of 4 washes were performed. To incorporate siRNA, purified nanoparticles were mixed with a siRNA solution (in Rnase free water) containing a mixture of a KRAS siRNA and AF 488 siRNA (120 nmol and 16 nmol, respectively). Control samples containing NC siRNA and AF 488 siRNA were also prepared in the same proportions for control purposes. Again, the addition was performed by adding dropwise the siRNA mixture to the purified nanoparticles, under stirring. Once more, the solutions were sonicated for extra 30 sec to allow particles–siRNA interaction/collision. Again, the particles were purified using another 300 kDa modified polyethersulfone hollow fiber module at a flow rate of 200 mL/min (no pressure applied). The purified polycation/siRNA nanoparticles were further mixed with a new solution of 1.5 mg/mL of the polycation PLA (5 – 15 kDa) in RNAse free water. The adding and purification procedure were the same as described above. Finally, the resulting particles were conjugated with a previously chilled (4 ºC) hyaluronic acid (HA) (40 kDa) solution (2 mg/mL) containing 100 nM dibasic sodium phosphate (pH 7.4). The HA solution was added in a single, strong and efficient mode to the purified nanoparticles placed in an ultrasonic bath, and placed at 4 ºC for 30 min. Further purification was performed using the same type of hollow fiber modules at a flow rate of 140 mL/min with a pressure of 0.07 MPa.

5.3.4 Physicochemical characterization of the LbL assemblies

All size, zeta potential and polydispersity index measurements were performed using a Malvern ZS90 zeta-sizer. Transmission electron microcopy (TEM) was assessed using a JEOL 2010 FEG Analytical Electron Microscope (JEOL). Samples were prepared by dropcasting nanoparticles suspensions onto carbon coated copper grids without any staining.

The loading of siRNA on the LbL nanoparticles was examined by (1) measuring the amount of fluorescent siRNA present in the nanoparticles after siRNA layering, against a standard fluorescent curve; and (2) using specific enzymes to digest HA (hyaluronidase)[184] and PLA (Proteinase K),[185] followed by an addition of an heparine solution (to compete for the siRNA), a quantification using Ribogreen assay and an siRNA integrity evaluation through electrophoresis in an agarose gel.

siRNA release assays were evaluated using 3 different buffer solutions: phosphate buffer saline solution at pH 7.4 to mimic cells' physiological pH, phosphate buffer saline solution at pH 6.8 to mimic the intracellular environment of cancer cells, and citrate buffer solution, pH 5.5 to mimic the endosomal environment of cancer cells.[186] The release assays were performed as the following: 500 µL of nanoparticle suspension (n = 3, for each pH) were centrifuged at high speed (30,000 x g, 15 min). The supernatant was recovered and stored for siRNA quantification. The nanoparticles were redispersed in 1 mL of each buffer solution and the siRNA released from the microparticles was evaluated during 3 days, with the aid of Ribogreen quantification assay, according to manufactures instructions. Prior to Ribrogreen quantification, heparine (10 mg/mL) was added to compete for the siRNA released to the medium.[187]

5.3.5 Preparation of CHT-LbL siRNA Powders by Supercritical Assisted Spray Drying (SASD)

A dry CHT-LbL siRNA and dry CHT-MSN powders (for aerodynamic properties assessment, X-Ray Diffraction, and specific surface area analysis) were both prepared based on the SASD method, already described in CHAPTER 4, with slightly modifications. The LbL assemblies were centrifuged at high speed (30,000 x g, 30 min) and the resultant pellet was placed in a casting solution of chitosan (CHT) (1 % w/v) prepared in 1 % (v/v) of acid water and 20 % (v/v) of ethanol and homogenized under stirring. Liquefied CO_2 was pumped with a high-pressure liquid pump (HPLC pump K-501, Knauer), which was then heated and sent to the static mixer (model 37-03-075, Kenics-Chemineer, 4.8 mm ID x mm L, 27 helical mixing elements). The casting solution containing both nanoparticles and CHT was pressurized through a high pressure pump (HPLC 305, Gilson) to the static mixer that promotes a near-equilibrium mixing of $scCO_2$ and the liquid solution. Pressure is measured with a Setra pressure transducer (0.1 psig stability). The solution was then sprayed through a 150 µm diameter nozzle into a thermostated aluminum precipitator (± 0.1 ºC), operating at near atmospheric pressure, where particles are formed by drying the droplets using a heated air flow (70 °C). The formed particles

exit the precipitator from the bottom and enter into a cyclone where they are separated from the gas stream and collected in a reservoir and in a filter bag (FSI, nylon mono-filament, 50 μm).[164] T_{mix} = 70 °C; T_{preci} = 90 °C; p_{CO2} = 10 MPa

5.3.6 Morphological and physical-chemical characterizations

Particle size analysis (sieve and Feret's diameter) was determined using an optical particle analyzer system (Morphologi G3 Essentials, from Malvern Instruments Ltd). The particles were characterized by the volume mean diameter (D_v) and the relative width of the distribution (Span), calculated as follows:

$$Span = \frac{D_{v,90} - D_{v,10}}{D_{v,50}} \qquad \text{Equation 5.1}$$

where $D_{v,90}$, $D_{v,10}$ and $D_{v,50}$ are the diameters at 90 %, 10 % and 50 % cumulative volume. To observe morphology, the microparticles were imaged via scanning electron microscopy (SEM) (JEOL) at various amplifications. All the samples were mounted on alumin stubs using carbon tape and were sputter-coated with 5 nm Pt/Pd.[165]

X-ray powder diffraction (XRD) analysis was performed in a RIGAKU X-ray diffractometer (model Miniflex II). Samples were placed in a holder and analyzed through CuKα radiation (30 KV/15 mA), with a 2θ angle ranging between 2° and 55° with a scan rate of 1°/min.

Moisture content of each formulation was accessed using Karl Fischer assay (Metrohm). 1.5 mg of powder were accurately weighted and introduced in the reaction cell. Moisture content was determined by subtracting the background signal.[36,166]

Surfaces areas were calculated by the Brunauer Emmett Teller (BET) method and were determined in a Micromeritics ASAP 2010 Physisorption Analyser, using 50 mg of samples. The analysis was performed in two phases first by heating the sample up to 320 K for 42 h, in order to release all adsorbed gases in the particle. Secondly, the temperature was lowered and maintained at 77.35 K during the time of analysis.

LBL siRNA nanoparticles distribution among CHT microparticles was evaluated through different techniques. Fluorescent siRNA spreading onto CHT microparticles was analyzed using Olympus FV1200 Laser Scanning Confocal (Olympus). Scanning TEM (STEM) and energy dispersive X ray spectroscopy (EDX) maps were simultaneously recorded using JEOL 2010 FEG Analytical Electron Microscope (JEOL), with the aid of Gatan Digital Micrograph soft-

ware. Such techniques combination enabled to visualize the surface of the solid template (microspheres) and assign specific elemental peaks.

5.3.7 Entrapment Efficiency

Since no fluorescence intensity decrease was noted due layers deposition, during the LbL assembly procedure, the entrapment efficiency was determined by measuring the amount of IR-780 dye presented in the powders. Briefly, 1 mg of CHT-LbL siRNA powders were dissolved in water and IR-780 dye fluorescence was assessed in a microplate reader.

The entrapment efficiency (E%) of IR-780 dye was calculated as follows:

$$E\% = \frac{m_r}{m_i} \times 100 \qquad \text{Equation 5.2}$$

where m_r is the amount of IR-780 dye remaining within the particles and m_i is the amount IR-780 dye presented in the LbL assemblies loaded into the casting solution. This percentage matches the percentage of the whole LbL nanosystems entrapped.

5.3.8 *In vitro* aerosolization study

An *in vitro* dry powder aerosolization study was carried out for the CHT-MSN formulations using seven stages Andersen Cascade Impactor (ACI) (Coopley Scientific). In a typical procedure 30 mg of powder were loaded into 5 hydroxypropylmethylcellulose capsules (Aerovaus). The capsules were individually placed in a handheld, dry powder, breath activated inhaler device (PlastiApe device HR model 7), previously weighted, which is coupled to the ACI device. The 7 metal plates within the cascade impactor were covered with pre weighted glass microfiber filters (MFV1 diameter 80 mm, Filter Lab). The DPI punctures the capsule prior to the inhalation and a high capacity pump is actuated to simulate an inspiration: air flow rate 60 L/min during 4 s, according to the European pharmacopeia.[167] After the dispersion, the filters and the dry powder inhalers (DPI) were weighted again. The emitted dose (ED %), which corresponds to the total loaded powder mass exiting the capsules and inhaler, was determined gravimetrically and can be expressed as follows:

$$\mathrm{ED}(\%) = \frac{\mathrm{m_{full}} - \mathrm{m_{empty}}}{\mathrm{m_{powder}}} \times 100 \qquad \text{Equation 5.3}$$

where m_{full} and m_{empty} are the weights (mg) of the capsule before and after simulating the inhalation and m_{powder} is the initial weight (mg) of the powder in the capsule.

The Fine Particle Fraction (FPF) was determined by the interpolation of the percentage of the particles with less than 5 μm diameter emitted from the capsules in each ACI experiment. The Mass Median Aerodynamic Diameter (MMAD) was determined as the particle diameter corresponding to 50 % of the cumulative distribution. The Geometric Standard Deviation (GSD) was determined by the following equation:

$$GSD = \sqrt{\frac{d_{84}}{d_{16}}} \qquad \text{Equation 5.4}$$

where d_{84} and d_{16} are the diameters corresponding to 84 % and 16 % of the cumulative distribution, respectively

5.3.9 *In vitro* cumulative release studies: nano and siRNA simultaneous release

The releases of LBL assemblies and simultaneous siRNA from the microparticles were evaluated at two distinct pHs: physiological pH (7.4) and a more acid H to mimic the lung-lining fluid of a lung cancer situation (6.8). Approximately 3 mg of the powders were transferred to a special membrane size cut off 1 μm, and incubated in 1.5 mL of different pH solutions in a shaking (35 rpm) water bath at 37 ºC. At pre-determined end points, the solutions were removed and replaced for 1.5 mL fresh buffer solutions. The removed solutions were centrifuged at 30,000 x g for 15 min and the supernatant was removed. Afterwards, 50 μL of water was added to resuspend the pellet. The samples were placed in a 384 Well Black with Clear Flat Bottom Polystyrene and read spectrophotometer microplate reader. From the fluorescence obtained and from the amount of IR-780 dye initially entrapped in the microparticles, it was possible to estimate the amount (%) of LbL nanoparticles being released from the micropowders.

In a simultaneous experiment, the amount of siRNA being released from the microcarriers was also quantified. Briefly, at determined time points, the 1.5 mL of buffer solutions were removed and replaced for fresh 1.5 mL of buffer solutions. To the removed buffer, 100 μL of a heparine solution (10 mg/mL) were added in order to compete for the siRNA. Afterwards, Ribrogreen assay was performed to quantify the amount of siRNA released to from the microspheres.

Nanoparticles and siRNA release from swelling-controlled systems was modelled by the Korsmeyer-Peppas equation as follows:

$$\frac{M_t}{M_\infty} = kt^n \qquad \text{Equation 5.5}$$

where M_t/M_∞ is the fraction of the drug release at time t, k is the rate constant and n is the diffusional exponent. The n-value is obtained from the slope of the Korsmeyer-Peppas plot and represent different release mechanisms. For spherical geometries: n = 0.43 for Fickian diffusion; 0.43 < n < 0.85 for anomalous non-Fickian diffusion; n = 0.85 for Case-II transport.[168,169]

5.3.10 *In vitro* performance of nano and nano-in-micro systems

KP tdTomato expressing cells were used in our experiments and grown in DMEM media supplemented with 10 % v/v heat-inactivated fetal bovine serum (FBS) and 1 % of antibiotic-antimycotic (penincilin G (100 U/mL)), spectromycin G (100 µg/mL)) at 37 °C, under 5 % CO_2 humidified atmosphere.[155]

Gene silencing of siRNA LbL nanoparticles was assessed in KP tdTomato-expressing cell line. Briefly, the cells were seeded on a 96-well plate overnight at a density of 1.2 x 10^4 cells/well, and treated with increasing concentrations of LbL nanoparticles of which the amounts were normalized to the siRNA loading (10, 50, 100 nM). The cells were treated with KRAS-targeting siRNA LbL nanoparticles, and compared with NC siRNA nanoparticles and lipofectamine controls. Three days after the treatment, cellular expression was evaluated through the QuantiGene RNA assay, according to the manufacturer's instructions. KRAS was used as the target gene and MRPL 53 was used as a reference gene. The experiment was repeated for the microformulations. The amount of powders administered was normalized to the amount of siRNA encapsulated. For this, two different concentrations of powders in solution were used: 0.45 mg/mL and 0.09 mg/mL, for either CHT or CHT-LbL siRNA microparticles.

Cytotoxicity assays were performed using CellTiter Glo, according to the manufactures instructions. Briefly, cells were seeded in a 96-well plate at a density of 1.2 x 10^4 cells/well for 24 h. Afterwards, cells were treated with the nanoparticles at various concentrations (normalized to siRNA concentrations: 10, 50, 100 nM). Cellular ATP was monitoring at 24 h and 72 h of incubation by replacing the medium by 100 µL of fresh media and 20 µL of the reagent mixture. Cell viabilities were normalized to an untreated control. The same procedure was repeated for the CHT-LbL siRNA powders. Again, the amount of powders administered was normalized to the amount of siRNA encapsulated and were the same as for the gene silencing assay.

Cellular uptake of nanoparticles was assessed by confocal microscopy and flow cytometry.

The confocal microscopic images were taken using an Olympus FV1200 Laser Scanning Confocal. Briefly, KP tdTomato cell line was seeded at a density of 1.2 x 10^4 cells/well on glass bottom dishes coated with collagen with 1 mL of DMEM supplemented with 10 % of FBS, during 24 h at 37 °C, under 5 % CO_2 humidified atmosphere. Afterwards LbL nanoparticles were placed in contact with cells. One and 4h after, the medium was replaced by DMEM supplement with 10 % of FBS and 1 % of antibiotic-antimycotic, and the cells were imaged. Further 3D reconstruction was performed using Imaris Bitplane (Vs7.6.1, Bitplane).

The quantity of uptake was measured by flow cytometry. Briefly, the cells were seeded in a 48-well plate at a density of 50 x 10^4 cells/well with 1 mL of DMEM supplemented with 10% of FBS, during 24 h at 37 °C, under 5 % CO_2 humidified atmosphere. Then, cells were treated with LbL fluorescently labeled nanoparticles at a concentration of 100 µg/mL for 1 and 4 h, followed by washing and trypsinization. The cell-associated fluorescence was analyzed by a BD LSRFortessa flow cytometer (BD Biosciences)

Microparticles' interactions with cells were carried out by seeding cells in glass bottom dishes coated with collagen at a density of 4 x 10^3 cells per well, for 24 h. Afterwards, nano-in-micro formulations were placed in contact with cells for 1 and 12 h and their interactions were imaged.

5.3.11 *In Vivo* experiments

Female BALB/c mice (4-6 weeks old) were purchased from Taconic, and the AIN-93 purified diet was from PharmaServ/Testdiets. Mice were kept on the AIN-93 diet for at least a week before experimentation to reduce levels of body autofluorescence. All in vivo experimentation as carried out under the supervision of the Division of Comparative Medicine (DCM), Massachusetts Institute of Technology, and in compliance with the Principles of Laboratory Animal Care of the National Institutes of Health.

Mice were divided in 4 groups: i) untreated; ii) treated with CHT-LbL siRNA (30 min); iii) treated with CHT-LbL siRNA (24 h); treated with CHT powders (24 h). Prior to the powders administration, the mice were anesthetized with isoflurane and hold on their back. The trachea was exposed to a dry powder insufflator® for mouse (Penn Century) and 1.5 mg of powders (2.8 µg of siRNA) was administered through the trachea.

After the pre-determined times points, the mice were sacrificed and lungs fluorescence derived from AF 488 siRNA (λ_{ex}= 465 nm ; λ_{em}: 520 nm) was detected using a Xenogen IVIS

Imaging System (Caliper Instruments). Imaging and biodistribution data were normalized to the autofluorescence of the untreated mice.

Further biodistribution analyses were performed both using confocal microscopy (Olympus FV1200 Laser Scanning Confocal) and two photon correlation microscopy with the aid of Olympus FV1000 Multiphoton Laser Scanning Confocal Microscope (Olympus) for deep tissue imaging of the lung, using a 25 x, N.A. 1.05 objective at 840 nm.

Quantigene analyses of target gene silencing were performed by isolating total RNA from the sliced lungs using quantigene processing kit for tissue (Affymetrix, Santa Clara, CA) according to the manufacturers' protocol. Again, KRAS was used as the target gene and MRPL 53 as a reference one.

In vivo toxicity of the CHT-LbL siRNA powders was assessed using serum and lung tissue samples isolated from both the treated and control mice at the end of the experiment. Blood biochemistry of liver and kidney panels was analyzed by Charles River Laboratories. Lungs tissues were fixed with O.C.T. and processed by the Swanson Biotechnology Histology Facility Core. The samples were sectioned for H&E staining. Sectioned images were collected using a Nikon light microscope, an Olympus FV1200 Laser Scanning Confocal and an Olympus FV1000 Multiphoton Laser Scanning Confocal Microscope.

5.3.12 *Statistical* Analysis

All statistical analysis, unless noted, (GraphPad Prism and Origin) were performed using one-way ANOVA analysis of variance following the Bonferroni post-hoc test with a significant set at $p < 0.05$.

5.4 RESULTS AND DISCUSSION

5.4.1 LbL nanoconstructs – characterization and *in vitro* performance

LbL architectures consisting of 4 layers (PLA-siRNA-PLA-HA) were engineered onto the surface of MSN_IR-780 (32 nm in hydrodynamic size and -32.2 mV in zeta potential) via sequential adsorption and TFF purifications from solutions of polycations and polyanions. Due their promising *in vivo* applications and several advantages, like low cytotoxicity, film stability, high transfection efficiency, among others, PLA was elected as the polycation to be used in this construct, and HA as the polyanion. The ability of HA to bind overexpressed CD44 receptors

existing in a vast majority of cancer cell lines, like KP-derived lung adenocarcinomas, promoting an active targeting and tumor cell uptake via HA-CD44 interactions, made HA an ideal surface polyanion.[25]

The deposition of PLA onto MSN_IR-780 was clearly demonstrated by the increase in the size of the particles as well as a complete reversal of surface charge, as shown in Figure 5.1A and B, respectively. Following additions of both siRNA, PLA, and HA were also corroborated by the increase in the particles' size (slightly for siRNA and PLA, and pronounced for HA layer) and complete surface charge reversal. The thick HA layer on the outer surface provides an enhanced degree of hydration to our particles, contributing to particles' steric stability. [180] The uniformity of the layer deposition was evidenced by the maintenance of the polydispersity following each layer, as depicted in Figure 5.1C. The electron micrographs of MSN_780-IR (Figure 5.1D) and LbL nanoparticles (Figure 5.1E) reveal the appearance of an outer shell, confirming the deposition of the polymeric film on the core particles.

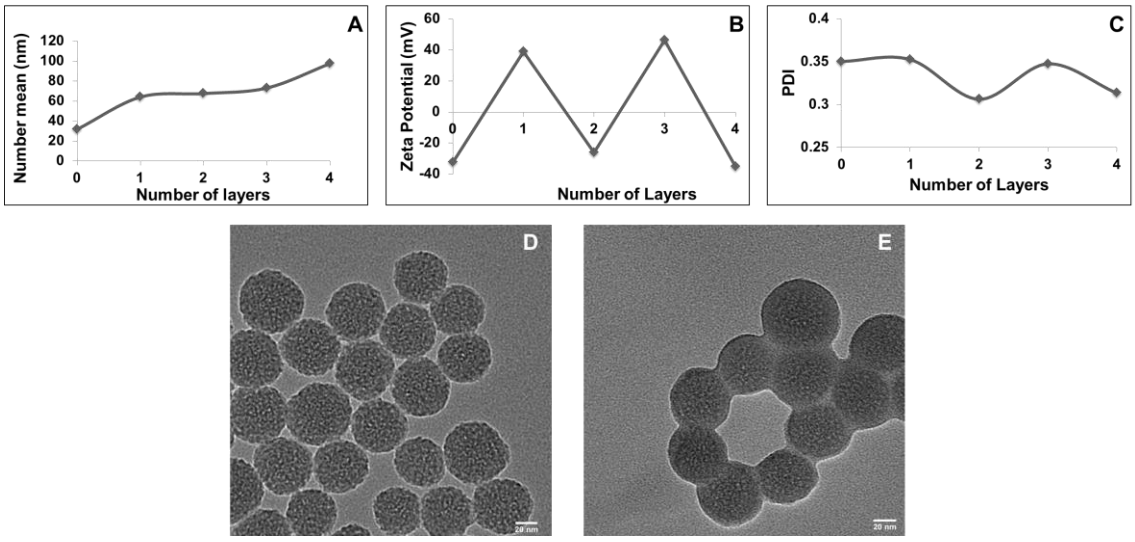

Figure 5.1-Physicochemical characterization of siRNA LbL nanoparticles. Effects of additional layers on (A) hydrodynamic diameter, (B) Zeta potential, and (C) polydispersity index (PDI) of the LbL nanosystems. TEM images of (D) MSN_IR-780 and (E) siRNA LbL nanoconstructs.

The layering of siRNA onto the MSN_IR-780/PLA construct was measured using Ribogreen assay immediately after siRNA deposition. The amount of AF 488 siRNA was also monitored by measuring the amount of fluorescent siRNA (no Ribrogreeen added) against a standard curve. The presence of siRNA after the remaining layers were deposited was also addressed by conjugating some specific enzymes like HAdase (for HA degradation), [184] Proteinase

K (for PLA degradation),[185] and a final conjugation of heparin to compete for the siRNA. [173] Ribogreen quantification was also performed, and the amount AF 488 siRNA was also measured. The results are displayed in Table 5.1.

Table 5. 1-siRNA loading onto LbL nanosystems

5 mg of MSN_IR-780	**siRNA (initial amount)**	**siRNA (LbL nanoparticles)**	**AF 488 siRNA (LbL nanoparticles)**
After siRNA layering	≈ 2040 µg (120 nmol of siRNA (Kras or NC + 16 nmol of AF 488 siRNA)	11.4 % of initial siRNA= 232.2 µg	1.2 % of initial siRNA = 25.1 µg
After enzymes degradation		10.7 % of initial siRNA = 219.1 µg	1.1 % of initial siRNA = 23.3 µg

The siRNA integrity was also evaluated using an agarose gel electrophoresis (Figure D.1, Appendix D). For this, heparin, generally used to unpack nucleic acids from nuclei acid/cationic vectors,[173] was used to enable the detection of electrophoretic band of siRNAs.

It was also found that the LbL constructs exhibited a controlled release over an extended period of time as depicted in Figure 5.2. Nevertheless, at pH 5.5 (that mimics the endosomal pH of a cancer cell) [186] the release is slightly higher than for pHs 6.8 and 7.4. The stability resolved temporally at these pHs is a key feature of this construct as it is undesirable to lose large amounts of siRNA during circulation until it reaches the tumor tissue. [25]. Moreover, the use of MSN is likely contributing to the sustained released due to a larger packing into particles pores. [22]

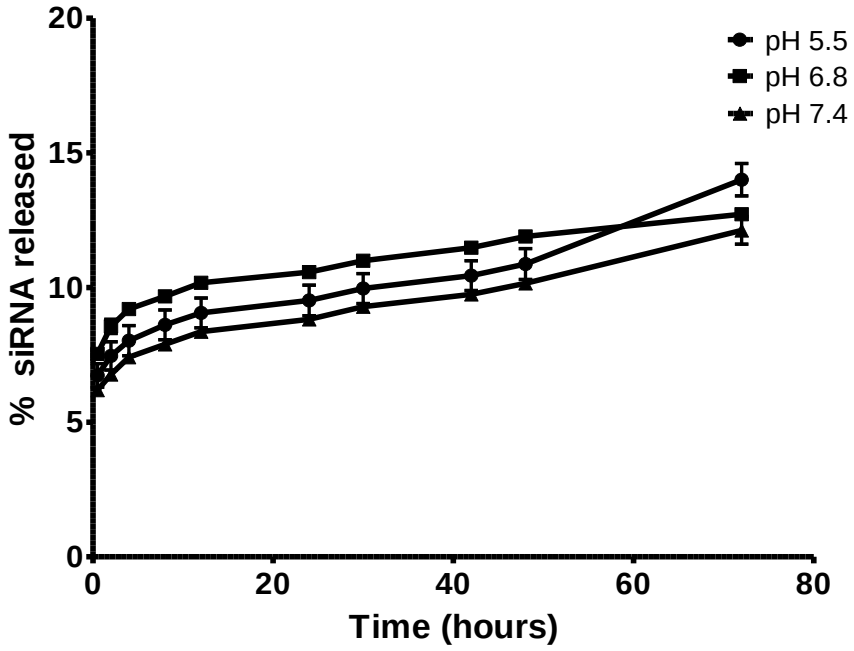

Figure 5.2-siRNA release from LbL nanoconstructs.

The ability of such nanoparticles to silence KRAS was investigated in tdTomato – expressing KP cells and is displayed on Figure 5.3. Increased concentrations of particles and, consequently, siRNA were investigated. Gene expression of treated cells was compared to un-treated ones. Lipofectamine controls of both types of siRNA were also performed. It was found that the LbL nanoparticles containing KRAS siRNA were able to achieve more than 50 % of gene silencing compared to the untreated cells, as LbL nanoparticles containing NC siRNA achieved only less than 30 % of gene silencing.

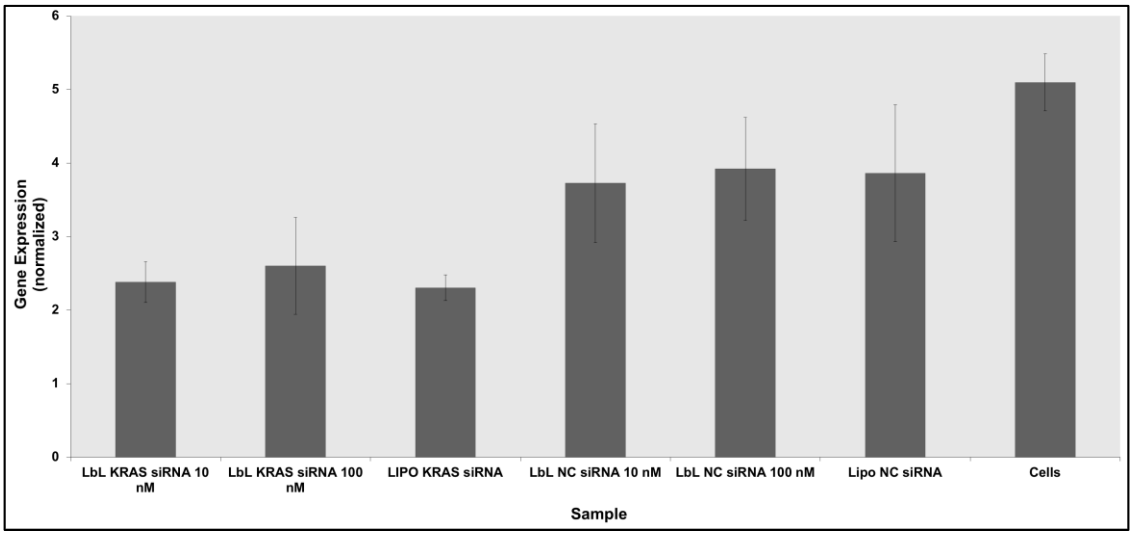

Figure 5.3-Gene expression of KRAS in tdTomato–expressing KP cell line.

The cytotoxic profile of the produced nanocarriers was also investigated. As Figure 5.4 demonstrates, little cytotoxicity was observed by the Lbl assemblies herein engineered. The results show that either HA or PLA are biocompatible and that there is little toxicity related to the use of this polymers, corroborating previous reports on literature. [25]

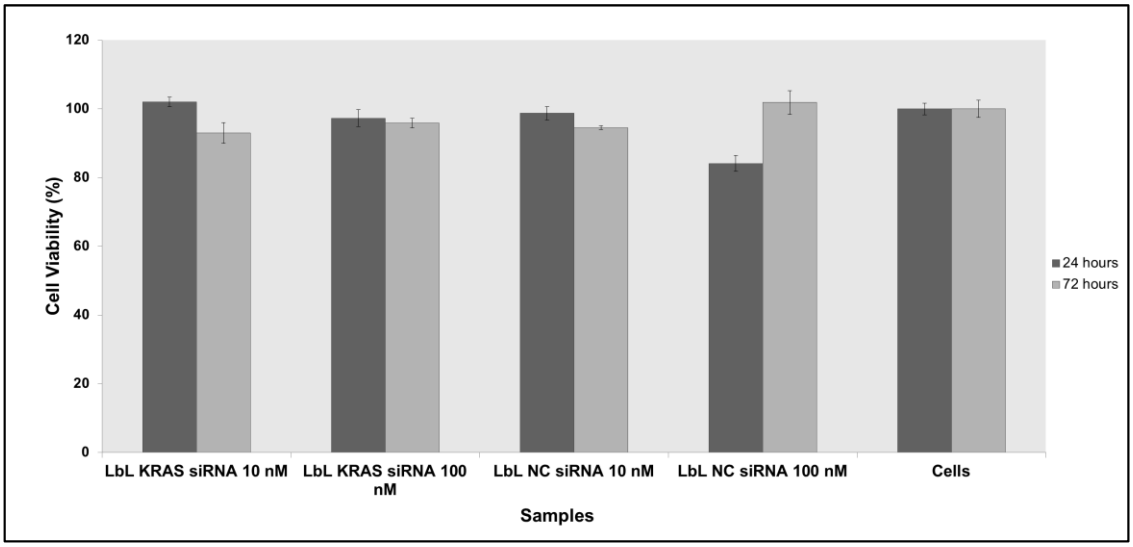

Figure 5.4-Cell viability of tdTomato-expressing KP cells 24 and 72 h after being in contact with the engineered LbL nanosystems**.**

Confocal laser scanning microscopy (CLSM) of the siRNA LbL nanosystems showed nanoparticles' binding to the cells after 1 h of incubation as displayed in Figure 5.5A. In fact,

some of the particles appear to be already internalized, evidenced by punctate fluorescence in the cytosolic compartments. After 4 h of incubation, brighter green spots (from AF 488 siRNA) associated with the nucleus are observed (in blue), as it can be seen in Figure 5.5B. Such increase in cellular internalization was corroborated by flow cytometry in Figure 5.5C. There is a two times increase in cellular uptake after 4 h of incubation (64.6 % of cells have nanoparticles internalized). Figure D.2 (Appendix D) also depicts a 3D reconstruction of such cells after 4 h using brightfield, where particles internalization is easily noted.

Such high internalization was already anticipated since HA-coated LbL nanoparticles can easily engage with CD44 receptor overexpressed by this type of cell line. In fact, HA is considered a native ligand to CD44 being therefore able to mediate cellular uptake through receptor-mediated interactions.[25,50,184]

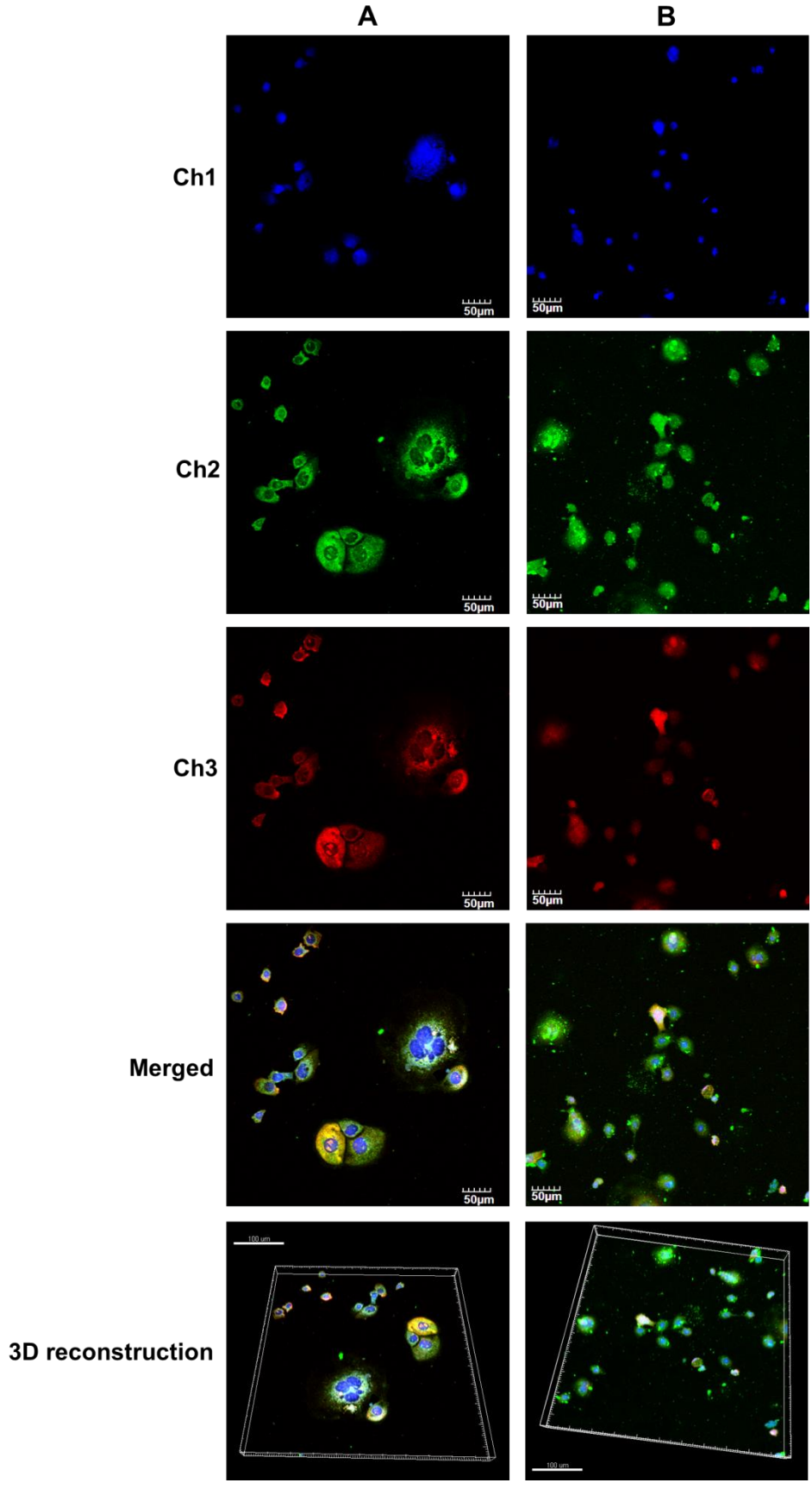
A
B
Ch1
Ch2
Ch3
Merged
3D reconstruction
50µm
100 µm

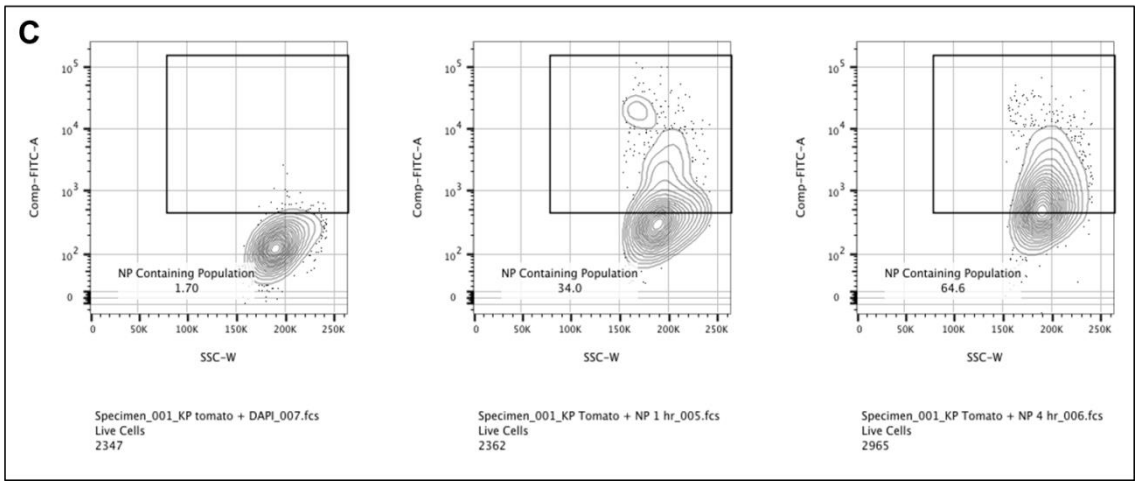

Figure 5.5-CLSM images of td Tomato-expressing KP cell line incubated with the LbL siRNA nanoparticles, after (A) 1 and (B) 4h. Ch1 – Hoechst, nuclear location (λ_{exc} = 405 nm; λ_{emm} = 461 nm); Ch2 – AF 488, siRNA (λ_{exc} = 463 nm; λ_{emm} = 520 nm); Ch3 – Ds-Red2 , tdTomato Kp cell line (λ_{exc} = 559 nm ; λ_{emm} = 581 nm); Merged – overlapping of channels 1,2 and 3; and 3D reconstruction. (C) Flow cytometry analysis of the nanoparticles uptake after 1 and 4 hours.

5.4.2 Morphology and physical-chemical characterizations of the micronized powders

Particle size and morphology are two critical factors affecting powder inhalation. The produced powders were characterized in terms of their volume mean diameter ($D_{v,50}$), which represents the cumulative diameter of 50 % of microparticles and provides an appropriate estimation of particle size for dry-powder inhalation purposes. Microparticles produced by SASD technology have no significant differences between the volume mean diameters. The mean diameters of 3.1 to 4.2 μm are ideal for inhalation purposes.[173] Similar span values were obtained for all types of CHT microparticles herein engineered, indicating that they have the same distribution width (Table 5.2). As we were only addressing biodistribution of the developed powders, both siRNA LbL nanosystems (KRAS and NC) were conjugated in a way to enhance the amount of fluorescent siRNA for a more accurate biodistribution panel.

Table 5.2-Powders physical characteristics.

Sample	$D_{v,50}$ (µm)	Span	Encapsulation Efficiency (%) [a]	Moisture Content (%)	Surface Area (m^2/g)	Pore volume (cm^3/g)	Pore size (nm)
CHT	4.2	0.9	-	1.4	7.1	0.008	4.7
CHT-MSN	3.1	0.8	-	0.7	6.3	0.009	5.9
CHT-LbL siRNA	3.5	1	28.7	0.9	-	-	-

[a] Based in IR-780 dye encapsulation efficiency.

The entrapment efficiency of the LbL nanosystems was assessed by measuring the fluorescence of IR-780 dye present in the microspheres. It is hypothesized that the remaining LbL siRNA nanosystems were lost during powder formation either by leaving the system with CO_2 flow or by degradation. Further measurements are depicted in Table D.1 (Appendix D). Due to the theragnostic properties of IR-780 dye, it can be used for future *in vivo* photothermal (PTT) application, enhancing the ability of our systems to kill cancer cells.[183]

The moisture content of each formulation was also assessed through a Karl Fisher assay and the results show a great improvement in comparison to our other studies (CHAPTER 4). Generally, in a drying operation the lower the moisture content, the better the product.[188] The residual moisture of less than 1 % indicates a complete drying process. Although the differences among the obtained values are not statistically significant, it seems that the moisture percentages decrease with the nanoparticles addition.

The XRD patterns of MSN and samples CHT and CHT-MSN are displayed in Figure D.3 (Appendix D). Due to the amount needed to perform an XRD analysis, the sample CHT-LbL siRNA was not investigated using this technique. However, the pattern is expected to be very similar to the one obtained for CHT-MSN. The characteristic spectra and peak of amorphous SiO_2 is depicted at $2\theta = 20^o$ for MSN. Similarly, the characteristic pattern of processed CHT also shows a broadening at $2\theta = 20^o$. This type of broadening is also depicted for CHT-MSN powders.

The results obtained for BET specific surface area analysis are also shown in Table 5.2 According to pores classification adopted by IUPAC, [98] the particles all present mesopores (1.5 nm < d < 50 nm). The analysis to BET isotherms (Figure D.4, Appendix D) shows that the produced microparticles follow a Type II isotherm. Such isotherm indicates the formation of an

adsorbed layer where the thickness increases with increasing relative pressure until it equals the saturation vapor pressure, when the adsorbed layer becomes a bulk liquid. The uptake at **A** represents the completion of the monolayer, and gives an estimation of how much adsorbate is required to form a monolayer covering solid surface. At this point begins a quasilinear section representing the formation of the multilayer.[189] The relative small values for surface area also indicate a more energetically favorable state.[101]

As displayed in Figure 5.6, the produced micronized powders present some difference in their morphology. CHT particles present a more rough surface and relatively distorted spheres. On the other hand, CHT-LbL siRNA powders show a smoother surface with different extended of regularity. STEM images and EDX analysis of such samples are displayed Figure D.5, Appendix D. From the obtained results, the LbL siRNA nanoparticles appear to be located in the outermost of the particle, even after 5 min of sonication (Figure D.5-C).

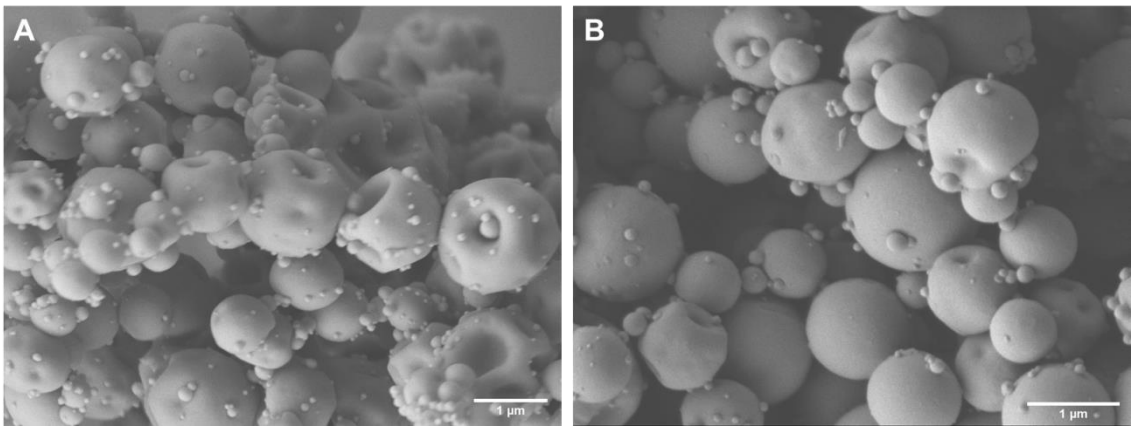

Figure 5.6-SEM images of the produced microparticles: (A) CHT (x 16,000); (B) CHT-LbL siRNA (x 30,000).

To further investigate nanoparticle localization inside the microparticles, the microspheres were observed using CLSM and a 3D reconstruction was performed with the aid of Imaris Bitplane. The whole microspheres were placed on glass-bottomed coverslips containing culture media. The particles were immediately visualized, and their images are depicted in Figure 5.7. Chitosan autofluorescence in DAPI region enabled the localization of whole particle. AF 488 siRNA can be seen in the images in green, representing nanoparticles location along the microparticle. As it can be observed, nanoparticles appear to be located on the outermost of the powders (Figure 5.7A), corroborating the results obtained by STEM and EDX conjugation. Upon a transversal cut, the blue color, correspondent to CHT autofluorescence, seems to be more

on the inside of the formed microparticle. However, the presence of siRNA LbL nanoparticles can be also denoted on the interior of the particle (Figure 5.7B**)**. As already described in the literature, there are no universal procedures to describe particles formation, but there are general tendencies that can be used to explain the particle formation step. The shriveling depicted in SEM images may be a result of a high Peclet number (*Pe*) or as changing *Pe* situation. Briefly, the *Pe* is influenced by a combination of material properties of the solute and the solvent processing parameters that, in turn, determine the evaporation rate. Therefore, the *Pe* number is a function of the ratio between solvent evaporation rate and the diffusion coefficient of the given solute. Hence, if the solvent evaporation rate is higher than the dissolved or suspended components diffusion, the surface will tend to become more enriched in the component with the higher *Pe* number, resulting on shriveled structures. As the nanoparticles possess even higher *Pe*, they will preferentially accumulate on the shell surface. The highest structural organization of nanoparticles hindrances the shell deformation mechanisms.[101,190] Again, the factors governing particle formation like the air temperature to aid particles drying process as well as the slightly increase in EtOH percentage (in comparison to our previous works), may be contributing factors to a rapid solvent evaporation. On the other hand, silica has also been described in literature as a drying auxiliary agent and as CO_2 absorbent.[191] The very low moisture content observed for this particles also corroborate an efficient drying process.

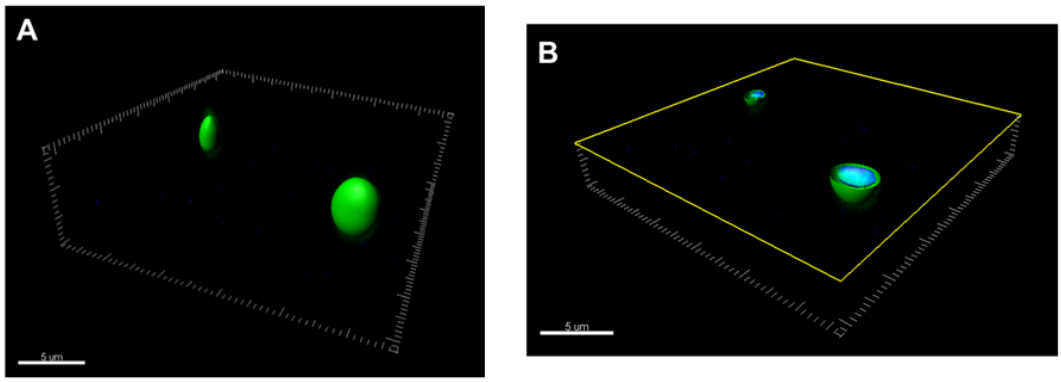

Figure 5.7-3D reconstruction of (A) LbL siRNA – CHT micronized powders and (B) their transversal cut. Green: AF 488 siRNA (λ_{exc} = 473 nm; λ_{emm} = 520 nm); Blue – DAPI, CHT autofluorescence (λ_{exc} = 405 nm; λ_{emm} = 461 nm).

5.4.3 *In vitro* aerosolization study

The powder aerosolization characteristics of CHT-MSN and CHT powders were assessed *in vitro* using a dry powder breath activated inhaler device with the aid of an Anderson Cascade Impactor (ACI). The percentage of powders deposited on each stage of the ACI, inhaler, cap-

sule and induction port was calculated gravimetrically and is plotted on Figure 5.8. In this particular study, the aerosolizable properties of CHT-LbL siRNA powders were not assessed due to the limited quantity of powder achieved, and needed for *in vivo* biodistribution assays.

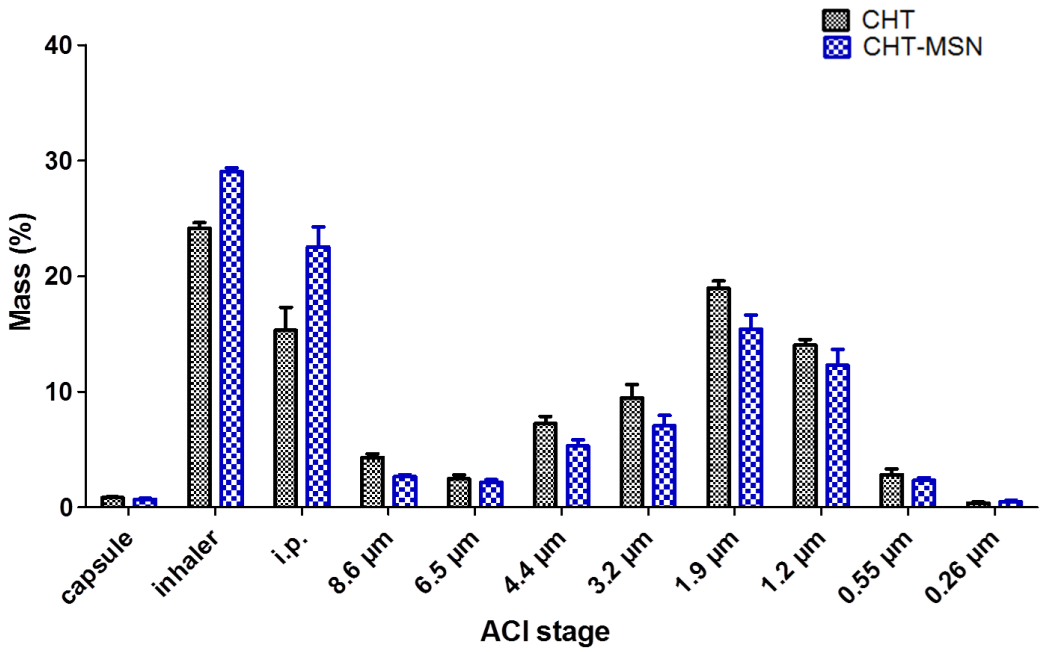

Figure 5.8-Powder dispersion among the micronized powders by ACI.

Cascade Impactor measurements displayed on Table 5.3 were obtained through the dispersion of 4 consecutive capsules (n = 3). The emitted dose which comprises the amount of powder that fluidize through the inhaler varied between 70.3 ± 1.7 % and 75 ± 2 %. It was also found for these formulations that the fine particle fraction (FPF %), the respirable fraction that that is most likely to deposit in the deep lung, was 54 ± 3 % to CHT and 44 ± 4 % for the CHT-MSN formulation, nearly matching the DPIs currently available on the market.[152,153] In Figure 5.8 it can be seen that the majority of the powder is lost in the inhaler and induction port, which simulates the upper airways. Such may be due to the formation of turbulent eddies in this area, humidity, chitosan mucoadhesive property or electrostatic energy of the produced powders.

Table 5.3-ACI measurements.

Sample	ED (%)	FPF (%)	MMAD (µm)	GSD
CHT	75±2	54±3	1.6±0.1	2.2±0.1
CHT-MSN	70±2	44±5	1.7±0.1	1.8±0.1

The results were analyzed using Graph Pad, performing a two-way analysis of variance (ANOVA) with a Bonferrroni's multiple comparison test for a significance level of 5%. Although a slight difference between the obtained values may be denoted, none of the samples show any significant difference in any of the ACI measurements. However, due to more pronounced shivering denoted for CHT microparticles, an enhanced flowability of this particular type of particles was already expected [190]

5.4.4 In *vitro* cumulative release studies: nano and siRNA simultaneous release

The cumulative release profile of the LbL siRNA nanoparticles and the siRNA *per se*, are depicted in Figure 5.9. Two different pHs were used in this study: 7.4 to mimic the physiologic pH; and 6.8 to mimic the lung lining-fluid of a lung cancer situation. For these *in vitro* studies, only CHT-LbL siRNA formulation was assessed. To evaluate the nanoparticles release from the microparticles, the IR-780 dye fluorescence was monitored at pre-determined end points. For the siRNA release from the powders, Ribrogreen assay was used to quantify the amount of siRNA released along the same end points.

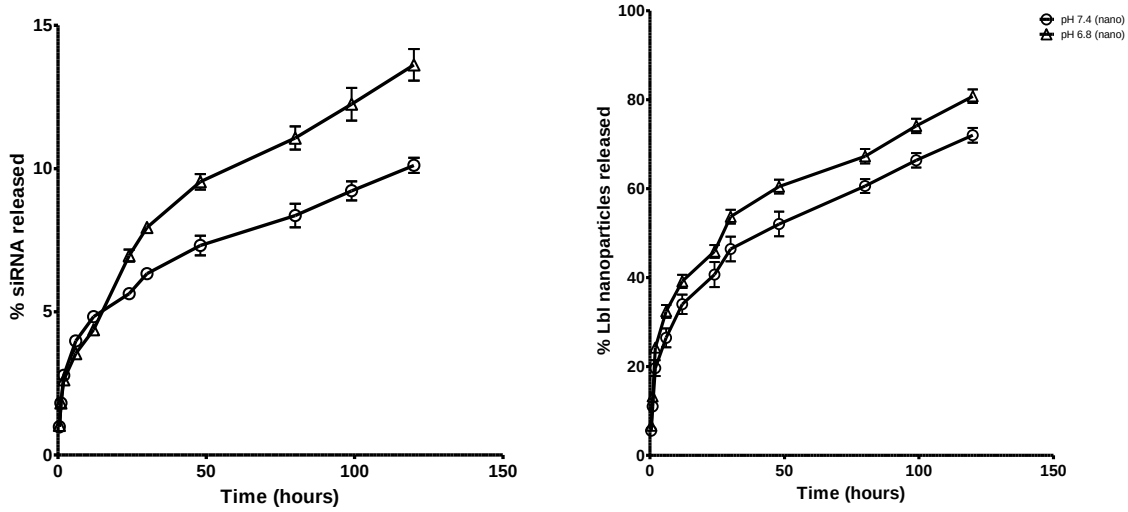

Figure 5.9-*In vitro* release assays of A) siRNA; B) LbL nanoparticles from micronized powders.

As demonstrated in the figure, siRNA is released from the micronized powders at a higher rate or pH 6.8, as already expected according to the release assays of siRNA from the LbL nanosystems. On the other hand, according to the IR-780 dye intensity, the release profile of the nanosystems from the micropowders varies between 72 and 80 % for pHs 7.4 and 6.8, respectively. Such result was already expected as described in the previous chapter. Briefly, since CHT pKa is 6.5, it is expected that at pH 6.8, CHT amino groups are partially protonated, leading to powders hydrolysis and consequently, a faster release.

The diffusion mechanism of the LbL nanosystems and siRNA through the microparticles were both evaluated by fitting the obtained data with Korsmeyer and Peppas equation (Figure D.6, Appendix D). Based on the diffusion exponent (n) of both systems in both pHs (between 0.38 and 0.44) their release profile from the microspheres is occurring through Fickian diffusion.[169]

5.4.5 *In vitro* performance of nano-in-micro formulations

The ability of the CHT-LbL siRNA powders to silence KRAS gene was investigated in tdTomato–expressing KP cells and is displayed on Figure 5.10. Increased concentrations of particles and, consequently, KRAS siRNA were investigated. Gene expression of treated cells was compared to untreated ones. It was found that the CHT-LbL siRNA microparticles were able to achieve more than 90 % of gene silencing compared to the untreated cells. Considering both the amount of siRNA entrapped per gram of powder (as displayed in Figure D.2, Appendix D), that

only half of that amount corresponds to LbL KRAS siRNA nanoparticles, and 13.3 % of the total siRNA that those particles cover AF 488 siRNA (and therefore only 86.7 % is KRAS siRNA) it is possible to say that 120 µg of powders contain approximately 33 nM of KRAS siRNA and 30 µg, 8.3 nM of KRAS siRNA.

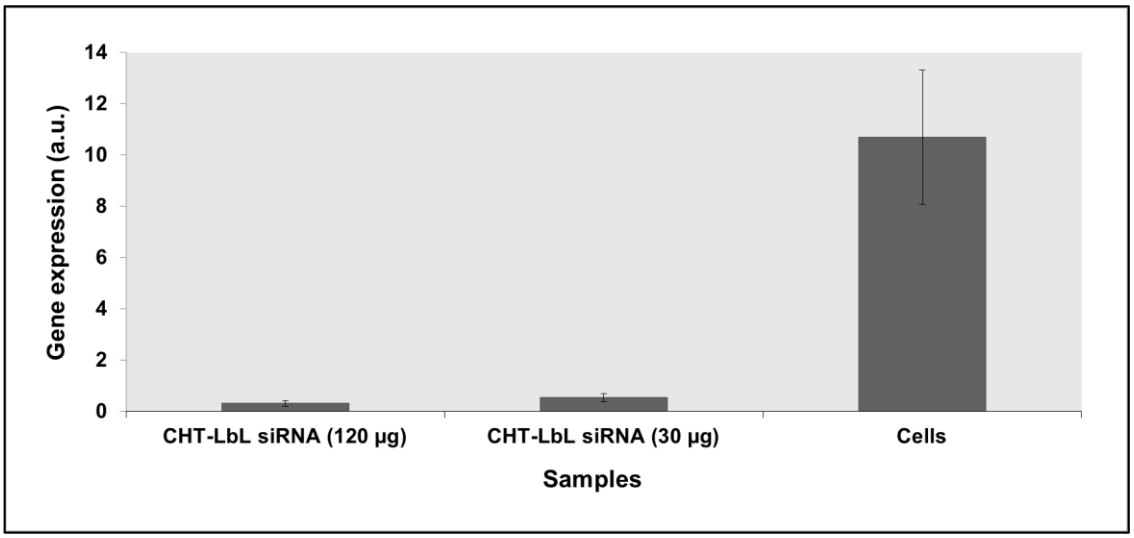

Figure 5.10-Effects of CHT-LbL siRNA microparticles on KRAS gene expression in tdTomato–expressing KP cell line (72 h).

Cell viability of the micronized powders was also addressed. As Figure 5.11 demonstrates, there is little cytotoxicity demonstrated by the micronized powders (cell viability always above 80 %). Although slight differences may be observed, there is no significant statistical difference between the negative control (cells) and the cells incubated with the powders.

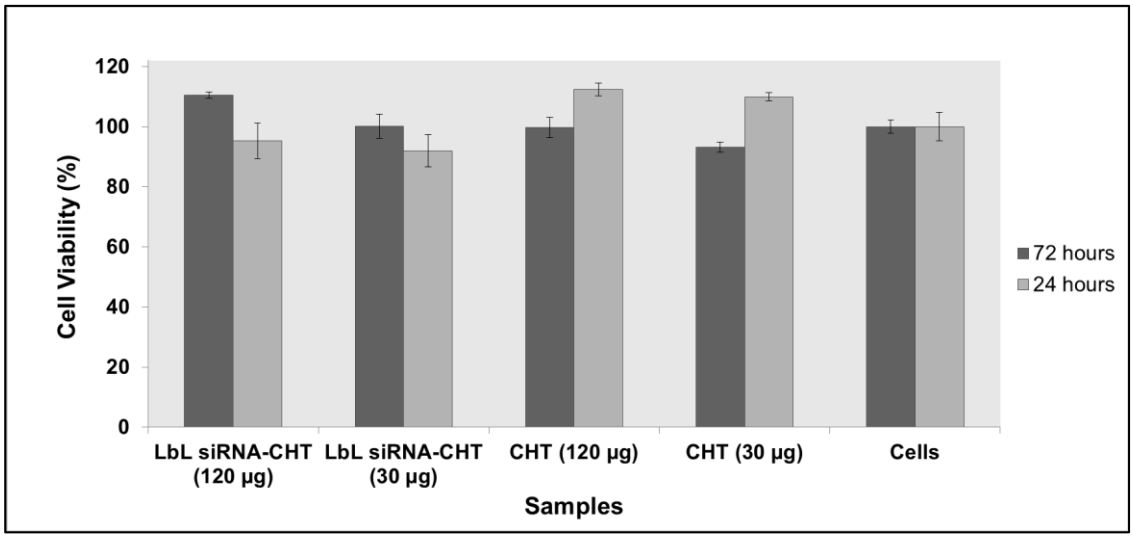

Figure 5.11-Cell viability of tdTomato–expressing KP cell line in the presence of micronized powders.

Powder interactions with cells after 1 and 12 h were also investigated using CSLM and their images are displayed in Figure 5.12. In this particular imaging, brightfield channel was also used to more clearly understand particle location. Also, no nuclear staining was used to avoid overlapping with CHT autofluorescence in DAPI region. After 1 h of incubation, green dots from AF 488 siRNA can be depicted among the cellular environment and already appear to be not confined to microparticles location (in blue) (Figure 5.12A). After 12 h of incubation, the siRNA spreading from the CHT microparticles is even more evidenced and accentuated among the cellular environment as demonstrated in Figure 5.12B. Such results are in agreement with the release profile obtained for both the LbL nanosystems as well as the labeled siRNA from the microspheres. It is also worth mentioning that microparticle adhesion to cells may be actually attributed to the outermost location of the LbL nanoparticles. In fact, since HA is the last layer in our LbL assembly, their interaction with CD44 receptors in tdTomato expressing KP cell line governs the higher levels of binding and internalization observed.

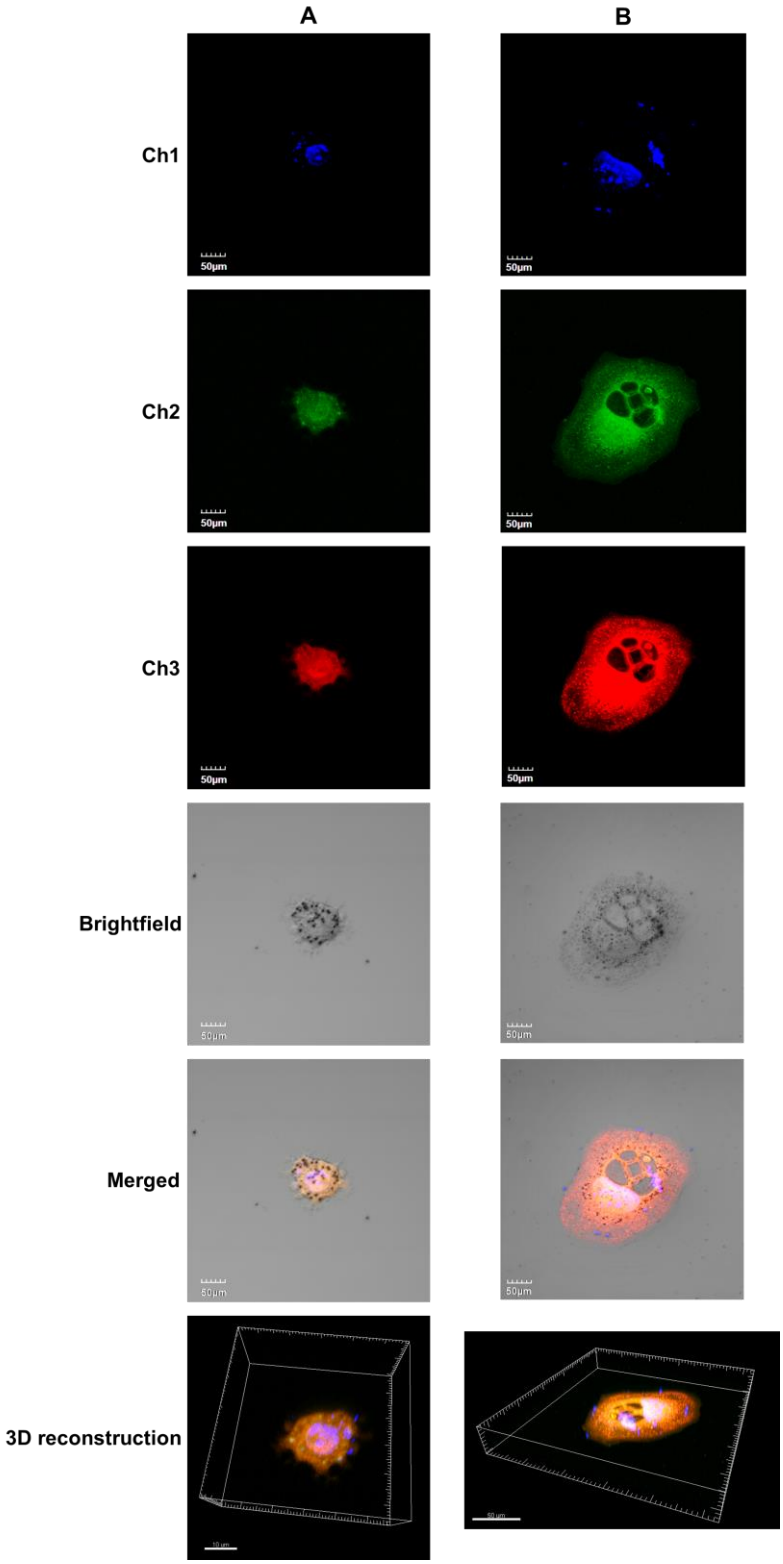

Figure 5.12-CLSM of td Tomato-expressing KP cell line incubated with the LbL siRNA microparticles after (A) 1 and (B) 12 h. Ch1 – DAPI, microparticles autofluorescence (λ_{exc} = 405 nm ; λ_{emm} = 461 nm); Ch2 – AF 488, siRNA (λ_{exc} = 473 nm ; λ_{emm} = 520 nm); Ch3 – Ds- Red2, tdTomato Kp cell line (λ_{exc} = 559 nm ; λ_{emm} = 581 nm); Merged – overlapping of channels 1,2,3 and brightfield; and 3D reconstruction.

5.4.6 *In* vivo biodistribution of the CHT-LbL siRNA powder

In order to achieve an effective gene silencing by siRNA *in vivo*, it is important to understand siRNA biodistribution and pharmacokinetics. It is well known that naked siRNA is easily degraded by the endonucleases presented in the bloodstream and, when injected intravenously, it is mostly accumulated in the kidneys and excreted in the urine (size below threshold for rapid renal excretion < 20nm). Nevertheless, biodistribution and pharmacokinetic behavior of siRNA after pulmonary administration are poorly described in the literature. In a proof-of-concept study, we attempted to address siRNA biodistribution following pulmonary delivery in healthy female BALB/c mice. CHT microparticles (no LbL nanosystems incorporation) were used as a control. Mice lungs treated with CHT-LbL siRNA microparticles were imaged using IVIS system after 30 min and 24 h (Figure 5.13). The administered dose to each mouse was 1.5 mg of powder, containing approximately 2.8 µg of siRNA (for CHT-LbL siRNA powders). Untreated lungs from healthy mice were also imaged in order to normalize lung autofluorescence. CHT microparticle autofluorescence is also easily depicted on IVIS imaging.

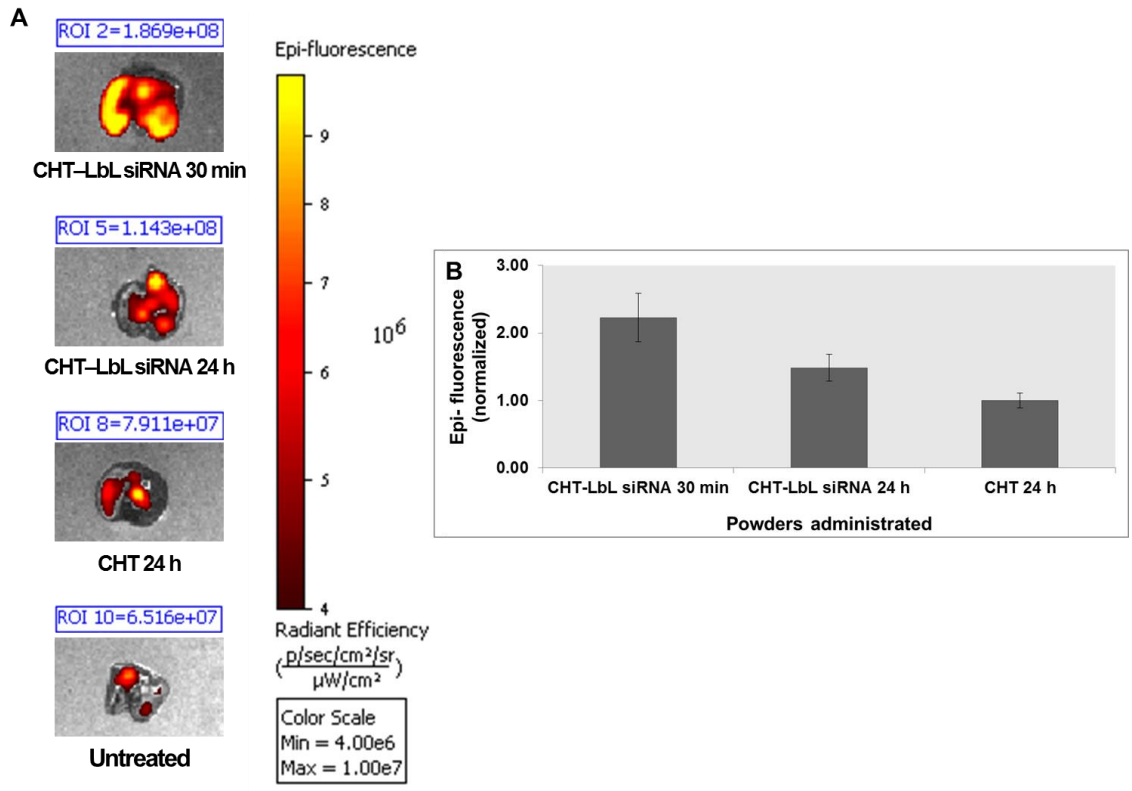

Figure 5.13-Micronized powders biodistribution in mice lungs: (A) Accumulation of the particles in mice lungs over pre-determined periods of time (λ_{exc} = 465 nm ; λ_{emm} = 520 nm); (B) Region-of- interest (ROI) analysis of lungs-specific accumulation.

The extracted lungs were scanned using two imaging techniques: two photon correlation microscopy (TPCM) and CLSM, as shown in Figure 5.14. Both microscopic imaging showed a higher fluorescence intensity on the green channel for samples CHT-LbL siRNA. By looking mainly to the TPCM images it appears that there is a higher particle density at 24 h than on 30 min, which is a contradictory result to IVIS epi-fluorescence measurement. Nevertheless, the high presence of collagen fibers (imaged by second harmonic generated polarized light) for the 30 min sample may also contribute to a lack of macroscopic perception for the particles there presented. CHT autofluorescence can be also corroborated by the presence of green dots in both images of both techniques. However, according to the TPCM image of CHT (where no tissue autofluorescence is presented) it is easily denoted that the green density and intensity is much lower than in the LbL siRNA-CHT particles. Lung tissue autofluorescence is mainly depicted in blue in CLSM.

As expected, untreated lungs do not exhibit any green fluorescence on TPCM, and only a limited autofluorescence in the green channel is observed in CLSM, proving that the green dots evidenced at the other samples do correspond to microparticles localization.

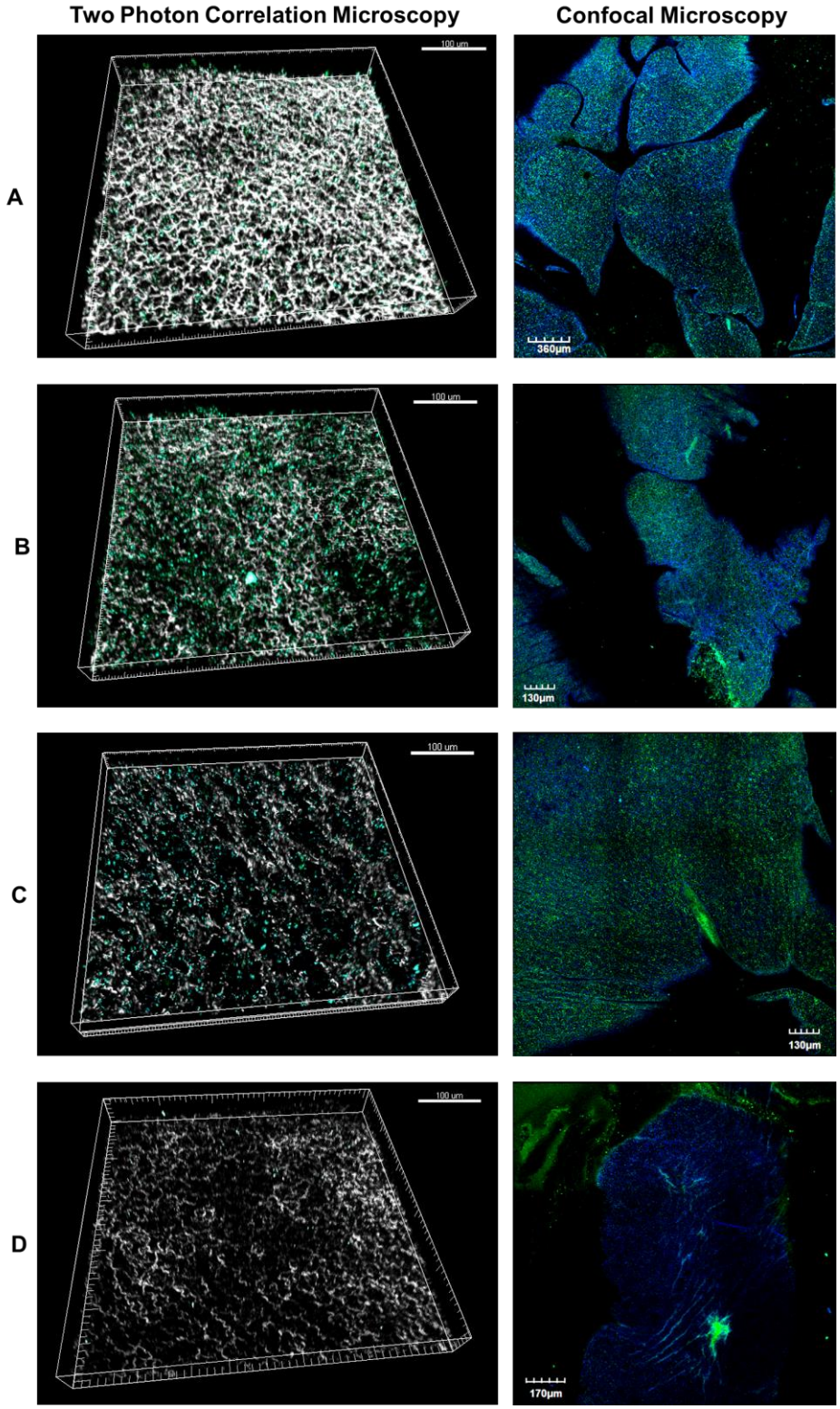

Figure 5. 14-Lung sections scans using TPCM and CLSM. Collagen fibers of lung tissue are depicted in white and microparticles depicted in green. (A) CHT-LbL siRNA 30 min; (B) CHT-LbL siRNA 24 h; (C) CHT 24 h; (D) Untreated lung tissue where only lungs autofluorescence is observed in CLSM. Both images were acquired using a using a 25 x, N.A. 1.05 objective at 840 nm.

Lungs section histology is displayed in Figure 5.15. Sections unstained (Figure 5.15-1) and stained with Hematoxylin and Eosin (H&E) (Figure 5.15-2 and 3). These results were analyzed using TPCM (Figure 5.15-1 and 2) and a Nikon light microscope (Figure 5.15-3). Figure 5.15-1 reveals the presence of microparticles in lung sections, mainly depicted in CHT-LbL siRNA 30 min and 24 hours (in green) (Figure 5.15 A1 and B1, respectively). H&E staining revealed the presence of more blue coloration (hematoxylin staining) in the lungs of animals treated with CHT-LbL siRNA powders (Figure 5.15-A3 and B3). Since hematoxylin stains acidic (or basophilic) structures it will bind to the siRNA presented in the powders. Nevertheless, animals receiving CHT microparticles showed evidence of mild inflammation, as corroborated by the slight increase in the blue staining from hematoxylin, probably related with the appearance of white cells. Such result is in agreement with some reports in the literature that showed pro-inflammatory effect in animals' lungs after administering CHT microparticles.[192] Yet, additional experiments are required to help clarify whether the produced CHT microparticles do trigger *in vivo* inflammatory response by the lung. The autofluorescence of the H&E staining sections are depicted in Figure 5.15-2.

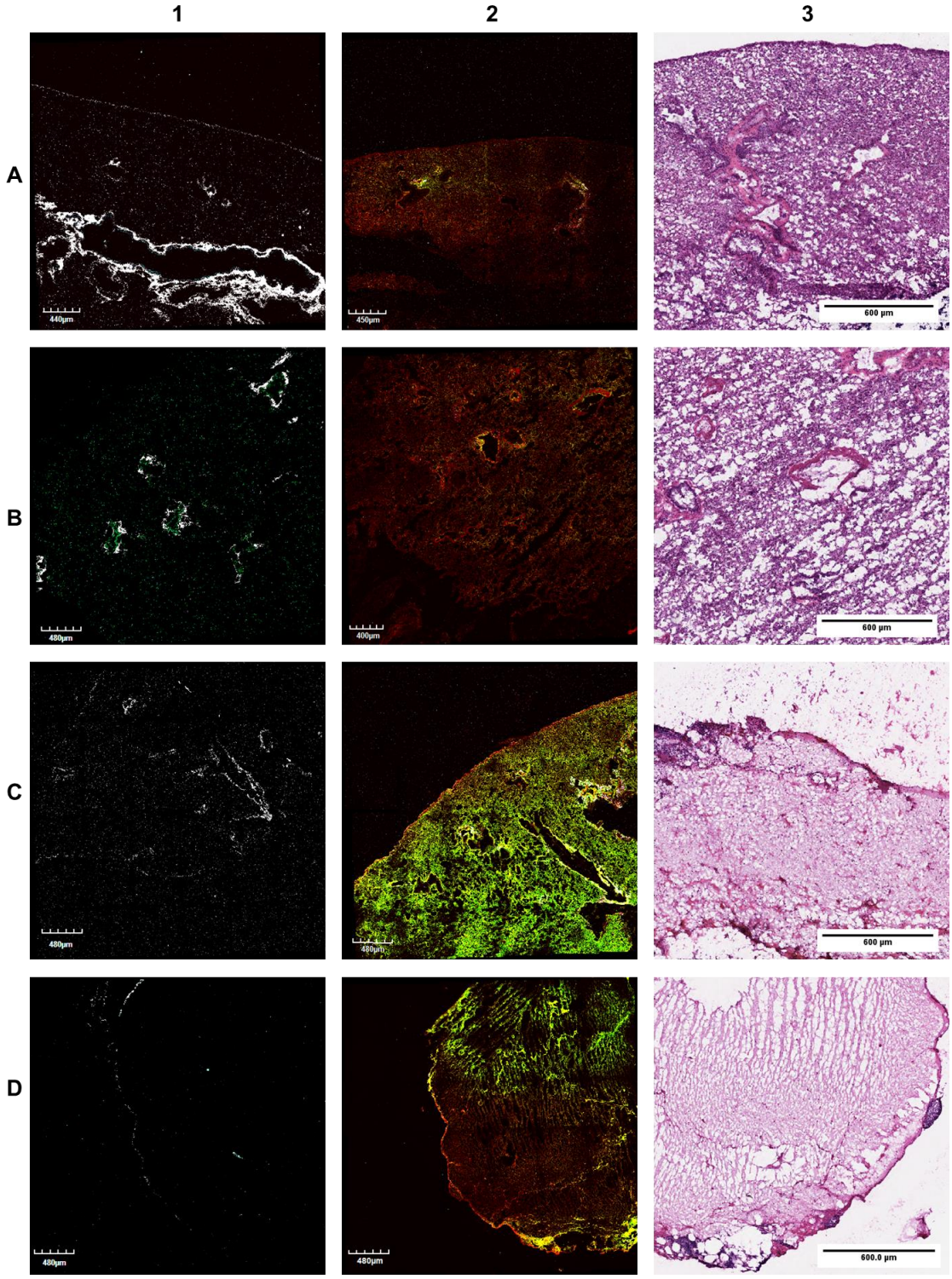

Figure 5.15- Histology analysis of lung sections: (A) CHT-LbL siRNA 30 min; (B) CHT-LbL siRNA 24 h; (C) CHT 24 h; (D) Untreated of (1) unstained; and (2),(3) H&E stained lung tissue sections isolated from the mice. (1**)** and (2**)** were imaged using TPCM (using a 25x, N.A. 1.05 objective at 840 nm) and (3**)** with Nikon light microscope (4x).

Serum biochemistry analysis of the blood recovered at the end of the experiment (24 h) is displayed on Table 5.4.

The results were compared to the dynamic reference range given by Charles River, and show no sign of liver or kidney damage, suggesting that the micronized powders and the LbL nanosystems exhibited little toxicity at the administered dose.

Table 5.4-Serum levels of ALT, AST, BUN and CREAT at the end of the 24 h treatment in BALB/c mice.

	ALT (U/L)	**AST (U/L)**	**BUN (mg/dL)**	**CREAT (mg/dL)**
CHT-LbL siRNA	151 ± 93	265 ± 102	14 ± 1.5	0.2 ± 0.03
CHT	295 ± 154	763 ± 194	15 ± 1.2	0.3 ± 0.07
Untreated	198 ± 114	626 ± 163	17 ± 2	0.3 ± 0.05
Dynamic Range	3-500	3-1000	2-130	0.2-25

[a] Data are mean ± error (n=3 per group). [b] ALT – alanine aminotransferase; AST – aspartate aminotransferase; BUN – blood urine nitrogen; CREAT – creatinine.

5.5 CONCLUSIONS

In the present study, LbL nanosystems comprising a nanolayer of KRAS siRNA were successfully engineered. The developed LbL assemblies were able to attain a significant impact on the reduction of KRAS gene expression in the KP lung cell line. Micronization of these nanosystems into CHT powders using SASD technology enabled the design and production of reliable systems for pulmonary delivery of siRNA. The ability of the micronized siRNA to reduce KRAS gene expression *in vitro* reveals the nucleic acid stability even after powder production. Moreover, the controlled and sustained release obtained for the biomolecules entrapped in the microparticles (both nanosystems and siRNA *per se*) proved that our micronized systems are suitable for a controlled pulmonary delivery. *In vivo* biodistribution of the micro formulations in healthy mice showed an alveolar distribution of the developed powders and no serum toxicity was noticed in the end of the treatment. However, some additional experiments may be required to clarify whether the CHT micropowders may trigger an *in vivo* inflammatory response by the lung. Nevertheless, the results provide a potential strategy to deliver siRNA to the lungs and address gene therapy in lung adenocarcinoma situation. The presence of the IR-780

dye in the MSN core of the LbL nanoassemblies will further allow combining therapeutic approaches, such as PTT, with gene therapy, potentially increasing lung cancer regression.

CHAPTER 6. Final overview, concluding remarks and future prospects

6.1 Final overview and concluding remarks

Local administration of biopharmaceutics to the lung is known as the most promising approach for deep lung delivery enabling both local and systemic treatments in several complications. Such type of treatment enables a targeted therapy while minimizing systemic toxicity. The advantages of such type of administration have been the focus of the most recent research regarding lung cancer treatment.

The work detailed in this thesis reveals the extraordinary advantages of combining nanotechnology, molecular biology, polymer science, chemical engineering and supercritical fluid technologies, to develop robust and reliable pulmonary delivery systems for the treatment of non-small cell lung cancer. The major goals of the present thesis were: i) to produce new biocompatible, biodegradable and targeted nanoplatforms that could be use in theragnosis lung cancer situations; ii) to produce nano-in-micro dry powders formulations with suitable aerodynamic properties and adequate release and degradation profiles, while preserving nanoparticles integrity; and iii) to evaluate *in vivo* powders biodistribution in mice lungs. For this purpose, nanoparticulated systems with therapeutic and/or diagnosis capabilities were embedded into respirable microparticles to be delivered to the lungs. In order to minimize costs, environmental impact, and eventual toxicity, the particles for pulmonary inhalation engineered during this PhD, were produced using sustainable methodologies like supercritical assisted spray drying (SASD), a process based on $scCO_2$ technology.

With the goal of designing a biocompatible, biodegradable theragnostic system, in the initial stages of the work (CHAPTER 2 and 3) there was a major concern on engineering robust functionalized nanosystems with environmental friendly coatings able to provide stealthy and fluorescence properties. Gold nanoparticles (AuNPs), having already shown remarkable impairments on lung cancer theragnosis, were elected as the nanocores to build our lung cancer theragnostic strategy.

In CHAPTER 2, AuNPs were coated with maleimide poly(ethylene glycol) (MPM) in order to provide a stealth character, improve nanoparticles' stability and foster their internalization. A second layer comprising of an oligoaziridine biosensor, polymerized under supercritical conditions, was added to the nanosystems in order to confer a fluorescent capability to the nanoparticles. Such straightforward incorporation avoids fluorescence quenching by the AuNPs' plasmon resonance effect, the major limitation of AuNPs fluorescent tagging. Moreover, the results showed that the produced biotags were able to enter into cells environment, and qualitative analysis using confocal laser scanning microscopy (CLSM) actually showed a nuclear

penetration of these biotags. These extraordinary features together with the biocompatibility demonstrated by the biotags enabled the production of feasible nanodevices that once conjugated with specific antibodies, anti-cancer drugs and photothermal therapy (PTT) can produce extraordinary outcomes in cancer theragnosis.

Notwithstanding, conscious that the use of synthetic compounds, like MPM, may lead to hepatotoxicity, the work in this PhD evolved in a way of substituting this type of polymers, while maintaining nanoparticles' stability, fluorescence and biocompatibility, as stated in CHAPTER 3. Further strengthen in the specific character towards particular tumor cell lines was also a requirement in order to improve nanoprobes specificity to tumor tissue. Hence, PEG coatings were substituted by "green" oligo(2-alkyl-2-oxazolines) produced using $scCO_2$ assisted protocols, a clean and friendly-environment technology built on the principles of green chemistry. Post–functionalization of the oligo-oxazolines (OOxs) enabled effective coatings on AuNPs' surface, resulting in stable and still, fluorescent nanoparticles. The placement of the fluorescent moiety on the OOxs, opposed to the moiety that grafts to the nanoparticles' surface, limits fluorescence quenching by the AuNPs' plasmon resonance effect. This remarkable finding allowed for the development of new, stable, stealthy and fluorescent AuNPs avoiding further steps of grafting with expensive probes. The developed systems presented ideal sizes for intracellular delivery and the additional conjugation of the peptide YIGSR strongly increased particles uptake by the lung cancer cell line under study (A549). The problematics around the use of PEGs are, therefore, circumvented and due to the optical and targeted capabilities of the produced particles, further conjugations with anti-cancer drugs or other therapeutic molecules enable the use of this type of nanosystems for cancer theragnosis applications.

The micronization of the developed gold nanoprobes (GNP) into chitosan (CHT) polymeric matrix, as reported in CHAPTER 4, was successfully achieved by making use of sustainable methodologies like SASD. Remarkably, the engineered powders exhibit suitable aerodynamic characteristics for inhalation and optimal biodegradation and release profiles. CHT, used as a polymeric carrier to the GNP proved to be a suitable material to be used in pulmonary delivery to treat lung cancer, as it releases from 50 to 90% of the nanocarriers (depending on the type of nanoparticles embedded) after 4 days, when incubated at pH 6.8.

It is believed that the new class of SASD formulations will impact the production pipeline of pharmaceutical companies. Notwithstanding, to rapidly take this particle engineering platform to clinical translation, there is a need to produce proof-of-concept studies using most common and, if possible, currently FDA approved nanocarriers and materials. In this attempt, a switch in the nanocore material was performed and mesoporous silica nanoparticles (MSN)

were used as the nanotemplate for layer-by-layer (LbL) assemblies, due its biocompatible and biodegradable character, as demonstrated in CHAPTER 5. LbL assemblies using a siRNA nanolayer and more common and/or FDA approved polyelectrolytes enabled an outstanding gene silencing in KRAS oncogene, mutated in lung adenocarcinoma cell lines. The combination of SASD and LbL technology with genetic therapy led to the manufacturing of nano-in-micro formulations with ideal release profiles and enhanced aerodynamic properties, moisture content and fine particle fractions (FPF). Controlled and sustained releases of either siRNA LbL (~ 80% after 5 days at pH 6.8) and siRNA *per se* (~ 14% after 5 days at pH 6.8) were obtained demonstrating, again, that CHT was an accurate choice for the carrier system. Although some additional experiments may be required to clarify whether the CHT micropowders may trigger an *in vivo* inflammatory response by the lung, the alveolar biodistribution of the nano-in-micro formulations and no serum toxicity evidenced in healthy mice, suggest that the developed formulations are suitable for future *in vivo* lung cancer gene therapy thought the pulmonary route. Additionally, the loaded IR-780 dye into MSN pores also enables the combination of gene therapy with PTT, potentially increasing therapeutic outcomes.

A comparison between the two different types of nano-in-micro platforms developed in this thesis is demonstrated in Table 6.1. Briefly, all the engineered formulations exhibit similar volume mean diameters ($D_{v,50}$) varying between 3.1 and 4.2 µm and span values varying between 0.8 to 2.9, being the highest value mainly attributed to the presence of aggregates. The high emitted dose percentages (ED %) and fine particle fractions (FPF) obtained for all the manufactured powders demonstrate that there are high percentages of powders likely to deposit in the deep lung. In fact, the majority of the values obtained for FPF, match the already marketed DPIs currently available, as already discussed along the respective chapters. The major difference depicted among the two types of formulations produced in CHAPTER 4 and 5 is related to particles moisture content. Such pronounced differences may be attributed to the improvements that the lab scale SASD apparatus suffered in order to produce excellent ultrafine particles for pulmonary delivery with sufficient siRNA loading to generate therapeutic effect. In this particular case, the amount of water used in the casting solution was extremely low, when compared to the ones used in CHAPTER 4, in order to provide a faster drying process enabling the preservation of siRNA integrity. Further centrifugation processes to remove the water excess of the GNP formulations in CHAPTER 4 could potentially decrease the moisture content of CHT-GNP formulations.

Nevertheless, the findings herein highlighted are of extreme importance and prove that our powders have the aerodynamic features ideal for deep lung delivery. These results, com-

bined with the optimal release profiles above mentioned, and with the sustainability beyond this type of manufacturing, make these nano-in-micro formulations, potential candidates for sustained pulmonary delivery, achieving, therefore, one of the major goals of this PhD.

Table 6.1 – Comparison of aerodynamic properties and cascade impactor measurements obtained through the course of this thesis.

Sample	$D_{v,50}$ (µm)	Span	E(%)	Moisture Content	ED (%)	FPF (%)	MMAD (µm)	GSD
CHT (chapter 4)	3.6	1.3	-	15.4	75±2.0	26±2	1.4±0.04	2.9±0.1
CHT-Au	3.2	2.9	34.7	14.8	86.8±0.3	32.8±0.4	3.2±0.1	2.8±0.1
CHT-Au-OEI-CS	3.7	1.7	17.2	12.4	66±2	41±1	1.5±0.1	3.3±0.1
CHT-Au-OEI-CS-YIGSR	3.4	1.7	51.8	16.2	72.2±0.1	44±2	1.8±0.07	3.1±0.1
CHT-Au-OEtOX-SH	3.8	1.4	38.6	14.9	70.2 ± 1	42±3	1.3±0.2	3.3±0.1
CHT-Au-OEtOX-SH-YIGSR	3.4	1.7	46.5	12.5	81±1	47±2	1.8±0.2	2.9±0.1
CHT (chapter 5)	4.2	0.9	-	1.4	75±2	54±3	1.6±0.1	2.2±0.1
CHT-MSN	3.1	0.8	-	0.7	70±2	44±4	1.7±0.1	1.8±0.1
CHT-LbL siRNA	3.5	1	28.7	0.9	n.a.	n.a.	n.a.	n.a.

Ultimately, the investigation conducted in this thesis and the findings that resulted from it enabled the successful development of potential aerosolizable systems for lung delivery. On the other hand, the nanosystems engineered along this PhD also empowered the developed micro powders allowing for their future use in lung cancer theragnosis. The goals of this thesis were successfully achieved and bring new insights for the use of pulmonary delivery in lung cancer situations.

6.2 Future prospects

"There's plenty of room at the bottom" was a lecture given by the physicist Richard Feyman at an American Physical Society in 1959. Since then, this well-known expression has been linked directly to the nanotechnology world and to the infinite possibilities that arise from it. Therefore, if there is plenty room to manipulate individual atoms, there is also plenty of room for improvement in the strategies described in this thesis.

Although the works herein detailed may present huge advances in particles' engineering for effective pulmonary delivery and lung cancer therapy, more efforts need to be done to translate these approaches into clinical applications. Additional *in vivo* contributions regarding the use of SASD technology must be addressed in order to convince the pharmaceutical industries to adopt such strategy. Accurate pharmacokinetics and pharmacodynamics studies, (meaning what happens to the particles after their deposition in the lungs and what are the effects of such particles/biomolecules in the body, respectively) need to be fully investigated to assure clinical relevance. There is also a need to perform *in vivo* toxicology studies of such type of formulations, mainly using CHT as carrier system. Pre-clinical studies involving the determination of a therapeutic margin, more histopathology evaluations (mainly of proximal and distal regions of the respiratory tract), and other *in vitro* specific methods, like growth factor release and enzymatic activities, should be addressed to bring these products to clinical trials.

Moreover, the use of supercritical technology to build nanoparticles coatings must also attain clinical relevance in order to evoke a change in industry mind-set.

Once these approaches are effectively implemented into industry, extraordinary therapeutic advances will definitely arise, improving to a great extend several pulmonary and systemic complications.

Forthcoming works that can arise from this thesis and be implemented in a near future include:

i) Evaluation of gene therapy efficacy in lung adenocarcinoma bearing mice, using the nano-in-micro systems developed in CHAPTER 5, and the investigation of possible improvements in tumor regression by combining such treatment with PTT;

ii) *In vivo* administration of the nano-in-micro platforms produced in CHAPTER 4 and assessment of the theragnosis potential of these systems, mainly in combination with PTT;

iii) Substitution of the water soluble oligomers produced in CHAPTER 3 by co-oligomers comprising both hydrophilic and hydrophobic parts (already synthetized by the author during this PhD), to enhance drug loading into the nanocarriers, and micronize such systems and assess their ability to chemically kill tumor cells in lung adenocarcinoma bearing mice.

Reference List

(1) Dufort, S., Bianchi, A., Henry, M., Lux, F., Le Duc, G., Josserand, V., Louis, C., Perriat, P., Crémillieux, Y., Tillement, O., and Coll, J.-L. (2015) Nebulized Gadolinium-Based Nanoparticles: A Theranostic Approach for Lung Tumor Imaging and Radiosensitization. *Small 11*, 215–221.

(2) Taratula, O., Garbuzenko, O. B., Chen, A. M., and Minko, T. (2011) Innovative strategy for treatment of lung cancer: targeted nanotechnology-based inhalation co-delivery of anticancer drugs and siRNA. *J. Drug Target. 19*, 900–914.

(3) Patil, J. S., and Sarasija, S. (2012) Pulmonary drug delivery strategies: A consice, systematic review. *Lung India 29*, 44–49.

(4) Ruge, C. A., Kirch, J., and Lehr, C. (2013) Pulmonary drug delivery : from generating aerosols to overcoming biological barriers — therapeutic possibilities and technological challenges. *Lancet Respir. 1*, 402–413.

(5) Lytton-jean, A. K. R., Kauffman, K. J., Kaczmarek, J. C., and Langer, R. (2015) Nanotechnology-Based Precision Tools for the Detection and Treatment of Cancer. *Cancer Treat. Res. 166*, 293–322.

(6) Sivadas, N., O'Rourke, D., Tobin, A., Buckley, V., Ramtoola, Z., Kelly, J. G., Hickey, A. J., and Cryan, S.-A. (2008) A comparative study of a range of polymeric microspheres as potential carriers for the inhalation of proteins. *Int. J. Pharm. 358*, 159–167.

(7) Kurmi, B. D., Kayat, J., Gajbhiye, V., and Tekade, R. K. (2010) Micro- and nanocarrier-mediated lung targeting. *Expert Opin. Drug Deliv.* 781–794.

(8) Akiyama, Y., Mori, T., Katayama, Y., and Niidome, T. (2009) The effects of PEG grafting level and injection dose on gold nanorod biodistribution in the tumor-bearing mice. *J. Control. Release 139*, 81–84.

(9) K. Lai, S., Wang, Y.-Y., and Hanes, J. (2010) Mucus-penetrating nanoparticles for drug and gene delivery to mucosal tissues. *Adv. Drug Deliv. Rev. 61*, 158–171.

(10) Ghosh, P., Han, G., De, M., Kim, C. K., and Rotello, V. M. (2008) Gold nanoparticles in delivery applications. *Adv. Drug Deliv. Rev. 60*, 1307–1315.

(11) Silva, A. S., Bonifácio, V. D. B., Raje, V. P., Branco, P. S., Machado, P. P. F., Correia, J., and Aguiar-ricardo, A. (2015) Design of oligoaziridine-PEG coatings for efficient nanogold cellular biotaging. *RSC Adv. 5*, 10733–10738.

(12) Conde, J., Rosa, J., de la Fuente, J. M., and Baptista, P. V. (2013) Gold-nanobeacons for simultaneous gene specific silencing and intracellular tracking of the silencing events. *Biomaterials 34*, 2516–2523.

(13) Solis David, J., Chang, W.-S., Khanal, B. P., Bao, K., Nordlander, P., Zubarev, E. R., and Link, S. (2010) Bleach-imaged plasmon propagation (BlIPP) in single gold nanowires. *Nano Lett. 10*, 3482–3485.

(14) Peer, D., Karp, J. M., Hong, S., Farokhzad, O. C., Margalit, R., and Langer, R. (2007) Nanocarriers as an emerging platform for cancer therapy. *Nat. Nanotechnol. 2*, 751–760.

(15) Farokhzad, O. C., and Langer, R. (2009) Impact of Nanotechnology on Drug\nDelivery. *ACS Nano 3*, 16–20.

(16) Hu, J., Dong, Y., Pastorin, G., Ng, W. K., and Tan, R. B. H. (2013) Spherical agglomerates of pure drug nanoparticles for improved pulmonary delivery in dry powder inhalers. *J. Nanoparticle Res. 15*, 1560–1572.

(17) Choi, S.-W., Xie, J., and Xia, Y. (2009) Chitosan-based inverse opals: three-dimensional scaffolds with uniform pore structures for cell culture. *Adv. Mater. 21*, 2997–3001.

(18) Odziomek, M., Sosnowski, T. R., and Gradoń, L. (2012) Conception, preparation and properties of functional carrier particles for pulmonary drug delivery. *Int. J. Pharm. 433*, 51–59.

(19) Li, Y.-Z., Sun, X., Gong, T., Liu, J., Zuo, J., and Zhang, Z.-R. (2010) Inhalable microparticles as carriers for pulmonary delivery of thymopentin-loaded solid lipid nanoparticles. *Pharm. Res. 27*, 1977–1986.

(20) Hickey, A. J., Mansour, H. M., Telko, M. J., Xu, Z., Smyth, H. D. C., Mulder, T., Mclean, R., Langridge, J., Papadopoulos, D., Hall, K., Hill, C., and Carolina, N. (2007) Physical Characterization of Component Particles Included in Dry Powder Inhalers . I . Strategy Review and Static Characteristics. *J. Pharm. Sci. 96*, 1282–1301.

(21) Klingler, C., Müller, B. W., and Steckel, H. (2009) Insulin-micro- and nanoparticles for pulmonary delivery. *Int. J. Pharm. 377*, 173–179.

(22) Malmsten, M. (2013) Inorganic nanomaterials as delivery systems for proteins, peptides, DNA, and siRNA. *Curr. Opin. Colloid Interface Sci. 18*, 468–480.

(23) Hammond, P. T. (2012) Polyelectrolyte multilayered nanoparticles: using nanolayers for controlled and targeted systemic release. *Nanomedicine 7*, 619–622.

(24) Conde, J., Tian, F., Hernández, Y., Bao, C., Cui, D., Janssen, K.-P., Ibarra, M. R., Baptista, P. V, Stoeger, T., and de la Fuente, J. M. (2013) In vivo tumor targeting via nanoparticle-mediated therapeutic siRNA coupled to inflammatory response in lung cancer mouse models. *Biomaterials 34*, 7744–7753.

(25) Deng, Z. J., Morton, S. W., Ben-akiva, E., Dreaden, E. C., Shopsowitz, K. E., and Hammond, P. T. (2013) Layer-by-Layer Nanoparticles for Systemic Codelivery of an Anticancer Drug and siRNA for Potential Triple-Negative Breast Cancer Treatment. *ACS Nano 11*, 9571–9584.

(26) Merkel, O. M., Rubinstein, I., and Kissel, T. (2014) siRNA Delivery to the lung: What's new? *Adv. Drug Deliv. Rev. 75*, 112–128.

(27) Conde, J., Ambrosone, A., Hernandez, Y., Tian, F., McCully, M., Berry, C. C., Baptista, P. V., Tortiglione, C., and de la Fuente, J. M. (2015) 15 years on siRNA delivery: Beyond the State-of-the-Art on inorganic nanoparticles for RNAi therapeutics. *Nano Today* 1–30.

(28) Geiser, M., Quaile, O., Wenk, A., Wigge, C., Eigeldinger-Berthou, S., Hirn, S., Schäffler, M., Schleh, C., Möller, W., Mall, M. a, and Kreyling, W. G. (2013) Cellular uptake and localization of inhaled gold nanoparticles in lungs of mice with chronic obstructive pulmonary disease. *Part. Fibre Toxicol. 10*, 19–29.

(29) Al-Qadi, S., Grenha, A., Carrión Recio, D., Seijo, B., and Remuñán-López, C. (2012) Microencapsulated chitosan nanoparticles for pulmonary protein delivery: in vivo evaluation of insulin-loaded formulations. *J. Control. Release 157*, 383–390.

(30) Hardy, J. G., and Chadwick, T. S. (2000) Sustained release drug delivery to the lungs: an option for the future. *Clin. Pharmacokinet. 39*, 1–4.

(31) Zhang, J., Wu, L., Chan, H.-K., and Watanabe, W. (2011) Formation, characterization, and fate of inhaled drug nanoparticles. *Adv. Drug Deliv. Rev. 63*, 441–455.

(32) Chow, A. H. L., Tong, H. H. Y., Chattopadhyay, P., and Shekunov, B. Y. (2007) Particle engineering for pulmonary drug delivery. *Pharm. Res. 24*, 411–437.

(33) Mohajel, N., Najafabadi, A. R., Azadmanesh, K., Vatanara, A., Moazeni, E., Rahimi, A., and Gilani, K. (2012) Optimization of a spray drying process to prepare dry powder microparticles containing plasmid nanocomplex. *Int. J. Pharm. 423*, 577–585.

(34) Powell, M. C., and Kanarek, M. S. (2006) Nanomaterial Health Effects — Part 1 : Background and Current Knowledge. *Wis. Med. J. 105*, 16–20.

(35) Borm, P. J. A., and Kreyling, W. (2004) Toxicological Hazards of Inhaled Nanoparticles—Potential Implications for Drug Delivery. *J. Nanosci. Nanotechnol. 4*, 521–531.

(36) Amidi, M., Pellikaan, H. C., de Boer, A. H., Crommelin, D. J. a, Hennink, W. E., and Jiskoot, W. (2008) Preparation and physicochemical characterization of supercritically dried insulin-loaded microparticles for pulmonary delivery. *Eur. J. Pharm. Biopharm. 68*, 191–200.

(37) Wanakule, P., Liu, G. W., Fleury, A. T., and Roy, K. (2012) Nano-inside-micro: Disease-responsive microgels with encapsulated nanoparticles for intracellular drug delivery to the deep lung. *J. Control. Release 162*, 429–437.

(38) Hoet, P. H., Brüske-Hohlfeld, I., and Salata, O. V. (2004) Nanoparticles - known and unknown health risks. *J. Nanobiotechnology 2*, 12–27.

(39) Oberdörster, G., Oberdörster, E., and Oberdörster, J. (2005) Nanotoxicology: An Emerging Discipline Evolving from Studies of Ultrafine Particles. *Environ. Health Perspect. 113*, 823–839.

(40) Kaur, G., Narang, R. K., Rath, G., and Goyal, A. K. (2012) Advances in pulmonary delivery of nanoparticles. *Artif. Cells. Blood Substit. Immobil. Biotechnol. 40*, 75–96.

(41) Tolman, J. A., and Williams, R. O. (2010) Advances in the pulmonary delivery of poorly water-soluble drugs: influence of solubilization on pharmacokinetic properties. *Drug Dev. Ind. Pharm. 36*, 1–30.

(42) Adami, R., Liparoti, S., and Reverchon, E. (2011) A new supercritical assisted atomization configuration, for the micronization of thermolabile compounds. *Chem. Eng. J. 173*, 55–61.

(43) Pulliam, B., Sung, J. C., and Edwards, D. A. (2007) Design of nanoparticle-based dry powder pulmonary vaccines. *Expert Opin. Drug Deliv. 4*, 651–63.

(44) Couzin-Frankel, J. (2013) Cancer Immunotherapy. *Science . 342*, 1432–1433.

(45) Choi, H. S., Ashitate, Y., Lee, J. H., Kim, S. H., Matsui, A., Insin, N., Bawendi, M. G., Semmler-Behnke, M., Frangioni, J. V, and Tsuda, A. (2010) Rapid translocation of nanoparticles from the lung airspaces to the body. *Nat. Biotechnol. 28*, 1300–1303.

(46) Yang, Y., Bajaj, N., Xu, P., Ohn, K., Tsifansky, M. D., and Yeo, Y. (2009) Development of highly porous large PLGA microparticles for pulmonary drug delivery. *Biomaterials 30*, 1947–1953.

(47) Yang, W., Peters, J. I., and Williams, R. O. (2008) Inhaled nanoparticles--a current review. *Int. J. Pharm. 356*, 239–247.

(48) Sadhukha, T., Wiedmann, T. S., and Panyam, J. (2013) Inhalable magnetic nanoparticles for targeted hyperthermia in lung cancer therapy. *Biomaterials 34*, 5163–5171.

(49) Duncan, B., Kim, C., and Rotello, V. M. (2010) Gold nanoparticle platforms as drug and biomacromolecule delivery systems. *J. Control. Release 148*, 122–127.

(50) Dreaden, E. C., Austin, L. A., Mackey, M. A., and El-Sayed, M. A. (2012) Size matters: gold nanoparticles in targeted cancer drug delivery. *Ther. Deliv. 3*, 457–478.

(51) Oishi, M., Tamura, A., Nakamura, T., and Nagasaki, Y. (2009) A Smart Nanoprobe Based On Fluorescence-Quenching PEGylated Nanogels Containing Gold Nanoparticles for Monitoring the Response to Cancer Therapy. *Adv. Funct. Mater. 19*, 827–834.

(52) Rogueda, P. G., and Traini, D. (2007) The nanoscale in pulmonary delivery . Part 2 : formulation platforms. *Expert Opin. Drug Deliv. 6*, 607–620.

(53) Telko, M. J., and Dsc, A. J. H. (2005) Dry Powder Inhaler Formulation. *Respir. Care 50*, 1209–1227.

(54) Packhaeuser, C. B., Lahnstein, K., Sitterberg, J., Schmehl, T., Gessler, T., Bakowsky, U., Seeger, W., and Kissel, T. (2009) Stabilization of aerosolizable nano-carriers by freeze-drying. *Pharm. Res. 26*, 129–138.

(55) Stegemann, S., Kopp, S., Borchard, G., Shah, V. P., Senel, S., Dubey, R., Urbanetz, N., Cittero, M., Schoubben, A., Hippchen, C., Cade, D., Fuglsang, A., Morais, J., Borgström, L., Farshi, F., Seyfang, K.-H., Hermann, R., van de Putte, A., Klebovich, I., and Hincal, A. (2013) Developing and advancing dry powder inhalation towards enhanced therapeutics. *Eur. J. Pharm. Sci. 48*, 181–194.

(56) Malcolmson, R. J., and Embleton, J. K. (1998) Dry powder formulations for pulmonary delivery. *Pharm. Sci. Technolo. Today 1*, 394–398.

(57) Newman, S. P., and Wilding, I. R. (1998) Gamma scintigraphy: an in vivo technique for assessing the equivalence of inhaled products. *Int. J. Pharm. 170*, 1–9.

(58) Pilcer, G., and Amighi, K. (2010) Formulation strategy and use of excipients in pulmonary drug delivery. *Int. J. Pharm. 392*, 1–19.

(59) Gabrio, B. J., Stein, S. W., and Velasquez, D. J. (1999) A new method to evaluate plume characteristics of hydrofluoroalkane and chlorofluorocarbon metered dose inhalers. *Int. J. Pharm. 186*, 3–12.

(60) Gil, M., Vicente, J., and Gaspar, F. (2010) Scale-up methodology for pharmaceutical spray drying. *Chem. today 28*, 18–22.

(61) Son, Y.-J., Worth Longest, P., and Hindle, M. (2013) Aerosolization characteristics of dry powder inhaler formulations for the excipient enhanced growth (EEG) application: effect of spray drying process conditions on aerosol performance. *Int. J. Pharm. 443*, 137–145.

(62) Millqvist-fureby, A., and Malmsten, M. (1999) Spray-drying of trypsin — surface characterisation and activity preservation. *Int. J. Pharm. 188*, 243–253.

(63) Ozeki, T., Beppu, S., Mizoe, T., Takashima, Y., Yuasa, H., and Okada, H. (2006) Preparation of polymeric submicron particle-containing microparticles using a 4-fluid nozzle spray drier. *Pharm. Res. 23*, 177–183.

(64) Dunbar, C. A., Concessio, N. M., and Anthony, J. (1998) Evaluation of Atomizer Performance in Production. *Pharm. Dev. Technol. 3*, 433–441.

(65) Elversson, J., Millqvist-fureby, A., Alderborn, G., and Elofsson, U. (2003) Droplet and particle size relationship and shell thickness of inhalable lactose particles during spray drying. *J. Pharm. Sci. 92*, 900–910.

(66) Elversson, J., and Millqvist-Fureby, A. (2005) Particle size and density in spray drying-effects of carbohydrate properties. *J. Pharm. Sci. 94*, 2049–2060.

(67) Li, H.-Y., and Birchall, J. (2006) Chitosan-modified dry powder formulations for pulmonary gene delivery. *Pharm. Res. 23*, 941–950.

(68) Girotra, P., Singh, S. K., and Nagpal, K. (2013) Supercritical fluid technology: a promising approach in pharmaceutical research. *Pharm. Dev. Technol. 18*, 22–38.

(69) Reverchon, E., and Adami, R. (2006) Nanomaterials and supercritical fluids. *J. Supercrit. Fluids 37*, 1–22.

(70) Sanli, D., Bozbag, S. E., and Erkey, C. (2011) Synthesis of nanostructured materials using supercritical CO2: Part I. Physical transformations. *J. Mater. Sci. 47*, 2995–3025.

(71) Türk, M. (1999) Formation of small organic particles by RESS : experimental and theoretical investigations. *J. Supercrit. Fluids 15*, 79–89.

(72) Martín, A., and Cocero, M. J. (2008) Micronization processes with supercritical fluids: fundamentals and mechanisms. *Adv. Drug Deliv. Rev. 60*, 339–350.

(73) Reverchon, E. (1999) Supercritical antisolvent precipitation of micro- and nano-particles. *J. Supercrit. Fluids 15*, 1–21.

(74) Martín, Á., Pham, H. M., Kilzer, A., Kareth, S., and Weidner, E. (2010) Micronization of polyethylene glycol by PGSS (Particles from Gas Saturated Solutions)-drying of aqueous solutions. *Chem. Eng. Process. Process Intensif. 49*, 1259–1266.

(75) Martín, Á., and Weidner, E. (2010) PGSS-drying: Mechanisms and modeling. *J. Supercrit. Fluids 55*, 271–281.

(76) Yeo, S.-D., and Kiran, E. (2005) Formation of polymer particles with supercritical fluids: A review. *J. Supercrit. Fluids 34*, 287–308.

(77) Adami, R., Osséo, L. S., and Reverchon, E. (2009) Micronization of lysozyme by supercritical assisted atomization. *Biotechnol. Bioeng. 104*, 1162–1170.

(78) Reverchon, E., Adami, R., and Caputo, G. (2006) Supercritical assisted atomization: Performance comparison between laboratory and pilot scale. *J. Supercrit. Fluids 37*, 298–306.

(79) Reverchon, E. (2002) Supercritical-Assisted Atomization To Produce Micro- and/or Nanoparticles of Controlled Size and Distribution. *Ind. Eng. Chem. Res. 41*, 2405–2411.

(80) Reverchon, E. Process for the production of micro and/or nano particles US Patent 7276190 B2.

(81) Chattopadhyay, P., and Gupta, R. B. (2001) Production of Antibiotic Nanoparticles Using Supercritical CO2 as Antisolvent with Enhanced Mass Transfer. *Ind. Eng. Chem. Res. 40*, 3530–3539.

(82) Ungaro, F., D'Angelo, I., Miro, A., La Rotonda, M. I., and Quaglia, F. (2012) Engineered PLGA nano-and micro-carriers for pulmonary delivery: challenges and promises. *J. Pharm. Pharmacol. 64*, 1217–1235.

(83) Tsapis, N., Bennett, D., Jackson, B., Weitz, D. a, and Edwards, D. a. (2002) Trojan particles: large porous carriers of nanoparticles for drug delivery. *Proc. Natl. Acad. Sci. U. S. A. 99*, 12001–12005.

(84) Sung, J. C., Padilla, D. J., Garcia-Contreras, L., Verberkmoes, J. L., Durbin, D., Peloquin, C. a, Elbert, K. J., Hickey, A. J., and Edwards, D. a. (2009) Formulation and pharmacokinetics of self-assembled rifampicin nanoparticle systems for pulmonary delivery. *Pharm. Res. 26*, 1847–1855.

(85) Yang, L., Luo, J., Shi, S., Zhang, Q., Sun, X., Zhang, Z., and Gong, T. (2013) Development of a pulmonary peptide delivery system using porous nanoparticle-aggregate particles for systemic application. *Int. J. Pharm. 451*, 104–111.

(86) Kaye S., R., Tol S., P., and H.Oya, A. (2009) Simultaneously Manufactured Nano-In-Micro (SIMANIM) Particles for Dry-Powder Modified-Release Delivery of Antibodies. *J. Pharm. Sci. 98*, 4055–4068.

(87) Moghaddam, P. H., Ramezani, V., Esfandi, E., Vatanara, a., Nabi-Meibodi, M., Darabi, M., Gilani, K., and Najafabadi, a. R. (2013) Development of a nano–micro carrier system for sustained pulmonary delivery of clarithromycin. *Powder Technol. 239*, 478–483.

(88) Genina, N., Räikkönen, H., Heinämäki, J., Veski, P., and Yliruusi, J. (2010) Nano-coating of β-galactosidase onto the Surface of Lactose by Using an Ultrasound-assisted Technique. *AAPS PharmSciTech 11*, 959–965.

(89) Chattopadhyay, P., and Gupta, R. B. (2002) Supercritical CO2 Based Production of Magnetically Responsive Micro- and Nanoparticles for Drug Targeting. *Ind. Eng. Chem. Res. 41*, 6049–6058.

(90) Rehman, M., Shekunov, B. Y., York, P., Lechuga-Ballesteros, D., Miller, D. P., Tan, T., and Colthorpe, P. (2004) Optimisation of powders for pulmonary delivery using supercritical fluid technology. *Eur. J. Pharm. Sci. 22*, 1–17.

(91) Koushik, K., Dhanda, D. S., Cheruvu, N. P. S., and Kompella, U. B. (2004) Pulmonary delivery of deslorelin: large-porous PLGA particles and HPbetaCD complexes. *Pharm. Res. 21*, 1119–1126.

(92) Okamoto, H., Nishida, S., Todo, H., Sakakura, Y., Iida, K., and Danjo, K. (2003) Pulmonary gene delivery by chitosan-pDNA complex powder prepared by a supercritical carbon dioxide process. *J. Pharm. Sci. 92*, 371–380.

(93) Gómez-Gaete, C., Fattal, E., Silva, L., Besnard, M., and Tsapis, N. (2008) Dexamethasone acetate encapsulation into Trojan particles. *J. Control. Release 128*, 41–49.

(94) Hadinoto, K., Zhu, K., and Tan, R. B. H. (2007) Drug release study of large hollow nanoparticulate aggregates carrier particles for pulmonary delivery. *Int. J. Pharm. 341*, 195–206.

(95) Tewa-Tagne, P., Briançon, S., and Fessi, H. (2006) Spray-dried microparticles containing polymeric nanocapsules: formulation aspects, liquid phase interactions and particles characteristics. *Int. J. Pharm. 325*, 63–74.

(96) Makadia, H. K., and Siegel, S. J. (2011) Poly Lactic-co-Glycolic Acid (PLGA) as Biodegradable Controlled Drug Delivery Carrier. *Polymers (Basel). 3*, 1377–1397.

(97) Cruz, L. J., Tacken, P. J., Fokkink, R., Joosten, B., Stuart, M. C., Albericio, F., Torensma, R., and Figdor, C. G. (2010) Targeted PLGA nano- but not microparticles specifically deliver antigen to human dendritic cells via DC-SIGN in vitro. *J. Control. Release 144*, 118–126.

(98) Sinsuebpol, C., Chatchawalsaisin, J., and Kulvanich, P. (2013) Preparation and in vivo absorption evaluation of spray dried powders containing salmon calcitonin loaded chitosan nanoparticles for pulmonary delivery. *Drug Des. Devel. Ther. 7*, 861–873.

(99) Grenha, A., Remuñán-López, C., Carvalho, E. L. S., and Seijo, B. (2008) Microspheres containing lipid/chitosan nanoparticles complexes for pulmonary delivery of therapeutic proteins. *Eur. J. Pharm. Biopharm. 69*, 83–93.

(100) Mansour, H. M., Rhee, Y.-S., and Wu, X. (2009) Nanomedicine in pulmonary delivery. *Int. J. Nanomedicine 4*, 299–319.

(101) Vehring, R. (2008) Pharmaceutical particle engineering via spray drying. *Pharm. Res. 25*, 999–1022.

(102) Rowe, R. C., Sheskey, P. J., and Quinn, M. E. (2009) Handbook of Pharmaceutical Excipients. Pharmaceutical Press.

(103) Linsenbühler, M., and Wirth, K.-E. (2005) An innovative dry powder coating process in non-polar liquids producing tailor-made micro-particles. *Powder Technol. 158*, 3–20.

(104) Storey, R. A., and Ingvar, Y. (2011) Solid State Charactrization of Pharmaceuticals. Wiley-Blackwell.

(105) Stephenson, G. A., Forbes, R. A., and Reutzel-Edens, S. M. (2001) Characterization of the solid state: quantitative issues. *Adv. Drug Deliv. Rev. 48*, 67–90.

(106) Pasquali, I., Bettini, R., and Giordano, F. (2006) Solid-state chemistry and particle engineering with supercritical fluids in pharmaceutics. *Eur. J. Pharm. Sci. 27*, 299–310.

(107) Sakagami, M. (2006) In vivo, in vitro and ex vivo models to assess pulmonary absorption and disposition of inhaled therapeutics for systemic delivery. *Adv. Drug Deliv. Rev. 58*, 1030–1060.

(108) Cryan, S.-A., Sivadas, N., and Garcia-Contreras, L. (2007) In vivo animal models for drug delivery across the lung mucosal barrier. *Adv. Drug Deliv. Rev. 59*, 1133–1151.

(109) Fineberg, S. E., Kawabata, T., Finco-Kent, D., Liu, C., and Krasner, A. (2005) Antibody response to inhaled insulin in patients with type 1 or type 2 diabetes. An analysis of initial phase II and III inhaled insulin (Exubera) trials and a two-year extension trial. *J. Clin. Endocrinol. Metab. 90*, 3287–3294.

(110) Misra, A., Hickey, A. J., Rossi, C., Borchard, G., Terada, H., Makino, K., Fourie, P. B., and Colombo, P. (2011) Inhaled drug therapy for treatment of tuberculosis. *Tuberculosis 91*, 71–81.

(111) Walle, C. Van Der. (2011) Peptide and Protein Delivery. Elsevier.

(112) Laube, B. L., Edwards, A. M., Dalby, R. N., Creticos, P. S., and Norman, P. S. (1998) Respiratory pathophysiologic responses: The efficacy of slow versus faster inhalation of cromolyn sodium in protecting against allergen challenge in patients with asthma. *J. Allergy Clin. Immunol. 101*, 475–483.

(113) Nolan, L. M., Li, J., Tajber, L., Corrigan, O. I., and Healy, A. M. (2011) Particle engineering of materials for oral inhalation by dry powder inhalers. II-Sodium cromoglicate. *Int. J. Pharm. 405*, 36–46.

(114) Tkachenko, A. G., Xie, H., Coleman, D., Glomm, W., Ryan, J., Anderson, M. F., Franzen, S., and Feldheim, D. L. (2003) Multifunctional gold nanoparticle-peptide complexes for nuclear targeting. *J. Am. Chem. Soc. 125*, 4700–4701.

(115) Gaspar, V. M., Correia, I. J., Sousa, A., Silva, F., Paquete, C. M., Queiroz, J. a, and Sousa, F. (2011) Nanoparticle mediated delivery of pure P53 supercoiled plasmid DNA for gene therapy. *J. Control. Release 156*, 212–222.

(116) Cho, K., Wang, X., Nie, S., Chen, Z. G., and Shin, D. M. (2008) Therapeutic nanoparticles for drug delivery in cancer. *Clin. Cancer Res. 14*, 1310–1316.

(117) Restani, R. B., Morgado, P. I., Ribeiro, M. P., Correia, I. J., Aguiar-Ricardo, A., and Bonifácio, V. D. B. (2012) Biocompatible polyurea dendrimers with pH-dependent fluorescence. *Angew. Chem. Int. Ed. Engl. 51*, 5162–5165.

(118) Restani, R. B., Conde, J., Baptista, P. V., Cidade, M. T., Bragança, A. M., Morgado, J., Correia, I. J., Aguiar-Ricardo, A., and Bonifácio, V. D. B. (2014) Polyurea dendrimer for efficient cytosolic siRNA delivery. *RSC Adv. 4*, 54872–54878.

(119) Yamamoto, K., An, Z., Saito, N., and Yamaguchi, M. (2013) Fluorescent gold nanoparticles: synthesis of composite materials of two-component disulfide gels and gold nanoparticles. *Chemistry 19*, 10580–10588.

(120) Eaton, P., Doria, G., Pereira, E., Baptista, P. V., and Franco, R. (2007) Imaging gold nanoparticles for DNA sequence recognition in biomedical applications. *IEEE Trans. Nanobioscience 6*, 282–288.

(121) H. Faraji, A., and Wipf, P. (2009) Nanoparticles in cellular drug delivery. *Bioorg. Med. Chem. 17*, 2950–2962.

(122) Khlebtsov, N., and Dykman, L. (2011) Biodistribution and toxicity of engineered gold nanoparticles: a review of in vitro and in vivo studies. *Chem. Soc. Rev. 40*, 1647–1671.

(123) Qiao, G., Gao, Y., Li, N., Yu, Z., Zhuo, L., and Tang, B. (2011) Simultaneous detection of intracellular tumor mRNA with bi-color imaging based on a gold nanoparticle/molecular beacon. *Chemistry 17*, 11210–11215.

(124) Yih, T. C., and Al-Fandi, M. (2006) Engineered nanoparticles as precise drug delivery systems. *J. Cell. Biochem. 97*, 1184–1190.

(125) Giljohann, D. a, Seferos, D. S., Daniel, W. L., Massich, M. D., Patel, P. C., and Mirkin, C. a. (2010) Gold nanoparticles for biology and medicine. *Angew. Chem. Int. Ed. Engl. 49*, 3280–3294.

(126) Zhao, J., Bo, B., Yin, Y.-M., and Li, G.-X. (2011) Gold nanoparticles-based biosensors for biomedical applications. *Nano Life 02*, 1230008–1230019.

(127) Llevot, A., and Astruc, D. (2012) Applications of vectorized gold nanoparticles to the diagnosis and therapy of cancer. *Chem. Soc. Rev. 41*, 242–257.

(128) Paul, A., Solis, D., Bao, K., Chang, W., Nauert, S., Vidgerman, L., Zubarev, E. R., Nordlander, P., and Link, S. (2012) Identi fi cation of Higher Order Plasmon Polariton Modes in Chemically Prepared Gold Nanowires. *ACS Nano 6*, 8105–8113.

(129) Kang, B., Mackey, M. a, and El-Sayed, M. a. (2010) Nuclear targeting of gold nanoparticles in cancer cells induces DNA damage, causing cytokinesis arrest and apoptosis. *J. Am. Chem. Soc. 132*, 1517–1519.

(130) Raje, V. P., Morgado, P. I., Ribeiro, M. P., Correia, I. J., Bonifácio, V. D. B., Branco, P. S., and Aguiar-Ricardo, A. (2013) Dual on-off and off-on switchable oligoaziridine biosensor. *Biosens. Bioelectron. 39*, 64–69.

(131) Gobbi, P., and Workentin, M. S. (2012) Improved Methodology for the Preparation of Water-Soluble Maleimide-Functionalized Small Gold Nanoparticles. *Langmuir 28*, 12357–12363.

(132) Oh, E., Susumu, K., Blanco-Canosa, J. B., Medintz, I. L., Dawson, P. E., and Mattoussi, H. (2010) Preparation of stable maleimide-functionalized au nanoparticles and their use in counting surface ligands. *Small 6*, 1273–1278.

(133) Hartlen, K. D., Ismaili, H., Zhu, J., and Workentin, M. S. (2012) Michael Addition Reactions for the Modification of Gold Nanoparticles Facilitated by Hyperbaric Conditions. *Langmuir 28*, 864–871.

(134) Zhu, J., Waengler, C., Lennox, R. B., and Schirrmacher, R. (2012) Preparation of water-soluble maleimide-functionalized 3 nm gold nanoparticles: a new bioconjugation template. *Langmuir 28*, 5508–5512.

(135) Frens, G. (1973) Controlled Nucleation for the Regulation of the Particle Size in Monodisperse Gold Suspensions. *Nat. Phys. Sci. 241*, 20–22.

(136) Gaspar, V. M., Marques, J. G., Sousa, F., Louro, R. O., Queiroz, J. a, and Correia, I. J. (2013) Biofunctionalized nanoparticles with pH-responsive and cell penetrating blocks for gene delivery. *Nanotechnology 24*, 275101–275117.

(137) Khatua, S., Manna, P., Chang, W., Tcherniak, A., Friedlander, E., Zubarev, E. R., and Link, S. (2010) Plasmonic Nanoparticles - Liquid Crystal Composites. *J. Phys. Chem. C 114*, 7251–7257.

(138) Ciesielski, J., Lebœuf, D., Stern, H. a, and Frontier, A. J. (2013) Gold (III) Chloride-Catalyzed 6-endo-trig Oxa-Michael Addition Reactions for Diastereoselective Synthesis of Fused Tetrahydropyranones. *Adv. Synth. Catal. 355*, 2077–2082.

(139) Liu, Y., Shipton, M. K., Ryan, J., Kaufman, E. D., Franzen, S., and Feldheim, D. L. (2007) Synthesis, stability, and cellular internalization of gold nanoparticles containing mixed peptide-poly(ethylene glycol) monolayers. *Anal. Chem. 79*, 2221–2229.

(140) Arvizo, R. R., Rana, S., Miranda, O. R., Bhattacharya, R., Rotello, V. M., and Mukherjee, P. (2011) Mechanism of anti-angiogenic property of gold nanoparticles: role of nanoparticle size and surface charge. *Nanomedicine 7*, 580–587.

(141) Caruso, F., Hyeon, T., Rotello, V., Lee, D., Koo, H., Sun, I., Ryu, J. H., Kim, K., and Kwon, I. C. (2012) Nanomedicine themed issue Multifunctional nanoparticles for multimodal imaging and theragnosis w. *Chem. Soc. Rev. 41*, 2656–2672.

(142) Kim, K., Kim, J. H., Park, H., Kim, Y.-S., Park, K., Nam, H., Lee, S., Park, J. H., Park, R.-W., Kim, I.-S., Choi, K., Kim, S. Y., Park, K., and Kwon, I. C. (2010) Tumor-homing multifunctional nanoparticles for cancer theragnosis: Simultaneous diagnosis, drug delivery, and therapeutic monitoring. *J. Control. Release 146*, 219–227.

(143) Viegas, T. X., Bentley, M. D., Harris, J. M., Fang, Z., Yoon, K., Dizman, B., Weimer, R., Mero, A., Pasut, G., and Veronese, F. M. (2011) Polyoxazoline : Chemistry , Properties , and Applications in Drug Delivery. *Bioconjug. Chem. 22*, 976–986.

(144) Nimesh, S., Goyal, A., Pawar, V., Jayaraman, S., Kumar, P., Chandra, R., Singh, Y., and Gupta, K. C. (2006) Polyethylenimine nanoparticles as efficient transfecting agents for mammalian cells. *J. Control. Release 110*, 457–468.

(145) Kievit, F. M., Veiseh, O., Bhattarai, N., Fang, C., Gunn, J. W., Lee, D., Ellenbogen, R. G., Olson, J. M., and Zhang, M. (2009) PEI-PEG-Chitosan Copolymer Coated Iron Oxide Nanoparticles for Safe Gene Delivery: synthesis, complexation, and transfection. *Adv. Funct. Mater. 19*, 2244–2251.

(146) Bonifácio, V. D. B., Correia, V. G., Pinho, M. G., Lima, J. C., and Aguiar-Ricardo, A. (2012) Blue emission of carbamic acid oligooxazoline biotags. *Mater. Lett. 81*, 205–208.

(147) Correia, V. G., Bonifácio, V. D. B., Raje, V. P., Casimiro, T., Moutinho, G., da Silva, C. L., Pinho, M. G., and Aguiar-Ricardo, A. (2011) Oxazoline-based antimicrobial oligomers: synthesis by CROP using supercritical CO2. *Macromol. Biosci. 11*, 1128–1137.

(148) De Macedo, C. V., da Silva, M. S., Casimiro, T., Cabrita, E. J., and Aguiar-Ricardo, A. (2007) Boron trifluoride catalyzed polymerisation of 2-substituted-2-oxazolines in supercritical carbon dioxide. *Green Chem. 9*, 948–953.

(149) Mukhopadhyay, S., Malik, P., Arora, S. K., and Mukherjee, T. K. (2013) Role of β1 Integrins in the Complication and Drug Resistance Against Lung Cancer: Targeting β1 Integrins to Eradicate Lung Cancer, in *Molecular Mechanisms of Tumor Cell Resistance to Chemotherapy*, pp 88–108.

(150) Wewer, U. M., Taraboletti, G., Sobel, M. E., Albrechtsen, R., and Liona, L. A. (1987) Role of Laminin Receptor in Tumor Cell Migration Role of Laminin Receptor in Tumor Cell Migration1. *Cancer Res. 47*, 5691–5698.

(151) Dubey, P. K., Singodia, D., and Vyas, S. P. (2010) Liposomes modified with YIGSR peptide for tumor targeting. *J. Drug Target. 18*, 373–380.

(152) El-Sherbiny, I. M., and Smyth, H. D. C. (2010) Biodegradable nano-micro carrier systems for sustained pulmonary drug delivery: (I) self-assembled nanoparticles encapsulated in respirable/swellable semi-IPN microspheres. *Int. J. Pharm. 395*, 132–141.

(153) Silva, A. S., Tavares, M. T., and Aguiar-Ricardo, A. (2014) Sustainable strategies for nano-in-micro particle engineering for pulmonary delivery. *J. Nanoparticle Res. 6*, 2602–2619.

(154) Azarmi, S., Roa, W. H., and Löbenberg, R. (2008) Targeted delivery of nanoparticles for the treatment of lung diseases. *Adv. Drug Deliv. Rev. 60*, 863–875.

(155) Connor, E. E., Mwamuka, J., Gole, A., Murphy, C. J., and Wyatt, M. D. (2005) Gold nanoparticles are taken up by human cells but do not cause acute cytotoxicity. *Small 1*, 325–327.

(156) Boisselier, E., and Astruc, D. (2009) Gold nanoparticles in nanomedicine: preparations, imaging, diagnostics, therapies and toxicity. *Chem. Soc. Rev. 38*, 1759–1782.

(157) Alvarenga, E. S. De. (2011) Characterization and Properties of Chitosan, in *Biotechnology of Biopolymers* M. Enashar., pp 91–108.

(158) Temtem, M., Barroso, T., Casimiro, T., Mano, J. F., and Aguiar-Ricardo, A. (2012) Dual stimuli responsive poly(N-isopropylacrylamide) coated chitosan scaffolds for controlled release prepared from a non residue technology. *J. Supercrit. Fluids 66*, 398–404.

(159) Temtem, M., Silva, L. M. C., Andrade, P. Z., dos Santos, F., da Silva, C. L., Cabral, J. M. S., Abecasis, M. M., and Aguiar-Ricardo, A. (2009) Supercritical CO2 generating chitosan devices with controlled morphology. Potential application for drug delivery and mesenchymal stem cell culture. *J. Supercrit. Fluids 48*, 269–277.

(160) Barroso, T., Viveiros, R., Casimiro, T., and Aguiar-Ricardo, A. (2014) Development of dual-responsive chitosan-collagen scaffolds for pulsatile release of bioactive molecules. *J. Supercrit. Fluids 94*, 102–112.

(161) Jae, H. P., Kwon, S., Lee, M., Chung, H., Kim, J. H., Kim, Y. S., Park, R. W., Kim, I. S., Sang, B. S., Kwon, I. C., and Seo, Y. J. (2006) Self-assembled nanoparticles based on glycol chitosan bearing hydrophobic moieties as carriers for doxorubicin: In vivo biodistribution and anti-tumor activity. *Biomaterials 27*, 119–126.

(162) Domínguez-delgado, C. L., Rodríguez-cruz, I. M., Fuentes-prado, E., Escobar-chávez, J. J., Vidal-romero, G., García-gonzález, L., and Puente-lee, R. I. (2014) Drug Carrier Systems Using Chitosan for Non Parenteral Routes, in *Pharmacology and Therapeutics* S. Gowder., pp 273–275.

(163) Kang, K. a, Wang, J., Jasinski, J. B., and Achilefu, S. (2011) Fluorescence manipulation by gold nanoparticles: from complete quenching to extensive enhancement. *J. Nanobiotechnology 9*, 16–25.

(164) Cabral, R. P. (2013) Development of chitosan-based microparticles for pulmonary delivery. *Diss. Univ. Nov. Lisboa*.

(165) Lim, E.-K., Sajomsang, W., Choi, Y., Jang, E., Lee, H., Kang, B., Kim, E., Haam, S., Suh, J.-S., Chung, S. J., and Huh, Y.-M. (2013) Chitosan-based intelligent theragnosis nanocomposites enable pH-sensitive drug release with MR-guided imaging for cancer therapy. *Nanoscale Res. Lett. 8*, 467–479.

(166) Naikwade, S. R., Bajaj, A. N., Gurav, P., Gatne, M. M., and Singh Soni, P. (2009) Development of budesonide microparticles using spray-drying technology for pulmonary

administration: design, characterization, in vitro evaluation, and in vivo efficacy study. *AAPS PharmSciTech 10*, 993–1012.

(167) Council of Europe. (2010) Preparations for Inhalation: Aerodynaminc Assessment of Fine Particles, in *European Pharmacopeia*, pp 274–285.

(168) Ritger, P. L., and Peppas, N. a. (1987) A simple equation for description of solute release I. Fickian and non-fickian release from non-swellable devices in the form of slabs, spheres, cylinders or discs. *J. Control. Release 5*, 23–36.

(169) Siepmann, J., and Siepmann, F. (2008) Mathematical modeling of drug delivery. *Int. J. Pharm. 364*, 328–343.

(170) Zhou, Q. F., Bao, J. C., and Xu, Z. (2001) Shape-controlled synthesis of nanostructured gold by a protection–reduction technique. *J. Mater. Chem. 12*, 384–387.

(171) Hirano, S., Tsuchida, H., and Nagao, N. (1989) N-acetylation in chitosan and the rate of its enzymic hydrolysis. *Biomaterials 10*, 574–576.

(172) Muzzarelli, R. a a. (2010) Chitins and chitosans as immunoadjuvants and non-allergenic drug carriers. *Mar. Drugs 8*, 292–312.

(173) Okuda, T., Kito, D., Oiwa, A., Fukushima, M., Hira, D., and Okamoto, H. (2013) Gene silencing in a mouse lung metastasis model by an inhalable dry small interfering RNA powder prepared using the supercritical carbon dioxide technique. *Biol. Pharm. Bull. 36*, 1183–1191.

(174) Jere, D., Jiang, H. L., Kim, Y. K., Arote, R., Choi, Y. J., Yun, C. H., Cho, M. H., and Cho, C. S. (2009) Chitosan-graft-polyethylenimine for Akt1 siRNA delivery to lung cancer cells. *Int. J. Pharm. 378*, 194–200.

(175) Hartmann, H., Hossfeld, S., Schlosshauer, B., Mittnacht, U., Pêgo, A. P., Dauner, M., Doser, M., Stoll, D., and Krastev, R. (2013) Hyaluronic acid / chitosan multilayer coatings on neuronal implants for localized delivery of siRNA nanoplexes. *J. Control. Release 168*, 289–297.

(176) Deng, Z. J., Morton, S. W., Ben-Akiva, E., Dreaden, E. C., Shopsowitz, K. E., and Hammond, P. T. (2013) Layer-by-layer nanoparticles for systemic codelivery of an anticancer drug and siRNA for potential triple-negative breast cancer treatment. *ACS Nano 7*, 9571–9584.

(177) Xue, W., Dahlman, J. E., Tammela, T., Khan, O. F., Sood, S., Dave, A., Cai, W., Chirino, L. M., Yang, G. R., Bronson, R., Crowley, D. G., Sahay, G., Schroeder, A., Langer, R., Anderson, D. G., and Jacks, T. (2014) Small RNA combination therapy for lung cancer. *Proc. Natl. Acad. Sci. U. S. A. 111*, 3553–3561.

(178) Xue, W., Dahlman, J. E., Tammela, T., Khan, O. F., Sood, S., Dave, A., Cai, W., Chirino, L. M., Yang, G. R., Bronson, R., Crowley, D. G., Sahay, G., Schroeder, A., Langer, R., Anderson, D. G., and Jacks, T. (2014) Small RNA combination therapy for lung cancer. *Proc. Natl. Acad. Sci. U. S. A.*

(179) Ihara, D., Hattori, N., Horimasu, Y., Masuda, T., Nakashima, T., Senoo, T., Iwamoto, H., Fujitaka, K., Okamoto, H., and Kohno, N. (2015) Histological Quantification of Gene Silencing

by Intratracheal Administration of Dry Powdered Small-Interfering RNA/Chitosan Complexes in the Murine Lung. *Pharm. Res.*, doi 10.1007/s11095-015-1747-6

(180) Dreaden, E. C., Morton, S. W., Shopsowitz, K. E., Choi, J., and Deng, Z. J. (2015) Bimodal Tumor-Targeting from Microenvironment Responsive. *ACS Nano 8*, 8374–8382.

(181) Zhang, K., Xu, L., Jiang, J., Calin, N., Lam, K., and Zhang, S. (2013) Facile Large-Scale Synthesis of Monodisperse Mesoporous Silica Nanospheres with Tunable Pore Structure Facile Large-Scale Synthesis of Monodisperse Mesoporous Silica Nanospheres with Tunable Pore Structure. *J. Am. Chem. Soc. 135*, 2427–2430.

(182) Moreira, A. F., Gaspar, V. M., Costa, E. C., de Melo-Diogo, D., Machado, P., Paquete, C. M., and Correia, I. J. (2014) Preparation of end-capped pH-sensitive mesoporous silica nanocarriers for on-demand drug delivery. *Eur. J. Pharm. Biopharm. 88*, 1012–1025.

(183) Yue, C., Liu, P., Zheng, M., Zhao, P., Wang, Y., Ma, Y., and Cai, L. (2013) IR-780 dye loaded tumor targeting theranostic nanoparticles for NIR imaging and photothermal therapy. *Biomaterials 34*, 6853–6861.

(184) Choi, K. Y., Chung, H., Min, K. H., Yoon, H. Y., Kim, K., Park, J. H., Kwon, I. C., and Jeong, S. Y. (2010) Self-assembled hyaluronic acid nanoparticles for active tumor targeting. *Biomaterials 31*, 106–114.

(185) Zeng, J., Chen, X., Liang, Q., Xu, X., and Jing, X. (2004) Enzymatic degradation of poly(L-lactide) and poly(epsilon-caprolactone) electrospun fibers. *Macromol. Biosci. 4*, 1118–1125.

(186) Costa, E. C., Gaspar, V. M., Marques, J. G., Coutinho, P., and Correia, I. J. (2013) Evaluation of nanoparticle uptake in co-culture cancer models. *PLoS One 8*, doi:10.1371/journal.pone.0070072.

(187) Krieg, B., Hirsch, M., Scholz, E., Nuhn, L., Tabujew, I., Bauer, H., Decker, S., Khobta, A., Schmidt, M., Tremel, W., Zentel, R., Peneva, K., Koynov, K., Mason, a. J., and Helm, M. (2014) New Techniques to Assess In Vitro Release of siRNA from Nanoscale Polyplexes. *Pharm. Res. 32*, 1957–1974.

(188) Tewa-Tagne, P., Degobert, G., Briançon, S., Bordes, C., Gauvrit, J. Y., Lanteri, P., and Fessi, H. (2007) Spray-drying nanocapsules in presence of colloidal silica as drying auxiliary agent: Formulation and process variables optimization using experimental designs. *Pharm. Res. 24*, 650–661.

(189) Kean, T., and Thanou, M. (2010) Biodegradation, biodistribution and toxicity of chitosan. *Adv. Drug Deliv. Rev. 62*, 3–11.

(190) Moura, C., Neves, F., and Costa, E. (2014) Design of Composite Particles via Spray Drying for DPI Formulations. *ONdrugDelivery 53*, 16–23.

(191) Wang, J., Huang, L., Yang, R., Zhang, Z., Wu, J., Gao, Y., Wang, Q., O'Hare, D., and Zhong, Z. (2014) Recent advances in solid sorbents for CO_2 capture and new development trends. *Energy Environ. Sci. 7*, 3478–3518.

(192) Huang, Y. C., Vieira, A., Huang, K. L., Yeh, M. K., and Chiang, C. H. (2005) Pulmonary inflammation caused by chitosan microparticles. *J. Biomed. Mater. Res. Part A 75*, 283–287.

Appendix

Appendix A

The information in this appendix is related to CHAPTER 2.

Estimation of the number of ligands per gold nanoparticle

According to TEM images and DLS measurements (Figure 2.2 and Table 2.1), the average diameter of the nanoparticles is 28 nm. Assuming the spherical shape for the particles, the volume of each particle is $(4/3)\pi(d/2)^3 = 1.15\text{x}10^{-17}$ cm^3. Hence the mass of each particle (M_{au}) is ($19.3\text{x}10^3$ mg/cm^3) x ($1.15\text{x}10^{-17}$ cm^3) = $2.22\text{x}10^{-13}$ mg. From TGA analysis of MPM coated AuNP (Figure A.1) the amount of gold core is 1.4 mg. So the number of gold nanoparticles (N_{Au}) is ($1.4 / 2.22\text{x}10^{-13}$) = $6.31\text{x}10^{12}$. Also, from the TGA data, the amount of MPM (M_w= 3400 g/mol) present is 0.10005 mg. Therefore, the number of MPM molecules (N_{MPM}) is ($0.100\text{x}10^{-3}$) x ($6.023\text{x}10^{23}$) / 3400 = $1.77\text{x}10^{16}$ and the number of MPM molecules per one AuNP is N_{MPM}/N_{Au} = 2807.

From TGA analysis of OA coated AuNP the amount of gold core is 2.63 mg. So the number of gold nanoparticles (N_{Au}) is ($2.63 / 2.22\text{x}10^{-13}$) = $1.19\text{x}10^{13}$. Also, from the TGA data, the amount of OA (M_w= 997.50g/mol) present is 0.171 mg. Therefore, the number of OA molecules (N_{OA}) is ($0.171\text{x}10^{-3}$) x ($6.023\text{x}10^{23}$) / 997.5 = $1.03\text{x}10^{17}$ and the number of OA molecules per one AuNP is N_{OA}/N_{Au} = 8712.

In order to understand how much OA and MPM are grafted onto particles' surface in the sample Au-MPM-OA, an ICP analysis for the sulfur atom was performed. Considering that each mol of S origins 1 mol of OA, the amount of OA/AuNP (grams) is $9.63\text{x}10^{-3}$. Therefore, considering the amount of gold core (1.6 – (0.04 x 1.6)) = 1.536 mg, the amount of OA is ($1.54\text{x}10^{-3}$) x ($9.63\text{x}10^{-3}$) = $1.48\text{x}10^{-5}$ g. Hence the mass of MPM in the weight loss from Au-MPM-OA (0.064 mg), is ($1.6 - 1.536 - 1.48\text{x}10^{-5}$) = $6.40\text{x}10^{-5}$g. Therefore, the number of molecules of OA would be ($1.48\text{x}10^{-5}$) x $6.023\text{x}10^{23}$ / 997.50 = $8.93\text{x}10^{15}$ (results obtained from TGA analysis. Consequently, the number of molecules of MPM is ($6.40\text{x}10^{-5}$) x $6.023\text{x}10^{23}$/ 3400 = $1.13\text{x}10^{16}$. Since the number of gold nanoparticles (N_{Au}) is ($1.536 / 2.22\text{x}10^{-13}$) = $6.93\text{x}10^{12}$, the number of molecules of MPM per one AuNP is 1636 as the number of molecules of OA per one AuNP is 1289. Thus, the total number of molecules per one nanoparticle is 2925.

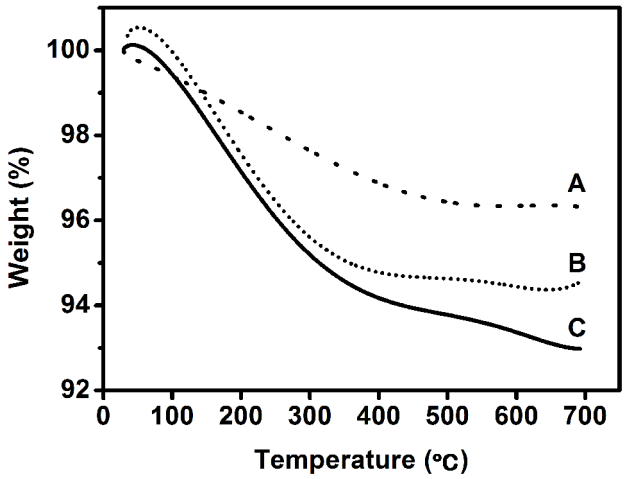

Figure A.1-TGA curves of (A) Au-MPM, (B) Au-OA and (C) Au-MPM-OA nanoparticles.

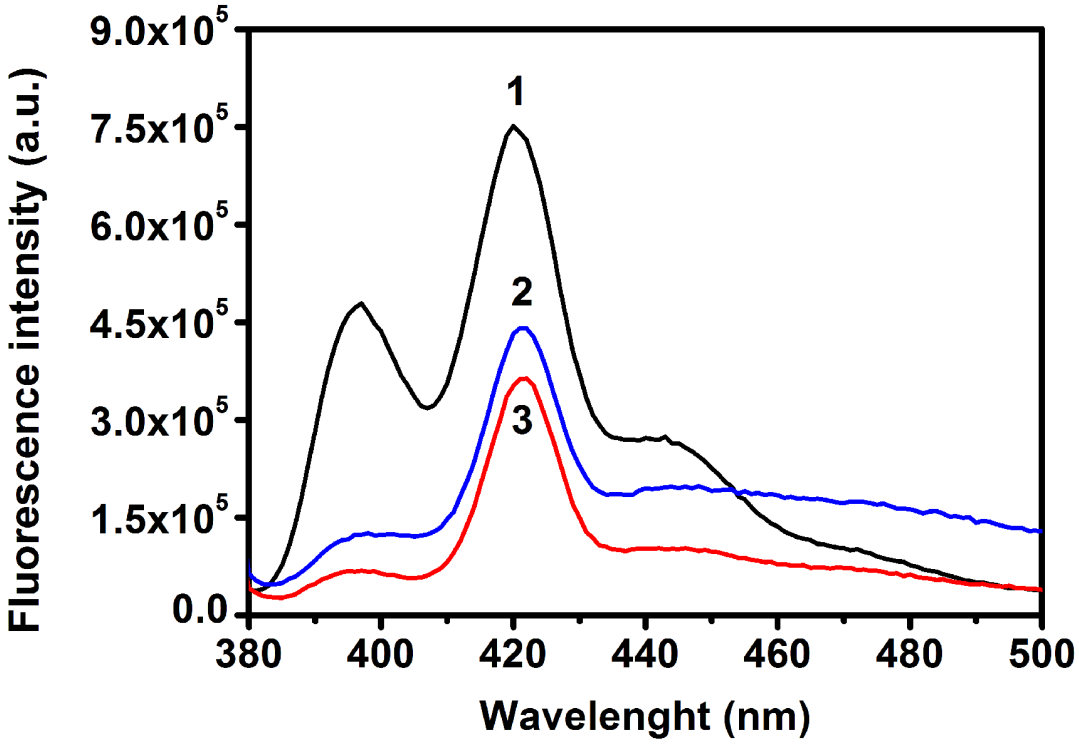

Figure A.2-Fluorescence spectra of (1) OA, (2) Au-OA and (3) Au-MPM-OA biosensors.

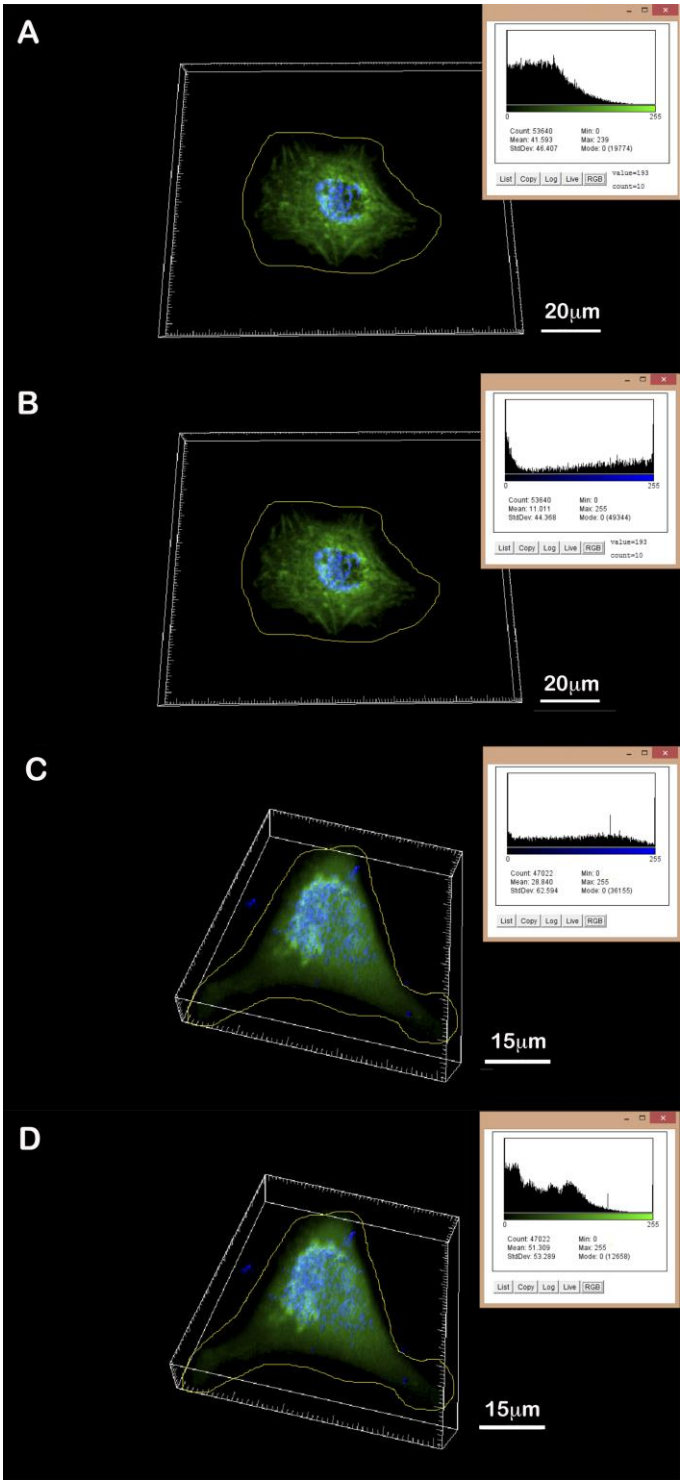

Figure A.3-Image J color histograms (A) CLSM images of A549 cells transfected with Au-OA, green histogram; (B) CLSM images of A549 cells transfected with Au-OA, blue histogram; (C) CLSM images of A549 cells transfected with Au-MPM-OA, green histogram; (D) CLSM images of A549 cells transfected with Au-MPM-OA, blue histogram. Green color – CellLight® Actin-GFP, BacMam 2.0; Blue color – GNP; Yellow color – region of interest selection.

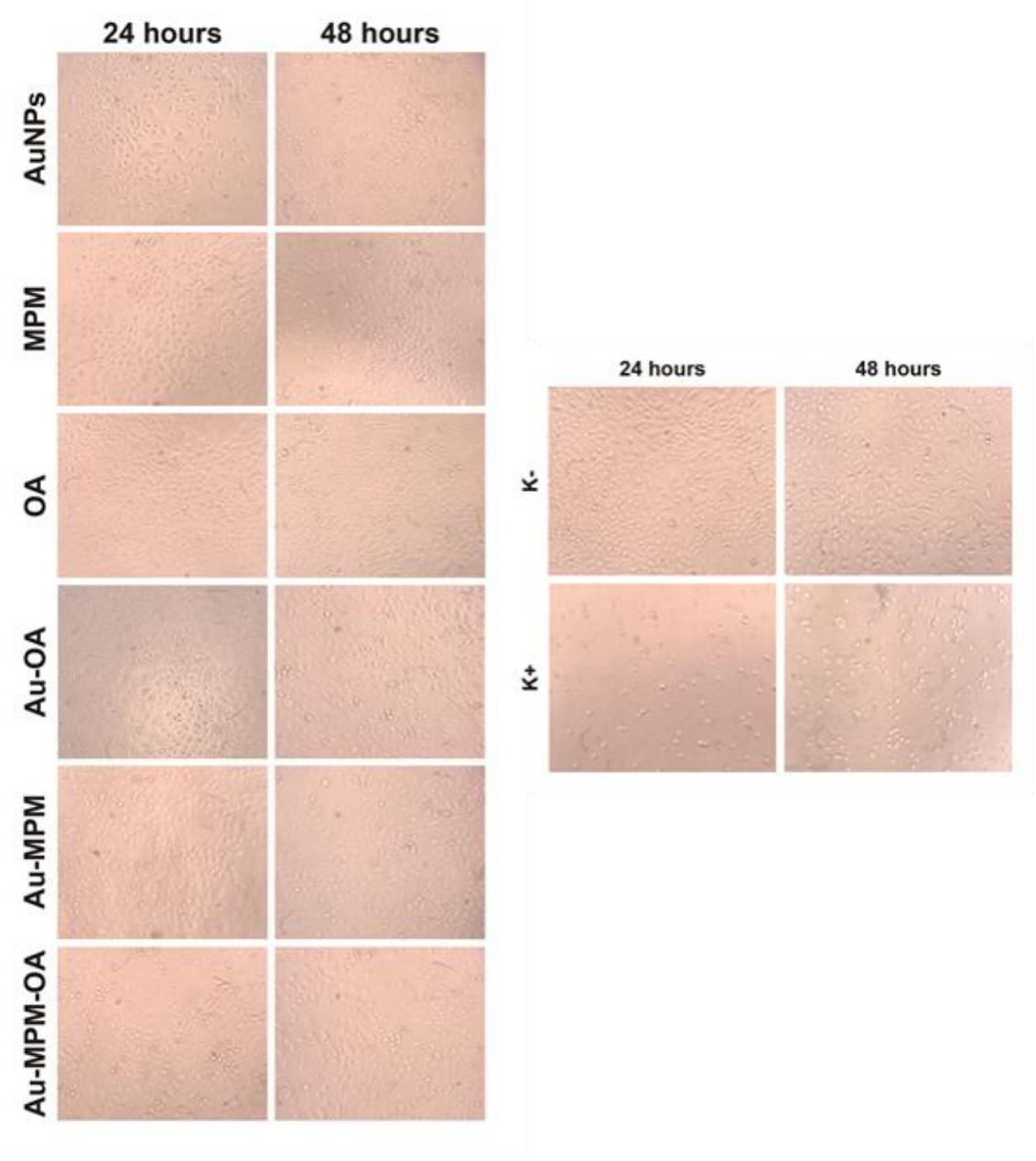

Figure A.4-Optical micrographs of A549 cell line transfected with the produced biotags and respective precursors after 24 h and 48 h of incubation: Gold nanoparticles (AuNPs); Maleimide-PEG-Maleimide (MPM); Oligoaziridine Biosensor (OA); Gold nanoparticles coated with oligoaziridine (Au-OA); Gold nanoparticles capped with Maleimide-PEG-Maleimide (Au-MPM); Gold nanoparticles capped with Maleimide-PEG-Maleimide and oligoaziridine (Au-MPM-OA); Negative control (K-) and Positive control (K+). Original magnification x 100.

Appendix B

The information in this appendix is related to CHAPTER 3.

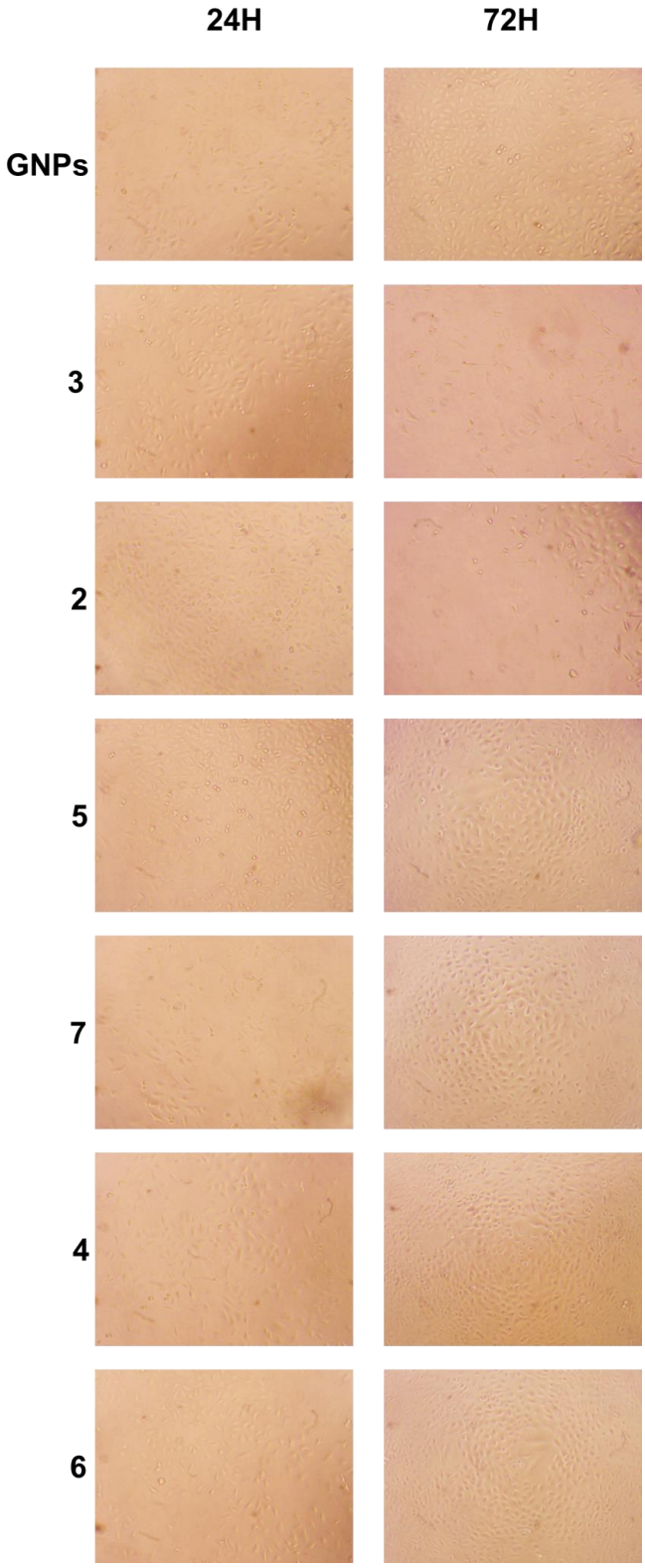

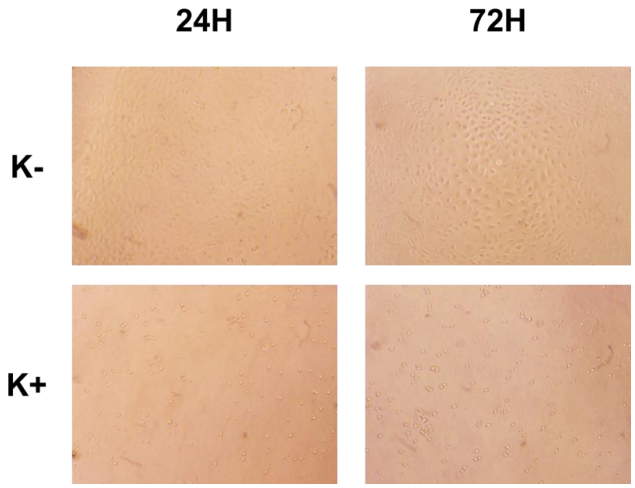

Figure B.1-Optical micrographs of A549 cell line transfected with the produced biotags and respective precursors after 24 h and 72 h of incubation: Gold nanoparticles (AuNPs), oligomers OEtOx-SH (2) and OEI-CS (3), and nanogold POxylated probes Au-OEtOx-SH (4), Au-OEI-CS (5), Au-OEtOx-SH-YIGSR (6) and Au-OEI-CS-YIGSR (7). Negative control (K-) and positive control (K+). Original magnification x100.

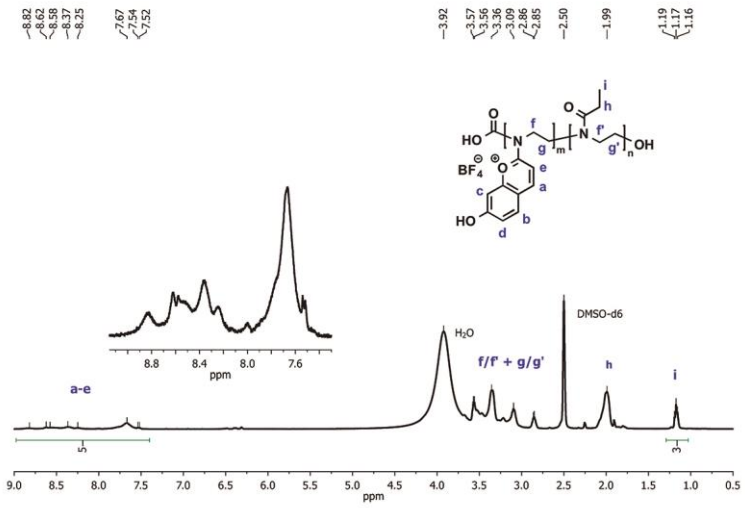

Figure B.2- H^1 NMR spectra of OEI-CS.

From MALDI-TOF analysis of oligomer **3**, eight different distributions were found: four with CO_2 incorporation (M_w= 974 g/mol) and four without (M_w= 1549 g/mol). The incorporation of CO_2 in the polymer chains was found to be ~ 48 %.

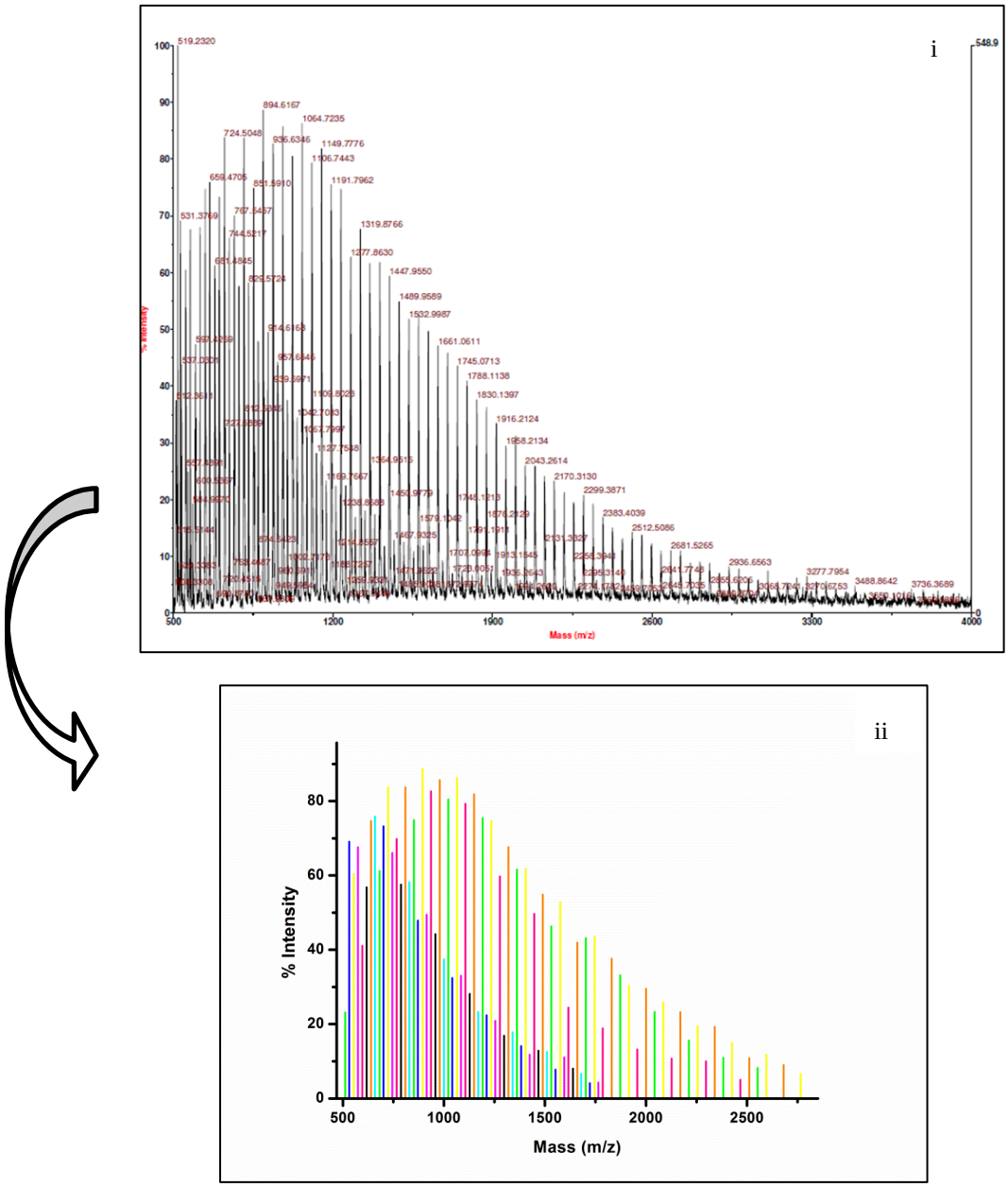

Figure B.3-MALDI-TOF spectra of OEI-CS. Matrix: DHB + Na. i) Raw data; ii) Treated data: **CO_2 insertion** – blue, black, cyan and red; **No CO_2 insertion** – yellow, green, orange and pink

Estimation of the number of ligands per gold nanoparticle

According to the DLS measurements (Table 3.1), the average diameter of the gold nanoparticles is 28 nm. Assuming the spherical shape for the particles, the volume of each particle is $(4/3)\pi(d/2)^3 = 1.14882\text{x}10^{-17}$ cm^3. Hence the mass of each particle (M_{Au}) is ($19.3\text{x}10^3$ mg/cm^3) x ($1.14882\text{x}10^{-17}$ cm^3) = $2.21723\text{x}10^{-13}$ mg.

The amount of YIGSR added to that was 5.17 $x10^{-5}$ M and the detection limit for the YIGSR was found to be 5.17 $x10^{-8}$ M (which is 0.1% of the original concentration). Considering both values and considering that no trace of peptide was found in the HPLC chromatogram and that the thiol groups from the peptide have high affinity to the AuNPs core, the binding of the peptide was considered to be 100%.

Bearing this, the amount of YIGSR per AuNP could be estimated. For this experiment, the amount of peptide added to the AuNPs was 1.36 $x10^{-6}$ g or 1.41 $x10^{-9}$ mol; based on the molar ratio 100:1 (peptide: AuNP). From TGA analysis of OEtOx-SH-YIGSR (**6**) (Figure 3.4) the amount of gold core is 1.47104 mg. So the number of gold nanoparticles (N_{Au}) is (1.47104 / $2.21723x10^{-13}$) = $6.6346x10^{12}$. Also, the weight of organic molecules was 0.12896 mg (1.6 mg of the initial sample – 1.47104 mg from the gold core). If the amount of peptide in the organic part is 1.36 $x10^{-6}$ g (or 1.36 $x10^{-3}$ mg) than, the amount of OEtOx-SH (M_w= 1449.15 g/mol, estimated through ^{1}H NMR) lost was (1.6 - 1.47104 - 1.36 $x10^{-3}$) = 1.28 $x10^{-4}$ g. Therefore, the number of OEtOx-SH molecules ($N_{OEtOx-SH}$) is (1.28 $x10^{-4}$) x ($6.023x10^{23}$) / 1449.15 = $5.30x10^{16}$ and the number of OEtOx-SH molecules per one AuNP is $N_{OEtOx-SH}/N_{Au}$ = 7993.49. As for the YIGSR sequence, the amount of YIGSR molecules (N_{YIGSR}) per GNP is N_{YIGSR}/N_{Au} = 127.64. Thus the total number of organic molecules per nanoparticle is 8121.13.

The same study was performed for Au-OEI-CS-YIGSR (**7**). Briefly, from TGA analysis (Figure 3.4) the amount of gold core is 2.447 mg. So the number of AuNPs (N_{Au}) is (2.447 / $2.21723x10^{-13}$) = $1.10363x10^{13}$. Again, the amount of peptide added to the AuNP was 1.36 $x10^{-6}$ g or 1.41 $x10^{-9}$ mol; based on the molar ratio 100:1 (peptide: AuNP). Therefore, the amount of OEI-CS (M_w= 1549 g/mol, estimated through MALDI-TOF) in the organic material is (3 - 2.447 - 1.36 $x10^{-3}$) = 9.46403 $x10^{-2}$ mg. Therefore, the number of OEI-CS molecules (N_{OEI-CS}) is (9.46403 $x10^{-5}$) x ($6.023x10^{23}$) / 1549 = $3.38x10^{16}$ and the number of OEI-CS molecules per one GNP is N_{OEI-CS}/N_{Au} = 2809.64. The amount of YIGSR molecules (N_{YIGSR}) per AuNP is N_{YIGSR}/N_{Au} = 64.66. Thus the total number of organic molecules per nanoparticle is 2874.3.

Appendix C

The information in this appendix is related to CHAPTER 4.

Table C.1-SASD Yields (%).

Sample	SASD Yield (%)
CHT-Au	74.5
CHT-Au-OEI-CS	56.9
CHT-Au-OEI-CS-YIGSR	61.6
CHT-Au-OEtOx-SH	61.9
CHT-Au-OEtOx-SH-YIGSR	83.0

Table C.2-Encapsulation efficiencies.

Sample	Au (mg/L) initial[a]	Au (mg) in total volume	Au (mg/L)[b]	Amount of powder used in ICP (mg)	Total amount of powder (mg)	mg of Au in the total amount of powder	E(%)
CHT-AuNP	95.2	5.71	8.94	20.14	4470	1.98	34.7
CHT-Au-OEI-CS	56.97	2.22	5.51	20.52	1549	0.38	17.2
CHT-Au-OEI-CS-YIGSR	61.06	3.66	10.35	20.18	3697	1.9	51.8
CHT-Au-OEtOx-SH	65.49	1.64	8.36	20.43	1423	0.63	38.6
CHT-Au-OEtOx-SH-YIGSR	88.65	3.42	6.391	20.04	4980	1.59	46.5

a – measured through ICP. The total amount of Au (mg) in the initial solution (next column) was calculated by multiplying Au concentration (mg/L) for the total volume used for the powders production: 60 mL for CHT-AuNP, CHT-Au-OEtOx-SH-YIGSR and CHT-Au-OEI-CS-YIGSR; 25 mL for CHT-Au-OEtOx-SH and CHT-Au-OEI-CS

b - measured through ICP. The total amount of Au (mg) in approximately 20 mg of powders was calculated by multiplying Au concentration (mg/L) for the volume in which the powders were dissolved (1 mL)

.

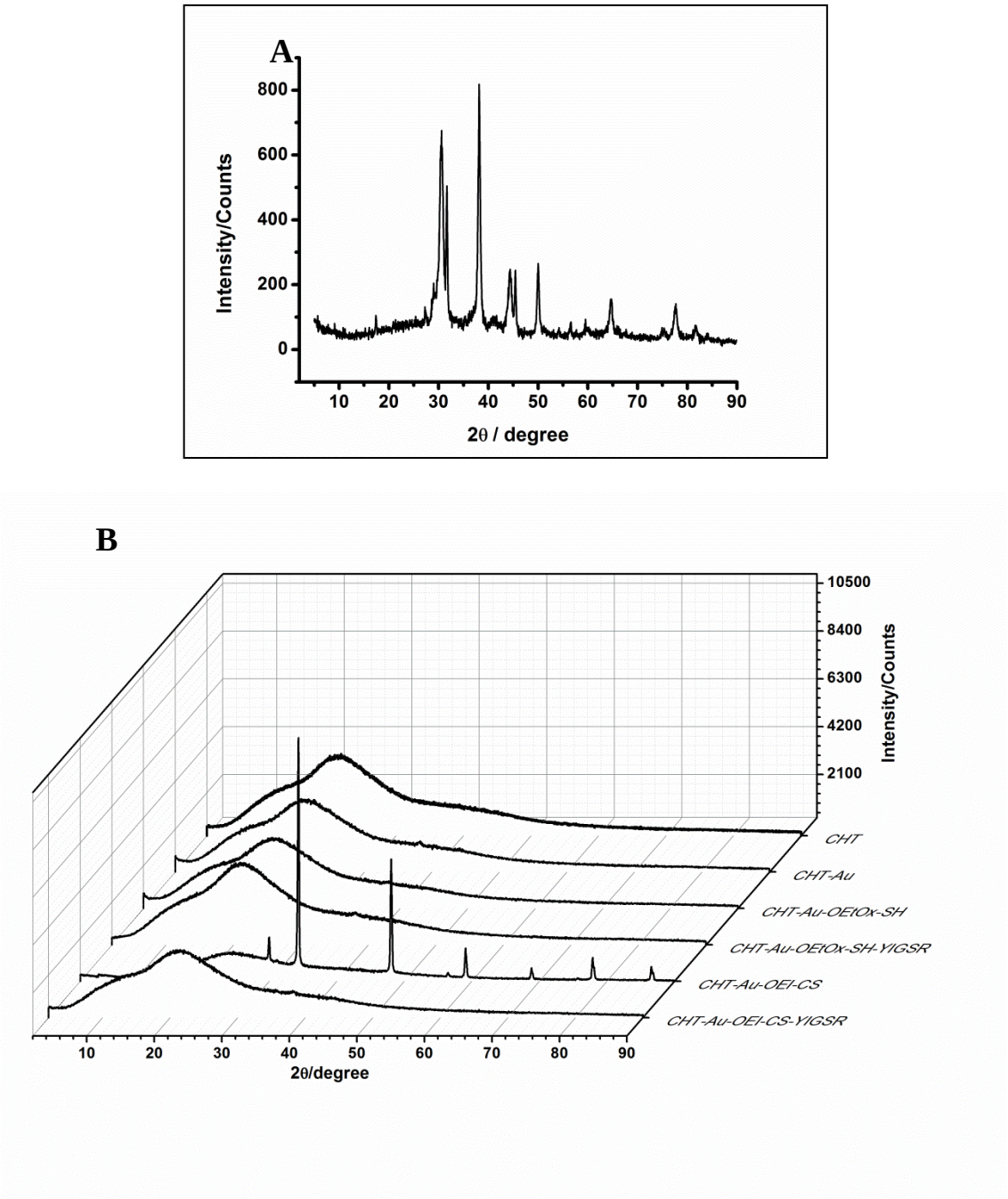

Figure C.1-X-ray diffraction patterns (A) AuNPs and of all the micronized powders (B).

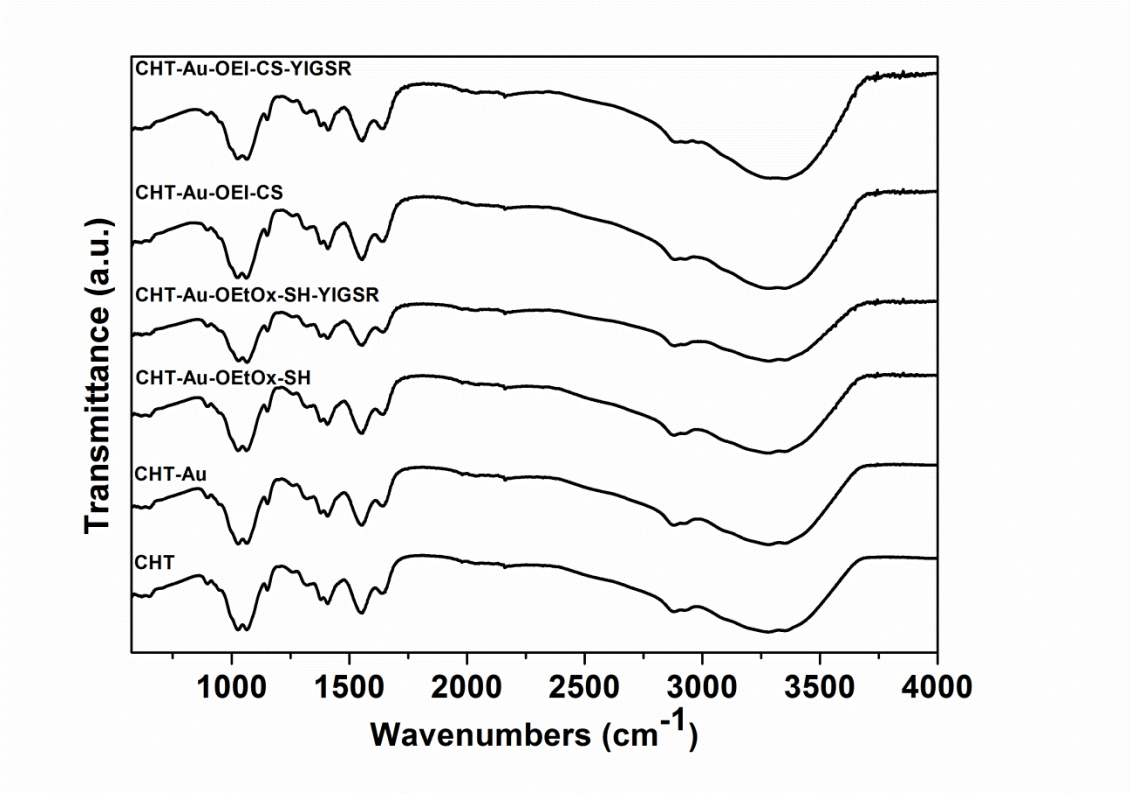

Figure C.2-FTIR-ATR of all the nano-in-micro formulations.

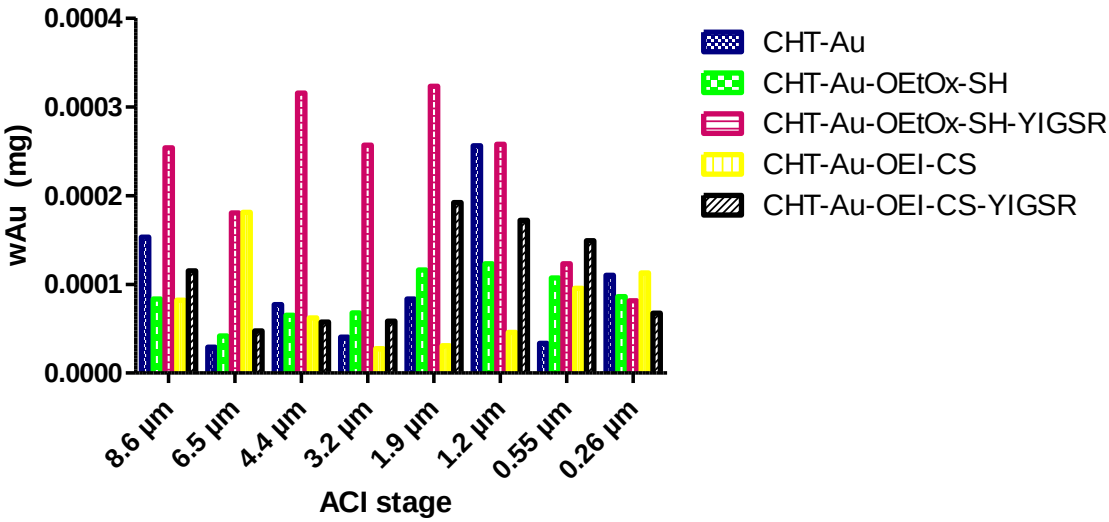

Figure C.3-Au powder content distribution among the different formulations.

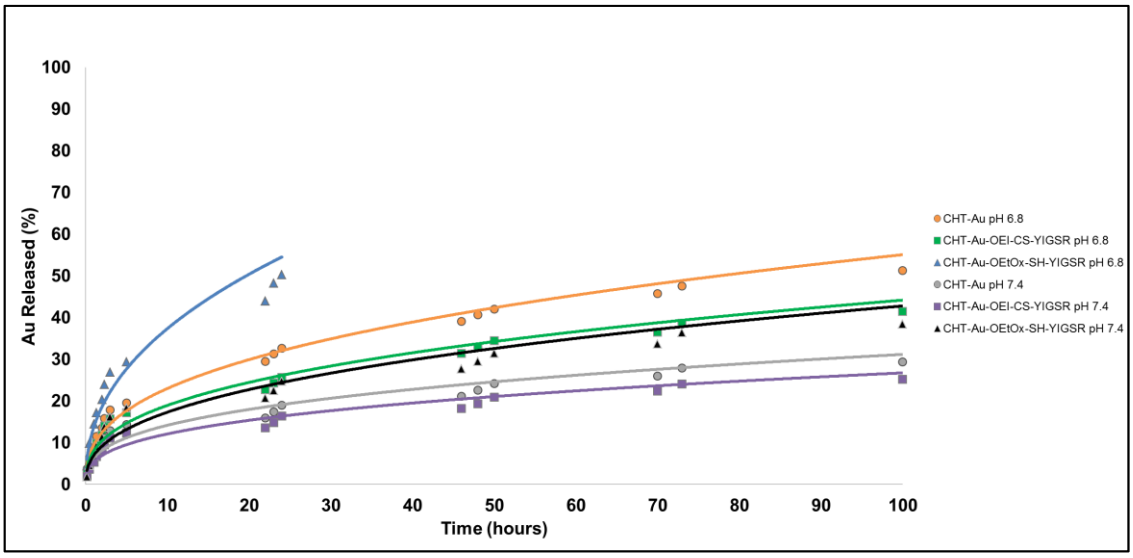

Figure C.4-Au release profile from CHT microspheres: Korsmeyer and Peppas fitting. The colors attributed to the adjustment curves are in agreement with the colors from the symbol.

Appendix D

The information in this appendix is related to CHAPTER 5.

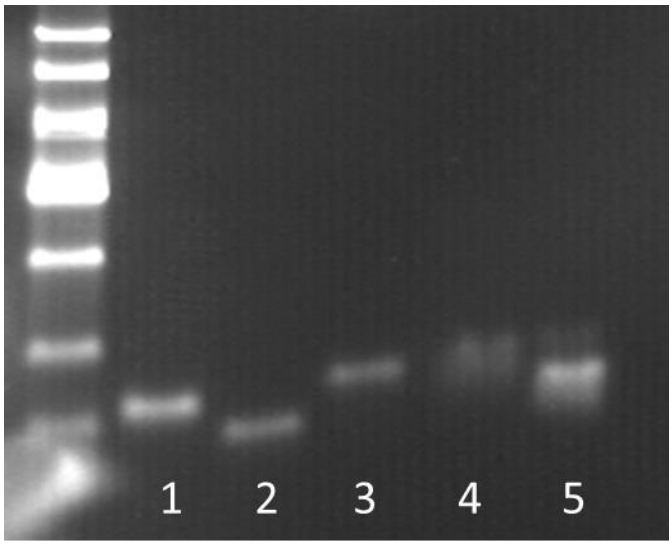

Figure D.1-Integrity of siRNA in the LbL siRNA nanosystems: (1) Kras siRNA; (2) NC siRNA; (3) AF 488 siRNA; (4) LbL Kras siRNA nanosystems; (5) LbL NC siRNA nanosystems. RNA ladder was used as marker and is depicted in at the most left of the gel.

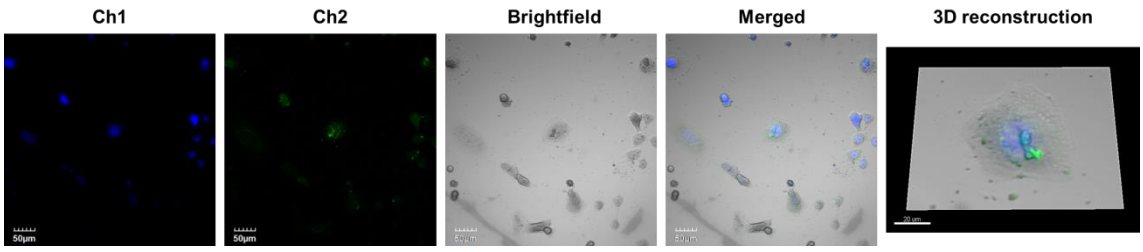

Figure D.2-CLSM images of td Tomato expressing KP cell line incubated with the LbL siRNA nanoparticles after 4h. Ch1 – Hoescht, nuclear location (λ_{exc} = 405 nm; λ_{emm} = 461 nm); Ch2 – AF 488 siRNA (λ_{exc} = 463 nm; λ_{emm} = 520 nm); Merged – overlappping of channels 1,2 and brightfield; and 3D reconstruction.

Table D.1-IR-780 dye and siRNA encapsulation efficiencies.

IR-780 dye initial amount	IR-780 dye loaded in MSN	IR-780 dye remaining after LbL assemblies	IR-780 dye within nano-in-micro formulations	siRNA (nano-in-micro particles)	siRNA in 1.5 mg of powder
0.13 mg/mL	92 %: 0.12 mg/mL	82.2%: 0.1 mg/mL	28.7%: 0.03 mg/mL (in 71.9 mg of powder)	133.4 ug (in 71.9 mg of powder)[a]	2.8 ug

[a] Based on the IR-780 dye loading efficiency

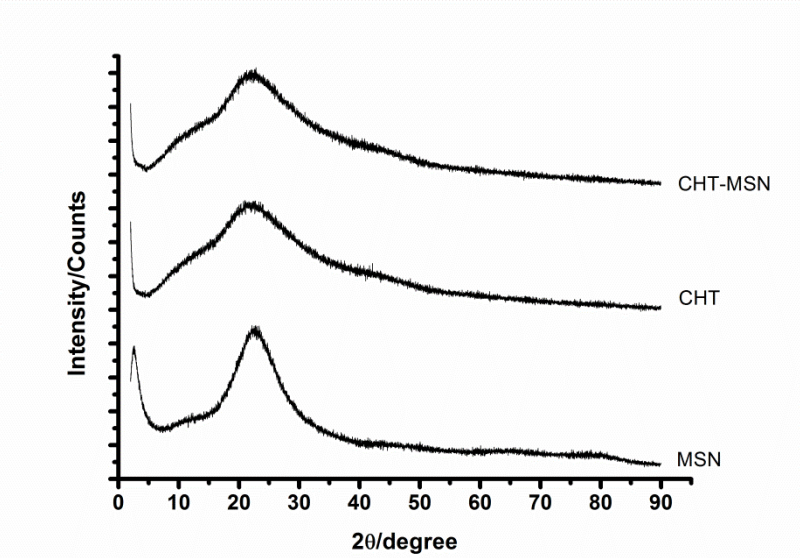

Figure D.3- X-ray diffraction patterns of MSN, CHT and CHT-MSN.

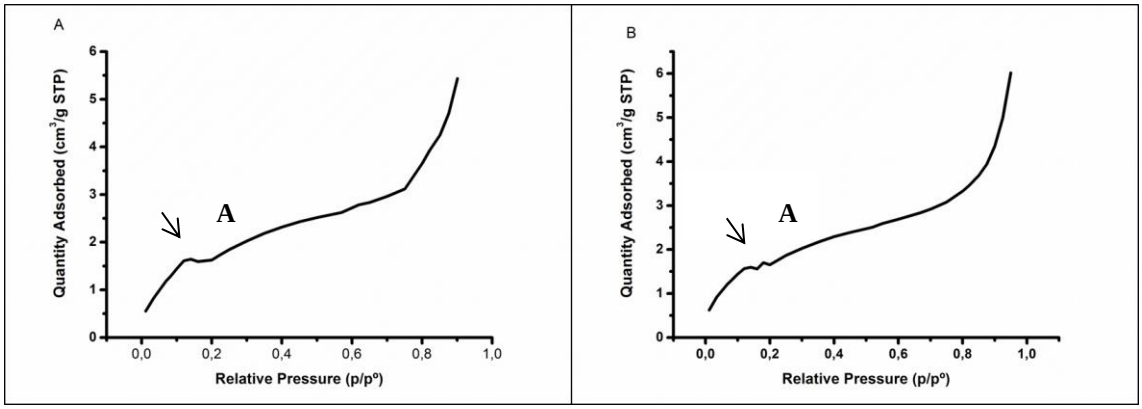

Figure D.4-Isotherm curves of (A) CHT and (B) CHT-MSN.

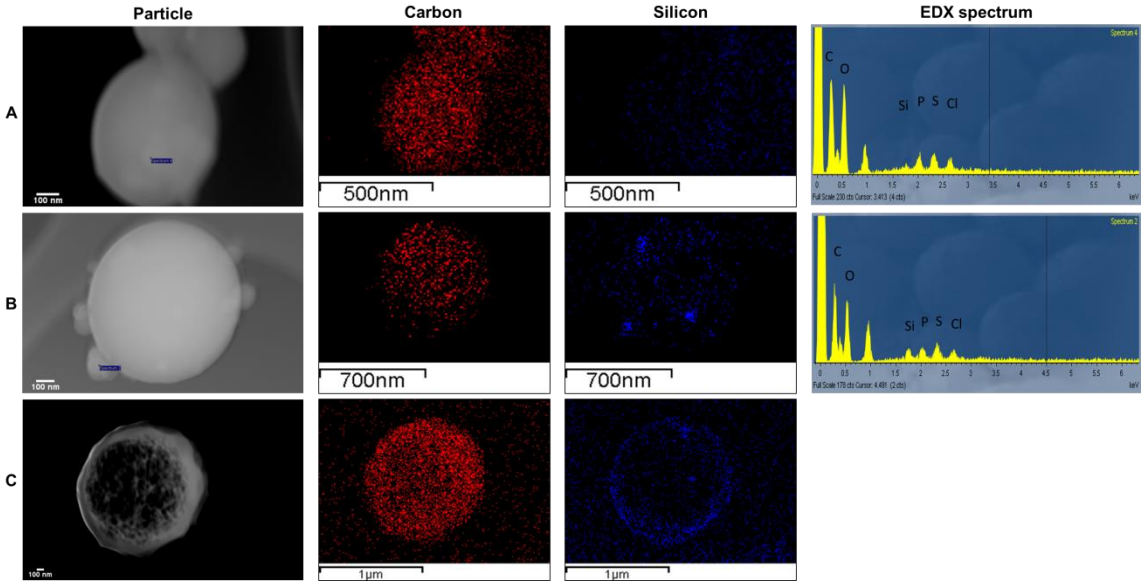

Figure D.5-STEM images and EDX spectrum of the micronized powders: (A) CHT; (B) CHT-LbL siRNA; and (C) CHT-LbL siRNA after 5 min in ultrasonic bath. Silicon atomic/weight % (respectively): CHT – 0.40 / 0.77 %; CHT-LbL siRNA - 1.69 / 3.19 %.

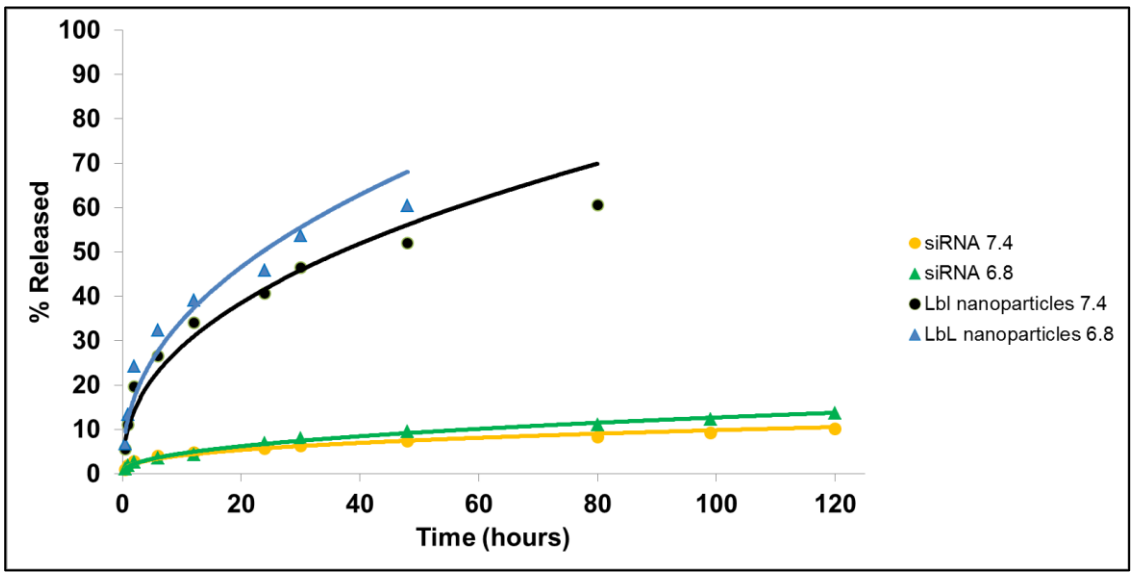

Figure D.6-Release profile from CHT microspheres: Korsmeyer and Peppas fitting. The colors from the adjustment curves are in agreement with the colors from the symbols.